T.R.
GEBZE TECHNICAL UNIVERSITY
GRADUATE SCHOOL OF NATURAL AND APPLIED SCIENCES

NON-LINEAR ANALYSIS OF SUPERELLIPTIC PANEL AND TUBULAR STRUCTURES

GÖKÇE AKGÜN
A THESIS SUBMITTED FOR THE DEGREE OF
DOCTOR OF PHILOSOPHY
DEPARTMENT OF MECHANICAL ENGINEERING

GEBZE
2019

T.R.

GEBZE TECHNICAL UNIVERSITY

GRADUATE SCHOOL OF NATURAL AND APPLIED SCIENCES

NON-LINEAR ANALYSIS OF SUPERELLIPTIC PANEL AND TUBULAR STRUCTURES

GÖKÇE AKGÜN

A THESIS SUBMITTED FOR THE DEGREE OF

DOCTOR OF PHILOSOPHY

DEPARTMENT OF MECHANICAL ENGINEERING

THESIS SUPERVISOR

PROF. DR. HASAN KURTARAN

GEBZE

2019

T.C.
GEBZE TEKNİK ÜNİVERSİTESİ
FEN BİLİMLERİ ENSTİTÜSÜ

SÜPERELİPTİK PANEL VE TÜP YAPILARIN DOĞRUSAL OLMAYAN ANALİZİ

GÖKÇE AKGÜN

DOKTORA TEZİ
MAKİNE MÜHENDİSLİĞİ ANABİLİM DALI

DANIŞMANI
PROF. DR. HASAN KURTARAN

GEBZE
2019

GEBZE TEKNİK ÜNİVERSİTESİ	**DOKTORA JÜRİ ONAY FORMU**

GTÜ Fen Bilimleri Enstitüsü Yönetim Kurulu'nun 13/11/2019 tarih ve 2019/51 sayılı kararıyla oluşturulan jüri tarafından 05/12/2019 tarihinde tez savunma sınavı yapılan Gökçe AKGÜN'ün tez çalışması Makine Mühendisliği Anabilim Dalında DOKTORA tezi olarak kabul edilmiştir.

JÜRİ

ÜYE (TEZ DANIŞMANI)	: Prof. Dr. Hasan KURTARAN	
ÜYE	: Doç. Dr. Ahmet Sinan ÖKTEM	
ÜYE	: Prof. Dr. Halit Süleyman TÜRKMEN	
ÜYE	: Prof. Dr. Mehmet Ali ARSLAN	
ÜYE	: Prof. Dr. Ekrem TÜFEKÇİ	

ONAY

Gebze Teknik Üniversitesi Fen Bilimleri Enstitüsü Yönetim Kurulu'nun

……/……./……. tarih ve ……../…….. sayılı kararı.

SUMMARY

In this thesis, geometrically nonlinear dynamic behavior of super-elliptic shells (both panel and tube type) made of laminated composite materials and functionally graded materials (FGMs) is investigated using generalized differential quadrature (GDQ) method. A super-elliptic shell can represent cylindrical, elliptical or quasi-rectangular shell by adjusting parameters in super-ellipse formulation (also known as Lamé curve formulation). In this study, geometric nonlinearity is taken into account using Green–Lagrange nonlinear strain–displacement relations that are derived for super-elliptic shells retaining full non-linear terms in all degree of freedom parameters. Transverse shear effect is considered through the first-order shear deformation theory (FSDT). Equations of motion are obtained using virtual work principle. Spatial derivatives in the equations of motion are expressed with generalized differential quadrature method and time integration is carried out using Newmark average acceleration method. Several super-elliptic shell problems under uniform distributed load are solved with the proposed method. Effects of laminated composite and functionally graded material properties (layer orientations, volume fraction coefficient of FGM, different ceramic/metal pairs like Alumina/Steel (Al_2O_3/Steel), Zirconia/Aluminum (ZrO_2/Al), Alumina/Aluminum (Al_2O_3/Al), Zirconia/Monel (ZrO_2/Ni-Cu) and Silicon Nitride/Steel (Si_3N_4/Steel)) on dynamic behavior are investigated. In addition, effects of super-elliptic shell geometric characteristics (ellipticity and ovality) and boundary conditions on dynamic behavior are examined. Transient dynamic responses are compared with the results that are obtained with the finite element models developed in this study.

Key Words: Super-Elliptic Shell, Functionally Graded, Generalized Differential Quadrature, Geometric Nonlinearity, Laminated Composite.

ÖZET

Bu tez çalışmasında, tabakalı kompozit ve fonksiyonel olarak derecelendirilmiş malzemelerden oluşan süper-eliptik kabuk yapıların (hem panel hem de tüp tipi) geometrik olarak doğrusal olmayan dinamik davranışı, genelleştirilmiş diferansiyel kareleme yöntemi kullanılarak incelenmiştir. Süper eliptik kabuk, süper-elips formülasyonundaki (Lamé eğrisi formülasyonu olarak da bilinir) parametrelere farklı değerler verilmesi vasıtasıyla silindirik, eliptik veya dikdörtgen benzeri bir kabuğu temsil edebilir. Bu çalışmada, geometrik doğrusalsızlık; süper-eliptik kabuklar için türetilmiş ve tüm serbestlik derecelerinde doğrusal olmayan terimlerin tamamını barındıran Green-Lagrange doğrusal olmayan gerinim-yer değiştirme ilişkileri kullanılarak dikkate alınmıştır. Enine kayma etkisi birinci dereceden kayma deformasyon teorisi kullanılarak dikkate alınmıştır. Hareket denklemleri sanal iş prensibi ile elde edilmiştir. Hareket denklemlerinde yer alan konumsal türevler genelleştirilmiş diferansiyel kareleme yöntemi ile ifade edilmiş olup, zaman integrasyonu için Newmark ortalama ivme metodu kullanılmıştır. Düzgün dağılı yük altındaki birkaç süper-eliptik kabuk problemi önerilen yöntemle çözülmüştür. Tabakalı kompozit ve fonksiyonel olarak derecelendirilmiş malzeme özelliklerinin (tabaka yönelimleri, fonksiyonel olarak derecelendirilmiş malzemeye ait hacim fraksiyon katsayısı, Alumina/Çelik (Al_2O_3/Çelik), Zirkonya/Alüminyum (ZrO_2/Al), Alumina/Alüminyum (Al_2O_3/Al), Zirkonya/Monel (ZrO_2/Ni-Cu) ve Silisyum Nitrür /Çelik (Si_3N_4/Çelik) gibi farklı seramik/metal çiftleri) dinamik davranışa olan etkileri incelenmiştir. Ayrıca süper-eliptik kabuğa ait geometrik özelliklerin (eliptiklik ve ovallik) ve sınır şartlarının dinamik davranış üzerindeki etkileri incelenmiştir. Dinamik geçici rejim cevapları, bu çalışma kapsamında geliştirilen sonlu elemanlar modeli ile elde edilen sonuçlar ile karşılaştırılmıştır.

Anahtar Kelimeler: Süper-Eliptik Kabuk, Fonksiyonel Olarak Derecelendirilmiş, Genelleştirilmiş Diferansiyel Kareleme, Geometrik Doğrusalsızlık, Tabakalı Kompozit.

ACKNOWLEDGEMENTS

I would like to express my deep appreciation and sincere gratitude to my supervisor, Prof. Hasan KURTARAN who inspired and encouraged me in this scientific work with his profound knowledge and experience.

I also express my special thanks to Assoc. Prof. Ahmet Zafer ŞENALP for his valuable supports, advices and guidance during my PhD studies.

I would like to extend my appreciation to the committee members, Assoc. Prof. Ahmet Sinan ÖKTEM, Prof. Halit Süleyman TÜRKMEN, Prof. Mehmet Ali ARSLAN and Prof. Ekrem TÜFEKÇİ for their time, guidance and valuable comments.

I wish to thank my dearest colleagues Tuğberk Hakan ÇETİN, Serhat DİNLEYEN, Erhan ÖZÇARE, İlke ALGÜL, Doğukan ARSLAN for their endless support during my PhD studies.

I wish to thank Asst. Prof. Fevzi Çakmak BOLAT and Özgür KALBARAN for their support and interest.

Finally, I would like to thank all of my friends, my family and my wife for their patience and support.

TABLE of CONTENTS

	Page
SUMMARY	v
ÖZET	vi
ACKNOWLEDMENTS	vii
TABLE of CONTENTS	viii
LIST of ABBREVIATIONS and ACRONYMS	x
LIST of FIGURES	xi
LIST of TABLES	xviii
1. INTRODUCTION	1
1.1. Literature Review	4
1.2. Objective and Content of the Thesis	7
1.3. Contribution of the Thesis	8
2. THEORETICAL FORMULATION	9
2.1. Theory of Surfaces	9
2.1.1. The First Fundamental Form	9
2.1.2. The Second Fundamental Form and Principle Radii of Curvature	11
2.2. Definition of Super-elliptic Cross-section	14
2.3. Strain-Displacement Relationship for Super-Elliptic Shell	15
2.4. Constitutive Equations and Equation of Motion	29
2.4.1. Super-Elliptic Shells Made of Laminated Composite Materials	29
2.4.2. Super-Elliptic Shells Made of FGMs	33
3. SOLUTION PROCEDURE	36
3.1. Geometric Mapping	36
3.2. Generalized Differential Quadrature (GDQ) Method	37
3.3. Solution of Equations of Motion	42
4. NUMERICAL RESULTS	45
4.1. Validation Examples	45

4.1.1. Validation Example for Laminated Composite Super-Elliptic Shell 45
4.1.2. Validation Example for FGM Super-Elliptic Shell 47
4.2. Examples for Laminated Composite Super-Elliptic Shells 48
4.2.1. Effect of Ovality Value (n) on Non-Linear Dynamic Behavior 50
4.2.2. Effect of Different Stacking Schemes on Non-Linear Dynamic Behavior 72
4.2.3. Effect of Ellipticity (a/b) on Non-Linear Dynamic Behavior 77
4.3. Examples for FGM Super-Elliptic Shells 81
4.3.1. Effect of Ovality Value (n) on Non-Linear Dynamic Behavior 82
4.3.2. Super-Elliptic Shells Made of Different FGMs 93
4.3.3. Effect of Volume Fraction Coefficient (k) on Nonlinear Dynamic Behavior 97
4.3.4. Effect of Ellipticity (a/b) on Nonlinear Dynamic Behavior 100
5. CONCLUSIONS 102

REFERENCES 105
BIOGRAPHY 110
APPENDICES 111

LIST of ABBREVIATIONS and ACRONYMS

Abbreviations and Acronyms		**Explanations**
GDQ	:	Generalized Differential Quadrature
DQM	:	Differential Quadrature Method
FSDT	:	First Order Deformation Theory
HSDT	:	Higher Order Deformation Theory
FGM	:	Functionally Graded Material
S-FGM	:	Sigmoid Functionally Graded Material
Al_2O_3	:	Alumina
ZrO_2	:	Zirconia
Ni-Cu	:	Monel
Si_3N_4	:	Silicon Nitride

LIST of FIGURES

Figure No:		Page
1.1:	Examples for engineering applications of shell structures a) composite pipe b) tunnel c) submarine d) aircraft.	1
1.2:	Representation of a) laminated composite material with different fiber orientations b) functionally graded material.	3
1.3:	Representation of a super-elliptic shell a) tube version b) panel version.	3
2.1:	Representation of a surface through parametric curves.	10
2.2:	Representation of super-ellipse curves according to different ovality (n) values.	15
2.3:	Position vector of a general point on shell surface.	17
2.4:	Representation of the super-elliptic shell.	19
3.1:	Geometric mapping process (transformation from Cartesian to natural coordinates).	37
3.2:	Discretized shell domain in natural coordinate system.	39
4.1:	Representation of the laminated composite cylindrical panel subjected to uniform internal pressure.	46
4.2:	Time history of transverse displacement at the center of laminated composite cylindrical panel.	46
4.3:	FGM plate under suddenly applied uniformly distributed pressure.	47
4.4:	Time history of non-dimensional transverse displacement at FGM plate center considering fully-clamped boundary condition.	48
4.5:	Super-elliptic shell parameters and fiber orientation angle (α) for laminated composite.	49
4.6:	Boundary and loading conditions of super-elliptic shell: a) CCCC b) CFCF c) CC boundary condition.	50
4.7:	Transverse displacement, strain and stress history at super-elliptic shell center for CCCC boundary condition for n=4 (left) and n=8 (right) ([0°/90°/0°/90°/0°]).	52

4.8: Transverse displacement, strain and stress history at super-elliptic shell center for CFCF boundary condition for n=4 (left) and n=8 (right) ([0°/90°/0°/90°/0°]). 53
4.9: Transverse displacement, strain and stress history at super-elliptic shell center for CCCC boundary condition for n=4 (left) and n=8 (right) ([30°/-30°/30°/-30°/30°]). 54
4.10: Transverse displacement, strain and stress history at super-elliptic shell center for CFCF boundary condition for n=4 (left) and n=8 (right) ([30°/-30°/30°/-30°/30°]). 55
4.11: Transverse displacement history of super-elliptic shells with different ovalities for CCCC boundary condition ([0°/90°/0°/90°/0°]). 56
4.12: Strain (in x direction) history of super-elliptic shells with different ovalities for CCCC boundary condition ([0°/90°/0°/90°/0°]). 57
4.13: Strain (in y direction) history of super-elliptic shells with different ovalities for CCCC boundary condition ([0°/90°/0°/90°/0°]). 57
4.14: Transverse displacement history of super-elliptic shells with different ovalities for CCCC boundary condition ([30°/-30°/30°/-30°/30°]). 58
4.15: Strain (in x direction) history of super-elliptic shells with different ovalities for CCCC boundary condition ([30°/-30°/30°/-30°/30°]). 58
4.16: Strain (in y direction) history of super-elliptic shells with different ovalities for CCCC boundary condition ([30°/-30°/30°/-30°/30°]). 59
4.17: Transverse displacement history of super-elliptic shells with different ovalities for CCCC boundary condition ([60°/-60°/60°/-60°/60°]). 59
4.18: Strain (in x direction) history of super-elliptic shells with different ovalities for CCCC boundary condition ([60°/-60°/60°/-60°/60°]). 60
4.19: Strain (in y direction) history of super-elliptic shells with different ovalities for CCCC boundary condition ([60°/-60°/60°/-60°/60°]). 60
4.20: Transverse displacement history of super-elliptic shells with different ovalities for CFCF boundary condition ([0°/90°/0°/90°/0°]). 61

4.21: Strain (in *x* direction) history of super-elliptic shells with different ovalities for CFCF boundary condition ([0°/90°/0°/90°/0°]). 61
4.22: Strain (in *y* direction) history of super-elliptic shells with different ovalities for CFCF boundary condition ([0°/90°/0°/90°/0°]). 62
4.23: Transverse displacement history of super-elliptic shells with different ovalities for CFCF boundary condition ([30°/-30°/30°/-30°/30°]). 62
4.24: Strain (in *x* direction) history of super-elliptic shells with different ovalities for CFCF boundary condition ([30°/-30°/30°/-30°/30°]). 63
4.25: Strain (in *y* direction) history of super-elliptic shells with different ovalities for CFCF boundary condition ([30°/-30°/30°/-30°/30°]). 63
4.26: Transverse displacement history of super-elliptic shells with different ovalities for CFCF boundary condition ([60°/-60°/60°/-60°/60°]). 64
4.27: Strain (in *x* direction) history of super-elliptic shells with different ovalities for CFCF boundary condition ([60°/-60°/60°/-60°/60°]). 64
4.28: Strain (in *y* direction) history of super-elliptic shells with different ovalities for CFCF boundary condition ([60°/-60°/60°/-60°/60°]). 65
4.29: Shear stress history of super-elliptic shells with different ovalities for CCCC boundary condition ([30°/-30°/30°/-30°/30°]). 66
4.30: Shear stress history of super-elliptic shells with different ovalities for CCCC boundary condition ([60°/-60°/60°/-60°/60°]). 67
4.31: Shear stress history of super-elliptic shells with different ovalities for CFCF boundary condition ([30°/-30°/30°/-30°/30°]). 67
4.32: Shear stress history of super-elliptic shells with different ovalities for CFCF boundary condition ([60°/-60°/60°/-60°/60°]). 68
4.33: Transverse displacement history of super-elliptic shells with different ovalities for CC boundary condition ([0°/90°/0°/90°/0°], at the upper center of tube). 69
4.34: Strain (in *x* direction) history of super-elliptic shells with different ovalities for CC boundary condition ([0°/90°/0°/90°/0°], at the upper center of tube). 69

4.35: Strain (in *y* direction) history of super-elliptic shells with different ovalities for CC boundary condition ([0°/90°/0°/90°/0°], at the upper center of tube). 70
4.36: Transverse displacement history of super-elliptic shells with different ovalities for CC boundary condition ([0°/90°/0°/90°/0°], at the lateral center of tube). 70
4.37: Strain (in *x* direction) history of super-elliptic shells with different ovalities for CC boundary condition ([0°/90°/0°/90°/0°], at the lateral center of tube). 71
4.38: Strain (in *y* direction) history of super-elliptic shells with different ovalities for CC boundary condition ([0°/90°/0°/90°/0°], at the lateral center of tube). 71
4.39: Transverse displacement history of super-elliptic shells with different layer orientations for CCCC boundary condition (*n*=2). 73
4.40: Transverse displacement history of super-elliptic shells with different layer orientations for CCCC boundary condition (*n*=4). 73
4.41: Transverse displacement history of super-elliptic shells with different layer orientations for CCCC boundary condition (*n*=8). 74
4.42: Transverse displacement history of super-elliptic shells with different layer orientations for CFCF boundary condition (*n*=2). 74
4.43: Transverse displacement history of super-elliptic shells with different layer orientations for CFCF boundary condition (*n*=4). 75
4.44: Transverse displacement history of super-elliptic shells with different layer orientations for CFCF boundary condition (*n*=8). 75
4.45: Transverse displacement history of super-elliptic tubes with different layer orientations for CC boundary condition (*n*=4, at the upper center of tube). 76
4.46: Transverse displacement history of super-elliptic tubes with different layer orientations for CC boundary condition (*n*=4, at the lateral center of tube). 76
4.47: Transverse displacement history of super-elliptic shells with different ellipticity for CCCC boundary condition (*n*=2, [60°/-60°/60°/-60°/60°]). 78

4.48: Transverse displacement history of super-elliptic shells with different ellipticity for CCCC boundary condition (n=4, [60°/-60°/60°/-60°/60°]). 79
4.49: Transverse displacement history of super-elliptic shells with different ellipticity for CCCC boundary condition (n=8, [60°/-60°/60°/-60°/60°]). 79
4.50: Transverse displacement history of super-elliptic shells with different ellipticity for CFCF boundary condition (n=2, [60°/-60°/60°/-60°/60°]). 80
4.51: Transverse displacement history of super-elliptic shells with different ellipticity for CFCF boundary condition (n=4, [60°/-60°/60°/-60°/60°]). 80
4.52: Transverse displacement history of super-elliptic shells with different ellipticity for CFCF boundary condition (n=8, [60°/-60°/60°/-60°/60°]). 81
4.53: FGM super-elliptic shell parameters. 82
4.54: Time history of non-dimensional displacement at FGM super-elliptic shell center for different grid numbers (1x8 elements). 83
4.55: Time histories of non-dimensional transverse displacement, strain and stress at FGM super-elliptic shell center (CCCC, n=4 (left) and n=8 (right), Zirconia/Aluminum, k=20). 85
4.56: Time histories of non-dimensional transverse displacement, strain and stress at FGM super-elliptic shell center (CFCF, n=4 (left) and n=8 (right), Zirconia/Aluminum, k=20). 86
4.57: The effect of ovality value (n) on transverse displacement time history (CCCC, Aluminum/Steel, k=1). 87
4.58: The effect of ovality value (n) on transverse displacement time history (CCCC, Zirconia/Aluminum, k=1). 87
4.59: The effect of ovality value (n) on transverse displacement time history (CCCC, Aluminum/Alumina, k=1). 88
4.60: The effect of ovality value (n) on transverse displacement time history (CCCC, Zirconia/Monel, k=1). 88

4.61: The effect of ovality value (n) on transverse displacement time history (CCCC, Silicon Nitride/Steel, k=1). 89
4.62: The effect of ovality value (n) on transverse displacement time history (CFCF, Aluminum/Steel, k=1). 89
4.63: The effect of ovality value (n) on transverse displacement time history (CFCF, Zirconia/Aluminum, k=1). 90
4.64: The effect of ovality value (n) on transverse displacement time history (CFCF, Aluminum/Alumina, k=1). 90
4.65: The effect of ovality value (n) on transverse displacement time history (CFCF, Zirconia/Monel, k=1). 91
4.66: The effect of ovality value (n) on transverse displacement time history (CFCF, Silicon Nitride/Steel, k=1). 91
4.67: The effect of ovality value (n) on transverse displacement time history (CC, Zirconia/Aluminum, k=2, at the upper center of tube). 92
4.68: The effect of ovality value (n) on transverse displacement time history (CC, Zirconia/Aluminum, k=2, at the lateral center of tube). 93
4.69: Non-dimensional transverse displacement time history of FGM super-elliptic shells made of different FGMs (CCCC, k=1): (a) ovality value n=2; (b) ovality value n=4; (c) ovality value n=8. 94
4.70: Non-dimensional transverse displacement time history of FGM super-elliptic shells made of different FGMs (CFCF, k=1): (a) ovality value n=2; (b) ovality value n=4; (c) ovality value n=8. 95
4.71: Non-dimensional transverse displacement time history of FGM super-elliptic shells made of different FGMs (CC, n=4, k=2, at the upper center of tube). 96
4.72: Non-dimensional transverse displacement time history of FGM super-elliptic shells made of different FGMs (CC, n=4, k=2, at the lateral center of tube). 96
4.73: The effect of volume fraction coefficient on transverse displacement time history for CCCC boundary condition (n=4): (a) Alumina/Steel; (b) Zirconia/Aluminum; (c) Alumina/Aluminum; (d) Zirconia/Monel; (e) Silicon Nitride/Steel. 98

4.74: The effect of volume fraction coefficient on transverse displacement time history for CFCF boundary condition (n=4): (a) Alumina/Steel; (b) Zirconia/Aluminum; (c) Alumina/Aluminum; (d) Zirconia/Monel; (e) Silicon Nitride/Steel. 99

4.75: The effect of ellipticity on transverse displacement time history for CCCC boundary condition (Silicon Nitride/Steel, k=1): (a) for ovality value n=2; (b) for ovality value n=4; (c) for ovality value n=8. 100

4.76: The effect of ellipticity on transverse displacement time history for CFCF boundary condition (Silicon Nitride/Steel, k=1): (a) for ovality value n=2; (b) for ovality value n=4; (c) for ovality value n=8. 101

LIST of TABLES

Table No:		Page
4.1:	First three natural frequencies (Hz) of super-elliptic shell (n=4, a/b=2, CCCC, [0°/90°/0°/90°/0°]) according to different mesh numbers.	51
4.2:	First three natural frequencies (Hz) of super-elliptic shell (n=8, a/b=2, CCCC, [0°/90°/0°/90°/0°]) according to different mesh numbers.	51
4.3:	Material specifications of FGM.	82
4.4:	Natural frequency values (Hz) of FGM super-elliptic shell (CCCC, a/b=2, n=4, Zirconia/Aluminum, k=20) considering different mesh numbers.	84
4.5:	Natural frequency values (Hz) of FGM super-elliptic shell (CCCC, a/b=2, n=8, Zirconia/Aluminum, k=20) considering different mesh numbers.	84

1. INTRODUCTION

Shell structures are extensively used in many areas such as aerospace, defense, marine and automotive industries where structures are commonly subjected to dynamic loadings rather than static loadings. Therefore, investigating the dynamic behavior of such structures is of common interest among many researchers. A shell structure may be defined as a body enclosed between two closely spaced and curved surfaces [Saada, 1974] where the thickness is small compared to middle surface dimensions (see Figure 2.2 in chapter 2). Shell structures can have various geometry types such as cylindrical, spherical, doubly-curved, conical, elliptical, oval shells etc. Such geometries are encountered in many engineering applications, e.g. airplanes, space ships, submarines, automobiles, pipes and so on (Figure 1.1 (a) [Web 1, 2019], (b) [Web 2, 2019], (c) [Web 3, 2019], (d) [Web 4, 2019]).

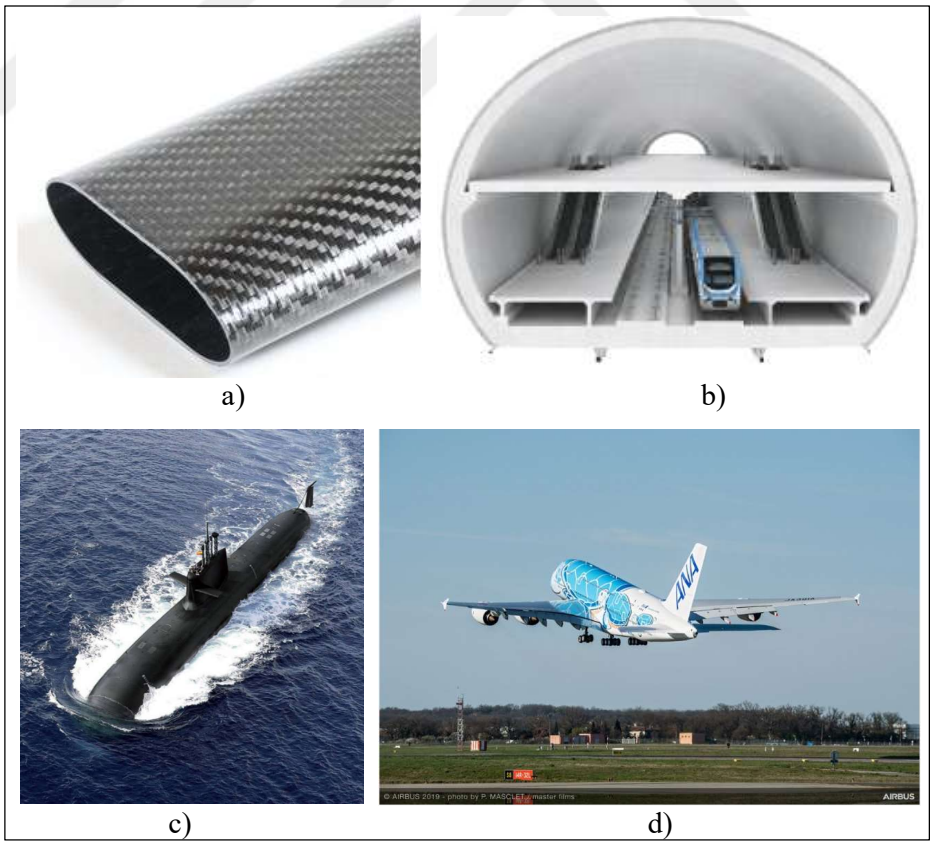

Figure 1.1**:** Examples for engineering applications of shell structures a) composite pipe b) tunnel c) submarine d) aircraft.

With the advancement of technology, manufacturing of innovative materials such as composite and functionally graded materials (FGMs) is facilitated, and their usage becomes more widespread. Composite materials consist of two or more materials which together produce desirable properties that cannot be achieved with any of the constituents alone [Reddy, 2003]. A fiber reinforced laminated composite material consists of two or more composite laminates which contain high strength and high modulus fibers in a matrix material (Figure 1.2 (a) [Reddy, 2003]). The desired mechanical properties for different directions can be provided by using different fiber orientation schemes. Moreover, composite materials are mostly preferred due to their light-weight feature by keeping high strength-to-weight ratio.

Besides the above-mentioned advantages of laminated composite materials, the main problem of these materials is material failure due to stress concentrations occurred between the layers. To overcome this issue, Japanese scientists bring forward a new idea referred as functionally graded materials (FGMs) in 1984. FGMs consist of different material pairs commonly metal and ceramic (Figure 1.2 (b)). Material properties of FGMs continuously vary through the thickness and are determined by changing volume fraction. FGMs were primarily utilized as thermal barriers to withstand high temperatures in fusion reactors and aero-space structures. Today, they are widely utilized as structural components in aerospace industry, biomedical, energy, defense and optoelectronics applications [Uemura, 2003], [Koizumi, 1997], [Hirai and Chen, 1999], [Chan, 2001].

This thesis presents the nonlinear transient dynamic behavior of super-elliptic shell structures made of laminated composite materials and FGMs subjected to dynamic loads under different boundary conditions. A super-elliptic shell can represent cylindrical, elliptical or quasi-rectangular shell (see Figure 2.1 and 2.3 in chapter 2) by adjusting parameters in super-ellipse formulation (also known as Lamé curve formulation, see chapter 2.1). From this point of view, a generic mathematical model is developed for both circular and non-circular (elliptic and super-elliptic) shells to investigate the nonlinear dynamic behavior. Here, only geometric nonlinearity is considered regardless of material and contact nonlinearities. Figure 1.3 shows the representation of a super-elliptic shell (panel and tube version). As it is investigated in this study, super-elliptic shell structures are encountered in engineering applications such as airplanes (cylindric shell case), tunnels (elliptic shell case), spacecrafts, helicopters, pipes, fuel tankers and submarines (super-elliptic shell case).

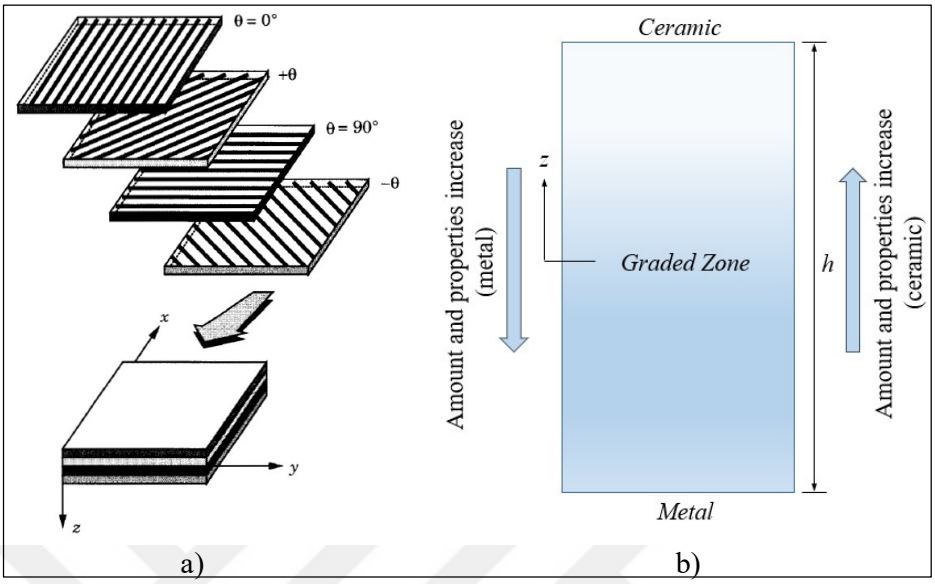

Figure 1.2**:** Representation of a) laminated composite material with different fiber orientations b) functionally graded material.

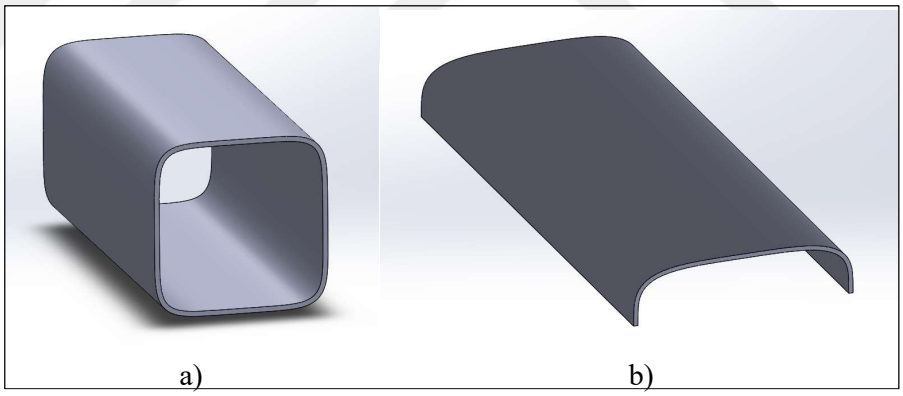

Figure 1.3**:** Representation of a super-elliptic shell a) tube version b) panel version.

In early 1970s, an efficient numerical method called differential quadrature method (DQM) was introduced by [Bellman and Casti, 1971], [Bellman et al., 1972]. They extended well-known integral quadrature method to the derivative calculation of a function [Tornabene and Bacciocchi, 2018]. The advantage of this method is to obtain accurate results using less grid points than well-known finite element method. However, first applications of DQM allows the use of a limited number of grids and it is not appropriate to calculate higher order derivatives. Later, [Shu, 2000] suggested a new technique which is the improved form of DQM called generalized differential

quadrature (GDQ) method. The advantage of GDQ method to DQM is that it is appropriate for arbitrary number and distribution of grid points. In addition, higher order derivatives can easily be calculated by using recursive formulations. Further information and the applications of GDQ technique can be found in relevant books [Chen, 2006], [Zong and Zhang, 2009], [Tornabene and Bacciocchi, 2018] and review articles [Bert and Malik, 1996], [Tornabene et al., 2015]. GDQ method was applied successfully in the efficient solution of structural problems [Choi and Chou, 2003], [Tornabene et al., 2015a], [Tornabene et al., 2015b], [Bacciocchi et al., 2016], [Kurtaran, 2015c], [Kurtaran, 2015b], [Kurtaran, 2015a], [Liu et al., 2016], [Zhang et al., 2015], [Tornabene et al., 2017]. Thus, in this study, GDQ method is applied to investigate the nonlinear transient behavior of super-elliptic shells.

1.1. Literature Review

Numerous studies about the structural analysis of shell structures have been conducted from past to present. Detailed explanations related to the structural analysis of shell structures made of laminated composite materials and FGMs can be found in specialized books [Fluegge, 1973], [Saada, 1974], [Vorovich, 1999], [Reddy, 2003], [Qatu, 2004], [Soedel, 2004], [Amabili, 2008], [Shen, 2009], [Elishakoff et al., 2016], [Tornabene and Bacciocchi, 2018]. In this thesis, literature review study is limited to dynamic analysis of circular and non-circular shell structures made of laminated composite materials and FGMs. In addition, the review mainly focused on linear and non-linear analysis of non-circular (elliptic, oval, etc.) shell structures.

Key research and review studies related to the non-linear dynamic analysis of shell structures that have constant radii of curvature (cylindrical, doubly-curved shells) made of laminated composite materials and FGMs are briefly mentioned as following. [Alijani and Amabili, 2014] conducted a survey about geometrically nonlinear free and forced vibration of shell structures made of isotropic, hyper-elastic, piezo-electric, laminated composite and functionally graded materials. [Amabili and Païdoussis, 2003] conducted a survey on large displacement free and forced vibrations of circular cylindrical shells and panels. [Dey and Ramachandra, 2017] investigated nonlinear transverse dynamic response of laminated composite circular cylindrical shells considering von Kármán type of non-linearity and simply supported boundary condition. [Sofiyev et al., 2017] studied non-linear vibration analysis of orthotropic

cylindrical shells resting on nonlinear elastic foundation. [Amabili, 2015] developed a nonlinear third-order shear deformation theory to examine static and dynamic behavior of laminated doubly curved shells and applied it to cylindrical shells. [Pradyumna and Nanda, 2013] studied on nonlinear dynamic analysis of FGM panels (hyperbolic paraboloid, spherical and cylindrical panels) with initial geometric imperfections under suddenly applied uniform load considering thermal effects. [Alijani et al., 2011] carried a study on nonlinear vibration responses of FGM doubly curved shells. [Duc et al., 2015] examined nonlinear dynamic behavior of sigmoid functionally graded (S-FGM) cylindrical shells considering elastic foundation and thermal effects.

Publications related to linear and non-linear analysis of non-circular (elliptic, oval, etc.) shell structures are mentioned below.

[Srinivasan and Bobby, 1976] utilized a matrix method to investigate the free vibration behavior of clamped non-circular cylindrical shell panels. In the study, effects of the curvature, thickness ratio and aspect ratio on natural frequencies has been studied. [Choi and Chou, 2003] examined free-vibration behavior of cantilever non-circular curved panels using DQM. The system is expressed in an orthogonal curvilinear co-ordinate system and the equations of motion are based on the Love's hypothesis. Effects of shallowness, thickness ratio and aspect ratio on free-vibration characteristics of a cantilever curved panel are examined. [Patel et al., 2004] carried out a study on thermal buckling behavior of laminated cross-ply oval cylindrical shells utilizing finite element method. In the study, higher order shear deformation theory (HSDT) is considered and the governing equations are obtained using the principle of minimum potential energy. Effects of geometric characteristics of shell and material properties on the critical temperature parameter is examined. [Patel et al., 2005] investigated the free vibration behavior of elliptical cylindrical shells made of FGM utilizing finite element method. In the study, HSDT is considered in both transverse and in-plane displacements. Effects of non-circularity, radius-to-thickness ratio, material composition and volume fraction coefficient on the free vibration frequencies and mode shape characteristics are examined. [Patel et al., 2007] studied the thermo-elastic buckling behavior of elliptical cylindrical shells made of angle-ply laminated composite materials subjected to uniform temperature rise. Combined effects of non-circularity and ply-angle on the critical temperature parameter and buckling mode shapes are investigated. [Ganapathi et al., 2003] investigated transient dynamic and free vibration behavior of laminated cross-ply oval cylindrical shells using finite

element method. Transverse shear effect is considered through HSDT. Effects of geometric characteristics of the shell, loading and lay-up on the vibration behavior are examined. [Tornabene et al., 2015a] conducted a study to investigate the free vibration behavior of thick and moderately thick elliptic cones, cylinders and plates made of laminated composite materials using GDQ method. In the study, HSDT is considered. It is shown that GDQ method has several advantages such as stability, accuracy and easy implementation. [Ganapathi et al., 2002] examined the dynamic behavior of thick non-circular cylindrical shell structures made of laminated cross-ply composite material under thermal/mechanical loading conditions considering HSDT. Effects of geometric characteristics and number of layers on thermal/mechanical behavior are investigated. [Khalifa, 2015] presented the free vibration analysis of an orthotropic elliptical cylindrical shell to investigate the effects of non-uniform Winkler elastic foundation and non-homogeneity on vibration characteristics. [Ganapathi et al., 2004] used finite element method to investigate the free vibration characteristics of non-circular cylindrical shells made of laminated angle-ply composite materials. In the study, FSDT is considered. Effects of geometric and material properties on natural frequencies are examined. [Tornabene et al., 2015b] implemented GDQ method to investigate free vibration behavior of composite oval and elliptic cylinders using linear strain-displacement relations. In the study, modal frequencies and modal shapes are obtained for elliptic and oval cylindrical tube structures. [Ma et al., 2008] investigated buckling behavior of super-ellipsoidal shells under uniform pressure using finite element approach. In this study, a super-ellipsoidal (box-like) shell structure is examined. The critical buckling pressures and buckling shapes are obtained. Besides, a simple approximate formula is developed to predict the critical buckling pressure of thick spherical shells. [Thamburaj and Sun, 2001] developed a method to examine the free and forced vibration behavior of a laminated non-circular cylindrical shell. The cross section of the shell is a square with rounded corners which leads difficulties in the analysis of the system. It is applied a conformal mapping to map the physical domain onto a circular cylindrical domain. The Rayleigh-Ritz method is utilized in the solution. Free and forced vibration solutions of the system are presented.

1.2. Objective and Content of the Thesis

The objective of this PhD thesis is to develop a mathematical model and a computer program to investigate the nonlinear transient dynamic behavior of super-elliptic shell structures (panel and tubular versions) made of laminated composite materials and FGMs subjected to dynamic loads under different boundary conditions. Obtained results are compared with the results in the literature and those obtained using well-known finite element method in order to validate the programs. This thesis consists of five chapters. Followings are the details of each chapter.

Chapter 1 deals with the brief information about shell structures and super-elliptic shells in particular, material models that is used in this study and solution method. Literature survey, objective and contribution of the thesis are mentioned in chapter 1.

In chapter 2, detailed definition of super-elliptic cross section of a super-elliptic shell is given first. Then, it is mentioned about the derivation of strain-displacement relations for super-elliptic shells. As a novelty, Green-Lagrange strain-displacement relations for super-elliptic shells were derived retaining full non-linear terms in all degree of freedom parameters using theory of surfaces and differential geometry [Saada, 1974], [Struik, 1988]. Transverse shear effect is considered through the first order shear deformation theory (FSDT). Constitutive equations for laminated composite materials and FGMs are explained in detail and equation of motion for each material model is obtained using virtual work principle.

In chapter 3, solution procedure of the equation of motion is explained in detail. In this context, geometric mapping process from cartesian to natural coordinates is applied since the domain is irregular. GDQ method is explained in detail. Another unique aspect of the thesis is to apply GDQ method in the calculation of spatial derivatives in equation of motion for super-elliptic shells. Time integration is carried out using Newmark average acceleration method and Newton Raphson iterative method is utilized in the solution.

In chapter 4, validation examples for developed GDQ codes are given and several super-elliptic shell problems are solved to investigate the following topics:

- Effect of super-elliptic shell geometric characteristics (ellipticity and ovality) on nonlinear dynamic behavior.
- Effect of different stacking schemes of laminated composite material on nonlinear dynamic behavior.
- Effect of FGM material properties using different ceramic/metal pairs like Alumina/Steel (Al_2O_3/Steel), Zirconia/Aluminum (ZrO_2/Al), Alumina/ Aluminum (Al_2O_3/Al), Zirconia/Monel (ZrO_2/Ni-Cu) and Silicon Nitride/Steel (Si_3N_4/Steel) on nonlinear dynamic behavior.
- Effect of the boundary conditions on nonlinear dynamic behavior.

In chapter 5, concluding remarks of the study and suggestions to the researchers for future studies are given.

1.3. Contribution of the Thesis

Analysis of shell structures that have constant radii of curvature such as cylindrical, spherical or doubly-curved shells is widely being studied by many researchers. As the geometry becomes more complex (like non-circular shells which have variable radii of curvature), the number of studies reduces. Mostly, linear free vibration and static analyses of such structures are encountered in the literature. However, there is still a gap in the literature related to nonlinear transient dynamic analysis of such complex shell geometries. In this context, nonlinear transient dynamic behavior of super-elliptic shell structures made of laminated composite materials and FGMs considering different boundary conditions is investigated in this thesis and novel nonlinear Green-Lagrange strain-displacement relations for super-elliptic shells are derived.

Computational cost of an analysis is another aspect for researchers. Grid numbers utilized in the analyses are playing an important role in computational cost. In this thesis, GDQ method is utilized where this method provides accurate results using less grid points than well-known finite element method. In this thesis, GDQ method is effectively and efficiently utilized in the analyses.

2. THEORETICAL FORMULATION

2.1. Theory of Surfaces

A shell structure may be defined as a body enclosed between two closely spaced and curved surfaces [Saada, 1974]. Before investigating the shell structures, a clear understanding of theory of surfaces, which is a subtopic of differential geometry, is a necessity. Detailed information about theory of surfaces can be found in relevant books of [Tornabene and Bacciocchi, 2018] (Chapter 2.1), [Saada, 1974] (Chapter 18) and [Amabili, 2008] (Chapter 2.3). However, for the sake of the reader, a brief information about the theory of surfaces is given below.

2.1.1. The First Fundamental Form

Consider a surface $\mathcal{S}$ defined in a three-dimensional Euclidean space with a global reference system of Cartesian coordinates x_1, x_2, x_3. This surface can be expressed as a function of ξ_1 and ξ_2 parameters as follows

$$x_1 = f_1(\xi_1, \xi_2), \quad x_2 = f_2(\xi_1, \xi_2), \quad x_3 = f_3(\xi_1, \xi_2) \tag{2.1}$$

where ξ_1 and ξ_2 denote the curvilinear coordinates of the surface. f_1, f_2 and f_3 are single-valued continuous functions of the parameters ξ_1 and ξ_2. Using a position vector $\mathbf{r}$ as illustrated in Figure 2.1, equation (2.1) can be stated in vector form as following

$$\mathbf{r}(\xi_1, \xi_2) = f_1(\xi_1, \xi_2)\mathbf{e}_1 + f_2(\xi_1, \xi_2)\mathbf{e}_2 + f_3(\xi_1, \xi_2)\mathbf{e}_3 \tag{2.2}$$

where $\mathbf{e}_1$, $\mathbf{e}_2$, $\mathbf{e}_3$ denote unit vectors along the axes of the global reference coordinate system $x_1x_2x_3$. As additional information, in this study, vectors are represented in **bold** form. As shown in Figure 2.1, by moving from the point $P(\xi_1,\xi_2)$ to $P'(\xi_1+d\xi_1,\xi_2+ d\xi_2)$ on the surface $\mathcal{S}$, the infinitesimal change of position vector $\mathbf{r}$ can be stated as

$$d\mathbf{r} = \frac{\partial \mathbf{r}}{\partial \xi_1} d\xi_1 + \frac{\partial \mathbf{r}}{\partial \xi_2} d\xi_2 = \mathbf{r}_{,\xi_1} d\xi_1 + \mathbf{r}_{,\xi_2} d\xi_2 \tag{2.3}$$

where $\mathbf{r}_{,\xi_1}$ and $\mathbf{r}_{,\xi_2}$ vectors are tangent to the ξ_1 and ξ_2 curves, respectively and sometimes are called as tangent vectors. Since the distance *ds* between *P* and *P′* points on the surface $\mathcal{S}$ is infinitesimal, the square of *ds* can be expressed as the scalar product of *d***r** by itself as following

$$(ds)^2 = d\mathbf{r} \cdot d\mathbf{r} = E(d\xi_1)^2 + 2F d\xi_1 d\xi_2 + G(d\xi_2)^2 \tag{2.4}$$

where

$$E = \mathbf{r}_{,\xi_1} \cdot \mathbf{r}_{,\xi_1}, \quad F = \mathbf{r}_{,\xi_1} \cdot \mathbf{r}_{,\xi_2}, \quad G = \mathbf{r}_{,\xi_2} \cdot \mathbf{r}_{,\xi_2} \tag{2.5}$$

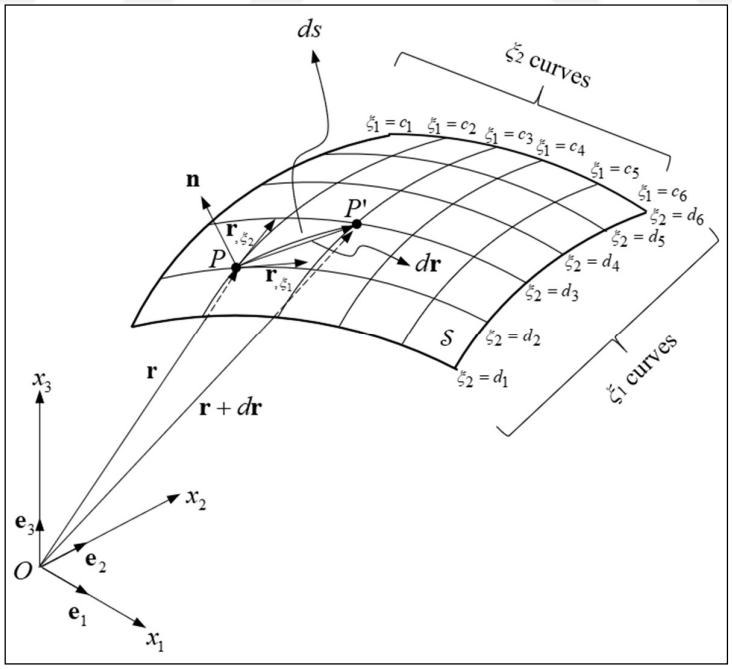

Figure 2.1**:** Representation of a surface through parametric curves.

Equation (2.4) indicates the first fundamental form of the surface $\mathcal{S}$ and *E*, *F*, *G* denote magnitudes of first fundamental form or metric coefficients. If ξ_1 and ξ_2 curves

are chosen as orthogonal (as in our case), then value of the metric F becomes 0. Therefore, equation (2.4) becomes

$$\left(ds\right)^2 = A_1^2\left(d\xi_1\right)^2 + A_2^2\left(d\xi_2\right)^2 \tag{2.6}$$

where

$$A_1 = \sqrt{E}, \quad A_2 = \sqrt{G} \tag{2.7}$$

In equation (2.6), the coefficients A_1 and A_2 are called as Lamé parameters. Metric coefficients E, F, G (in particular, Lamé parameters) are the link between the length of an element on the surface $\mathcal{S}$ and the differentials $d\xi_1$ and $d\xi_2$. Thus, first fundamental form allows to measure the distances on the surface $\mathcal{S}$.

2.1.2. The Second Fundamental Form and Principle Radii of Curvature

As it is illustrated in Figure 2.1, there exists a unit normal vector $\mathbf{n}(\xi_1,\xi_2)$ that is orthogonal to the tangent plane of the surface $\mathcal{S}$ at any point P. The unit vector $\mathbf{n}$ parallel to the vector product of $\mathbf{r}_{,\xi_1}$ and $\mathbf{r}_{,\xi_2}$ tangent vectors and since it has a magnitude of 1, it can be expressed as following

$$\mathbf{n}(\xi_1,\xi_2) = \frac{\mathbf{r}_{,\xi_1} \times \mathbf{r}_{,\xi_2}}{\left|\mathbf{r}_{,\xi_1} \times \mathbf{r}_{,\xi_2}\right|} \tag{2.8}$$

Considering φ as the angle between the tangent vectors $\mathbf{r}_{,\xi_1}$ and $\mathbf{r}_{,\xi_2}$, by using following relations

$$\left|\mathbf{r}_{,\xi_1} \times \mathbf{r}_{,\xi_2}\right| = \left|\mathbf{r}_{,\xi_1}\right| \cdot \left|\mathbf{r}_{,\xi_2}\right| \cdot \sin\varphi \tag{2.9}$$

$$\mathbf{r}_{,\xi_1} \cdot \mathbf{r}_{,\xi_2} = \left|\mathbf{r}_{,\xi_1}\right| \cdot \left|\mathbf{r}_{,\xi_2}\right| \cdot \cos\varphi \tag{2.10}$$

$$\cos\varphi = \frac{\mathbf{r}_{,\xi_1} \cdot \mathbf{r}_{,\xi_2}}{\sqrt{(\mathbf{r}_{,\xi_1} \cdot \mathbf{r}_{,\xi_1}) \cdot (\mathbf{r}_{,\xi_2} \cdot \mathbf{r}_{,\xi_2})}} = \frac{F}{\sqrt{EG}} \tag{2.11}$$

$$\sin\varphi = \sqrt{1-\cos^2\varphi} = \sqrt{EG - \frac{F^2}{EG}} \tag{2.12}$$

unit vector **n** can be stated as

$$\mathbf{n}(\xi_1, \xi_2) = \frac{\mathbf{r}_{,\xi_1} \times \mathbf{r}_{,\xi_2}}{H} \tag{2.13}$$

where

$$H = \sqrt{EG - F^2} \neq 0 \tag{2.14}$$

As it is illustrated in Figure 2.1, moving from the point P to P' on the surface $\mathcal{S}$ leads to a change in the position vector **r** and unit normal vector **n** as $d\mathbf{r}$ and $d\mathbf{n}$, respectively. These can be expressed as following

$$d\mathbf{r} = \frac{\partial \mathbf{r}}{\partial \xi_1} d\xi_1 + \frac{\partial \mathbf{r}}{\partial \xi_2} d\xi_2 \tag{2.15}$$

$$d\mathbf{n} = \frac{\partial \mathbf{n}}{\partial \xi_1} d\xi_1 + \frac{\partial \mathbf{n}}{\partial \xi_2} d\xi_2 \tag{2.16}$$

By forming the scalar product of $d\mathbf{n}$ and $d\mathbf{r}$, one can get

$$d\mathbf{n} \cdot d\mathbf{r} = L\left(d\xi_1\right)^2 + 2M d\xi_1 d\xi_2 + N\left(d\xi_2\right)^2 \tag{2.17}$$

where

$$L = \mathbf{n}_{,\xi_1} \cdot \mathbf{r}_{,\xi_1}, \quad M = \frac{1}{2}\left(\mathbf{n}_{,\xi_1} \cdot \mathbf{r}_{,\xi_2} + \mathbf{n}_{,\xi_2} \cdot \mathbf{r}_{,\xi_1}\right), \quad N = \mathbf{n}_{,\xi_2} \cdot \mathbf{r}_{,\xi_2} \tag{2.18}$$

Equation (2.17) is called as the second fundamental form of the surface $\mathcal{S}$. L, M, N denote magnitudes of second fundamental form, and they are connected with the curvature properties of the surface $\mathcal{S}$. Since $\mathbf{n}$ is normal to the surface, and since $\mathbf{r}_{,\xi_1}$ and $\mathbf{r}_{,\xi_2}$ are tangent to the surface, thus

$$\mathbf{n} \cdot \mathbf{r}_{,\xi_1} = \mathbf{n} \cdot \mathbf{r}_{,\xi_2} = 0 \tag{2.19}$$

and partial differentiation of the scalar products in equation (2.19) respect to ξ_1 and ξ_2 parameters yields to the following expressions:

$$\mathbf{n}_{,\xi_1} \cdot \mathbf{r}_{,\xi_1} = -\mathbf{n} \cdot \mathbf{r}_{,\xi_1\xi_1} \tag{2.20}$$

$$\mathbf{n}_{,\xi_2} \cdot \mathbf{r}_{,\xi_2} = -\mathbf{n} \cdot \mathbf{r}_{,\xi_2\xi_2} \tag{2.21}$$

$$\mathbf{n}_{,\xi_2} \cdot \mathbf{r}_{,\xi_1} = -\mathbf{n} \cdot \mathbf{r}_{,\xi_1\xi_2} \tag{2.22}$$

$$\mathbf{n}_{,\xi_1} \cdot \mathbf{r}_{,\xi_2} = -\mathbf{n} \cdot \mathbf{r}_{,\xi_1\xi_2} \tag{2.23}$$

Therefore, magnitudes of second fundamental form L, M and N in equation (2.17) can be rewritten as follows

$$L = -\mathbf{n} \cdot \mathbf{r}_{,\xi_1\xi_1}, \quad M = -\mathbf{n} \cdot \mathbf{r}_{,\xi_1\xi_2}, \quad N = -\mathbf{n} \cdot \mathbf{r}_{,\xi_2\xi_2} \tag{2.24}$$

Defining the normal curvature C_n of the surface $\mathcal{S}$, the reciprocal of normal curvature is called as radius of curvature $R_n = 1 / C_n$. Normal curvature C_n can be expressed in terms of first and second fundamental form as

$$C_n = \frac{L\left(d\xi_1\right)^2 + 2Md\xi_1 d\xi_2 + N\left(d\xi_2\right)^2}{E\left(d\xi_1\right)^2 + 2Fd\xi_1 d\xi_2 + G\left(d\xi_2\right)^2} \tag{2.25}$$

By setting the parametric curves (see Figure 2.1) as the lines of curvature, F value becomes 0 in equation (2.25) since parametric curves are orthogonal and also $M = 0$. Setting $d\xi_2 = 0$ (because along the ξ_1 curves, ξ_2 is constant), one can obtain

$$C_1 = \frac{L}{E} = \frac{1}{R_1} \tag{2.26}$$

and setting $d\xi_1 = 0$ (because along the ξ_2 curves, ξ_1 is constant), one can obtain

$$C_2 = \frac{N}{G} = \frac{1}{R_2} \tag{2.27}$$

where C_1 and C_2 are called as principle curvatures and reciprocals R_1 and R_2 are denoted as principle radii of curvature.

2.2. Definition of Super-elliptic Tube Cross-section

Super-elliptic shells have a cross-section formed with Lamé curves on which the set of all points (X, Y) satisfy following equation

$$\left|\frac{X}{a}\right|^n + \left|\frac{Y}{b}\right|^n = 1 \tag{2.28}$$

where a and b denote the semi-axes of the super-ellipse and a/b ratio is defined as the ellipticity of the cross-section. n is a positive number representing the ovality of the cross-section. A super-elliptic curve represents an ellipse in case of n=2 (in particular, a circle if a=b) and a hyper-ellipse for $n > 2$. Figure 2.2 shows that super-elliptic curve

evolves into a quasi-rectangular form as the value of n increases. Equation (2.28) can be defined parametrically as following

$$X(\theta) = R_0(\theta)\cos\theta \tag{2.29}$$

$$Y(\theta) = R_0(\theta)\sin\theta \tag{2.30}$$

where R_0 denotes the distance between the origin and a point on super-ellipse curve with θ angle from the X axis and can be written as

$$R_0(\theta) = \frac{ab}{(b^n|\cos\theta|^n + a^n|\sin\theta|^n)^{1/n}} \tag{2.31}$$

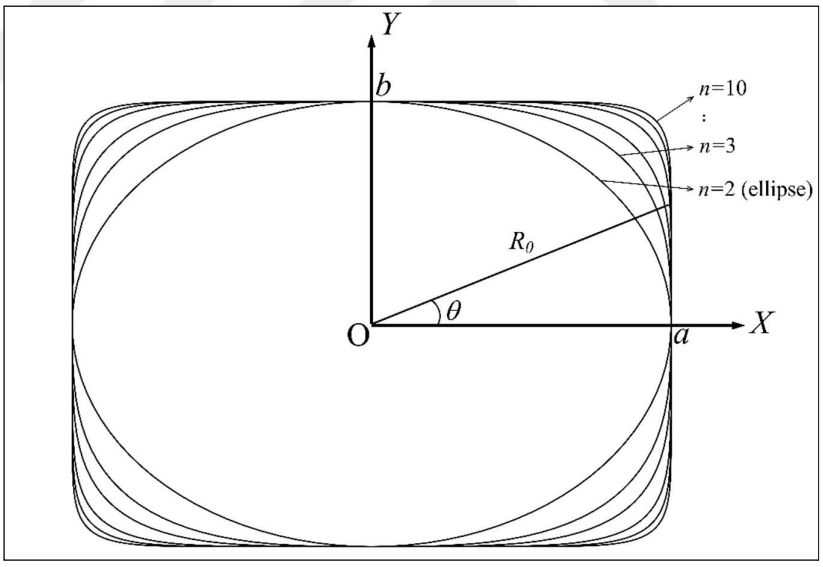

Figure 2.2**:** Representation of super-ellipse curves according to different ovality (*n*) values.

2.3. Strain-Displacement Relationship for Super-Elliptic Shell

Considering shell theory, an arbitrary point P' within the shell can be represented by a position vector **R**(x, y, z) as shown in Figure 2.3. Position vector **R**(x, y, z) can be expressed in terms of a position vector **r**(x, y) on the reference surface (middle surface)

and a normal vector $\mathbf{n}(x, y)$ defined by orthogonal curvilinear principal co-ordinates x, y. In Figure 2.3, *O'xyz* indicates the orthogonal curvilinear coordinate system on the shell reference surface and h is the thickness of the shell ($-h/2 \leq z \leq h/2$).

$$\mathbf{R}(x, y, z) = \mathbf{r}(x, y) + z\mathbf{n}(x, y) \tag{2.32}$$

Position vector for a general point in the super-ellipse formulation as shown in Figure 2.4 can be given as

$$\mathbf{r}(x, y = \theta) = \frac{ab\cos y}{(b^n|\cos y|^n + a^n|\sin y|^n)^{1/n}}\mathbf{i} + \frac{ab\sin y}{(b^n|\cos y|^n + a^n|\sin y|^n)^{1/n}}\mathbf{j} - x\mathbf{k} \tag{2.33}$$

where a and b denote the semi-axes of the super-ellipse, n is a positive number determining the ovality of the shell. **i, j** and **k** represent unit vectors of the global reference system *OXYZ*. Using the position vector in equation (2.33), cylindrical, elliptical and quasi-rectangular shell surfaces can be obtained. Position vector $\mathbf{r}(x, y)$ can be simplified as

$$\mathbf{r}(x, y) = r_X(x, y)\mathbf{i} + r_Y(x, y)\mathbf{j} + r_Z(x, y)\mathbf{k} \tag{2.34}$$

where r_X, r_Y, r_Z are the components of **r** in the global coordinate system *OXYZ*. The first and second order derivatives of the position vector **r** with respect to the x and y are

$$\mathbf{r}_{,x} = -\mathbf{k} \tag{2.35}$$

$$\mathbf{r}_{,y} = r_{X,y}\mathbf{i} + r_{Y,y}\mathbf{j} \tag{2.36}$$

$$\mathbf{r}_{,yy} = r_{X,yy}\mathbf{i} + r_{Y,yy}\mathbf{j} \tag{2.37}$$

$$\mathbf{r}_{,xx} = \mathbf{0} \tag{2.38}$$

$$\mathbf{r}_{,xy} = \mathbf{0} \tag{2.39}$$

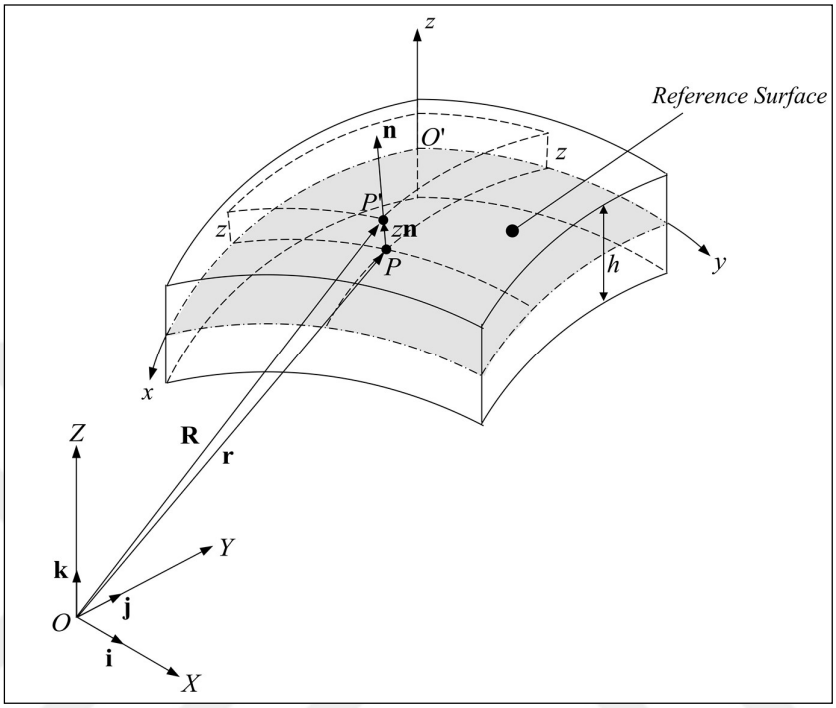

Figure 2.3**:** Position vector of a general point on shell surface.

Magnitudes of first fundamental form can be obtained using the equations (2.35-39)

$$E(x,y) = \mathbf{r}_{,x} \cdot \mathbf{r}_{,x} = 1 \tag{2.40}$$

$$F(x,y) = \mathbf{r}_{,x} \cdot \mathbf{r}_{,y} = 0 \tag{2.41}$$

$$G(x,y) = \mathbf{r}_{,y} \cdot \mathbf{r}_{,y} = r_{X,y}^2 + r_{Y,y}^2 \tag{2.42}$$

Defining the quantity

$$H(x,y) = \sqrt{EG - F^2} = \sqrt{r_{X,y}^2 + r_{Y,y}^2} \tag{2.43}$$

normal vector expression becomes

$$\mathbf{n}(x,y)=\frac{\mathbf{r}_{,x}\times\mathbf{r}_{,y}}{H}=\frac{1}{\sqrt{r_{X,y}^2+r_{Y,y}^2}}\left(-r_{X,y}\mathbf{j}+r_{Y,y}\mathbf{i}\right) \tag{2.44}$$

Magnitudes of second fundamental form are as follows

$$L(x,y)=-\mathbf{r}_{,xx}\cdot\mathbf{n}=0 \tag{2.45}$$

$$M(x,y)=-\mathbf{r}_{,xy}\cdot\mathbf{n}=0 \tag{2.46}$$

$$N(x,y)=-\mathbf{r}_{,yy}\cdot\mathbf{n}=\frac{1}{\sqrt{r_{X,y}^2+r_{Y,y}^2}}\left(r_{X,y}r_{Y,yy}-r_{Y,y}r_{X,yy}\right) \tag{2.47}$$

Using the magnitudes of first and second fundamental form principal radii of curvature can be obtained as

$$R_1=\frac{E}{L}=\infty \tag{2.48}$$

$$R_2=\frac{G}{N}=\frac{(r_{X,y}^2+r_{Y,y}^2)^{3/2}}{r_{X,y}r_{Y,yy}-r_{Y,y}r_{X,yy}} \tag{2.49}$$

and Lamé parameters are

$$A_1=\sqrt{E}=1 \tag{2.50}$$

$$A_2=\sqrt{G}=\sqrt{r_{X,y}^2+r_{Y,y}^2} \tag{2.51}$$

Since derivatives of r_X and r_Y expressions become complex and difficult, they are calculated numerically in this study.

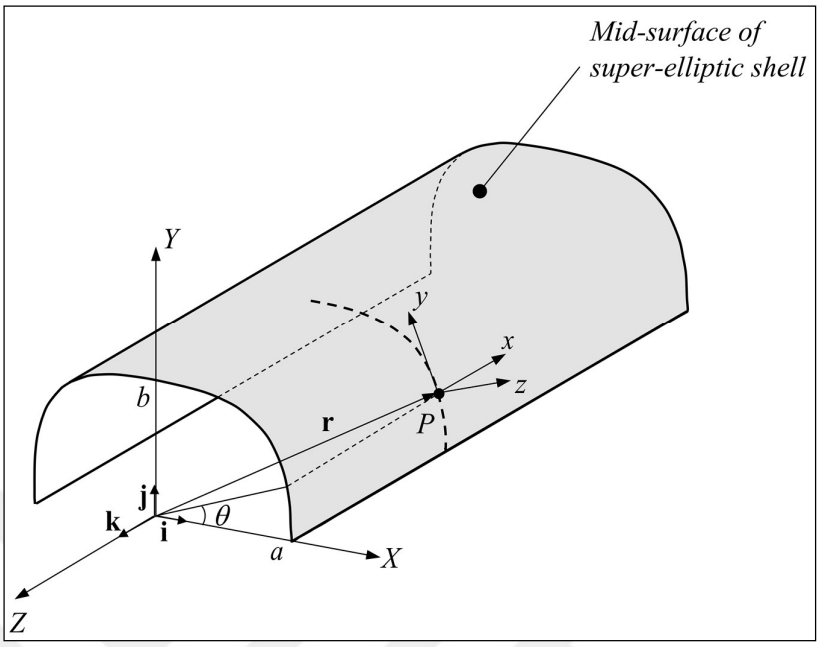

Figure 2.4**:** Representation of the super-elliptic shell.

Defining the infinitesimal change in position vector **R** as *d***R**, one can obtain using the equation (2.32),

$$d\mathbf{R} = d\mathbf{r} + zd\mathbf{n} + \mathbf{n}dz \tag{2.52}$$

and the magnitude of *d***R** can be expressed as

$$(ds)^2 = d\mathbf{R}d\mathbf{R} = A_1^2\left(1+\frac{z}{R_1}\right)^2(dx)^2 + A_2^2\left(1+\frac{z}{R_2}\right)^2(dy)^2 + (dz)^2 \tag{2.53}$$

Since $A_1 = 1$ and $R_1 = \infty$ for super-elliptic shells, equation (2.53) takes the form

$$(ds)^2 = d\mathbf{R}d\mathbf{R} = (dx)^2 + A_2^2\left(1+\frac{z}{R_2}\right)^2(dy)^2 + (dz)^2 \tag{2.54}$$

or

$$(ds)^2 = d\mathbf{R}d\mathbf{R} = g_{xx}(dx)^2 + g_{yy}(dy)^2 + g_{zz}(dz)^2 \tag{2.55}$$

where g_{ii} represents the metric coefficients, which can also be expressed as following

$$g_{xx} = h_x^2 \tag{2.56}$$

$$g_{yy} = h_y^2 \tag{2.57}$$

$$g_{zz} = h_z^2 \tag{2.58}$$

where h_i indicates the scale factors and for super-elliptic shells they are given as follows

$$h_x = 1 \tag{2.59}$$

$$h_y = A_2\left(1 + \frac{z}{R_2}\right) \tag{2.60}$$

$$h_z = 1 \tag{2.61}$$

Denoting **u** as the displacement vector of the arbitrary point P' in the shell medium, the deformed shell can be expressed in vectoral form as follows

$$\mathbf{R}^*(x,y,z) = \mathbf{R}(x,y,z) + \mathbf{u}(x,y,z) \tag{2.62}$$

and following expression can be obtained:

$$(ds^*)^2 - (ds)^2 = d\mathbf{R}^* d\mathbf{R}^* - d\mathbf{R}d\mathbf{R} = 2\lambda_{ij}dx_i dx_j \tag{2.63}$$

From the great book of [Saada, 1974], one can obtain the Green-Lagrange non-linear strain-displacement relationships using equation (2.63) and the scale factors as following

$$\varepsilon_{ij} = \frac{\lambda_{ij}}{h_i h_j} \tag{2.64}$$

where λ_{ij} are given as follows

$$\begin{aligned}\lambda_{xx} = h_x \frac{\partial u}{\partial x} + \frac{h_x v}{h_y}\frac{\partial h_x}{\partial y} + \frac{h_x w}{h_z}\frac{\partial h_x}{\partial z} + \frac{1}{2}\left(\frac{\partial u}{\partial x} + \frac{v}{h_y}\frac{\partial h_x}{\partial y} + \frac{w}{h_z}\frac{\partial h_x}{\partial z}\right)^2 \\ + \frac{1}{2}\left(\frac{\partial v}{\partial x} - \frac{u}{h_y}\frac{\partial h_x}{\partial y}\right)^2 + \frac{1}{2}\left(\frac{\partial w}{\partial x} - \frac{u}{h_z}\frac{\partial h_x}{\partial z}\right)^2\end{aligned} \tag{2.65}$$

$$\begin{aligned}\lambda_{yy} = h_y \frac{\partial v}{\partial y} + \frac{h_y w}{h_z}\frac{\partial h_y}{\partial z} + \frac{h_y u}{h_x}\frac{\partial h_y}{\partial x} + \frac{1}{2}\left(\frac{\partial v}{\partial y} + \frac{w}{h_z}\frac{\partial h_y}{\partial z} + \frac{u}{h_x}\frac{\partial h_y}{\partial x}\right)^2 \\ + \frac{1}{2}\left(\frac{\partial w}{\partial y} - \frac{v}{h_z}\frac{\partial h_y}{\partial z}\right)^2 + \frac{1}{2}\left(\frac{\partial u}{\partial y} - \frac{v}{h_x}\frac{\partial h_y}{\partial x}\right)^2\end{aligned} \tag{2.66}$$

$$\begin{aligned}\lambda_{xy} = \frac{1}{2}\left(h_x \frac{\partial u}{\partial y} + h_y \frac{\partial v}{\partial x} - v\frac{\partial h_y}{\partial x} - u\frac{\partial h_x}{\partial y}\right) \\ + \frac{1}{2}\left(\frac{\partial u}{\partial y} - \frac{v}{h_x}\frac{\partial h_y}{\partial x}\right)\left(\frac{\partial u}{\partial x} + \frac{v}{h_y}\frac{\partial h_x}{\partial y} + \frac{w}{h_z}\frac{\partial h_x}{\partial z}\right) \\ + \frac{1}{2}\left(\frac{\partial v}{\partial x} - \frac{u}{h_y}\frac{\partial h_x}{\partial y}\right)\left(\frac{\partial v}{\partial y} + \frac{u}{h_x}\frac{\partial h_y}{\partial x} + \frac{w}{h_z}\frac{\partial h_y}{\partial z}\right) \\ + \frac{1}{2}\left(\frac{\partial w}{\partial x} - \frac{u}{h_z}\frac{\partial h_x}{\partial z}\right)\left(\frac{\partial w}{\partial y} - \frac{v}{h_z}\frac{\partial h_y}{\partial z}\right)\end{aligned} \tag{2.67}$$

$$\lambda_{yz}=\frac{1}{2}\left(h_z\frac{\partial w}{\partial y}+h_y\frac{\partial v}{\partial z}-v\frac{\partial h_y}{\partial z}-w\frac{\partial h_z}{\partial y}\right)$$
$$+\frac{1}{2}\left(\frac{\partial v}{\partial z}-\frac{w}{h_y}\frac{\partial h_z}{\partial y}\right)\left(\frac{\partial v}{\partial y}+\frac{w}{h_z}\frac{\partial h_y}{\partial z}+\frac{u}{h_x}\frac{\partial h_y}{\partial x}\right)$$
$$+\frac{1}{2}\left(\frac{\partial w}{\partial y}-\frac{v}{h_z}\frac{\partial h_y}{\partial z}\right)\left(\frac{\partial w}{\partial z}+\frac{v}{h_y}\frac{\partial h_z}{\partial y}+\frac{u}{h_x}\frac{\partial h_z}{\partial x}\right)$$
$$+\frac{1}{2}\left(\frac{\partial u}{\partial y}-\frac{v}{h_x}\frac{\partial h_y}{\partial x}\right)\left(\frac{\partial u}{\partial z}-\frac{w}{h_x}\frac{\partial h_z}{\partial x}\right) \tag{2.68}$$

$$\lambda_{zx}=\frac{1}{2}\left(h_z\frac{\partial w}{\partial x}+h_x\frac{\partial u}{\partial z}-u\frac{\partial h_x}{\partial z}-w\frac{\partial h_z}{\partial x}\right)$$
$$+\frac{1}{2}\left(\frac{\partial u}{\partial z}-\frac{w}{h_x}\frac{\partial h_z}{\partial x}\right)\left(\frac{\partial u}{\partial x}+\frac{w}{h_z}\frac{\partial h_x}{\partial z}+\frac{v}{h_y}\frac{\partial h_x}{\partial y}\right)$$
$$+\frac{1}{2}\left(\frac{\partial w}{\partial x}-\frac{u}{h_z}\frac{\partial h_x}{\partial z}\right)\left(\frac{\partial w}{\partial z}+\frac{u}{h_x}\frac{\partial h_z}{\partial x}+\frac{v}{h_y}\frac{\partial h_z}{\partial y}\right)$$
$$+\frac{1}{2}\left(\frac{\partial v}{\partial x}-\frac{u}{h_y}\frac{\partial h_x}{\partial y}\right)\left(\frac{\partial v}{\partial z}-\frac{w}{h_y}\frac{\partial h_z}{\partial y}\right) \tag{2.69}$$

where u, v, w denote displacements along the orthogonal curvilinear principal co-ordinates x, y and z, respectively. By substituting scale factors in equations (2.59-61) into equation (2.64) and after rearrangement, Green-Lagrange strain-displacement relationships for the super-elliptic shell can be obtained as following

$$\varepsilon_x=\frac{\partial u}{\partial x}+\frac{1}{2}\left[\left(\frac{\partial u}{\partial x}\right)^2+\left(\frac{\partial v}{\partial x}\right)^2+\left(\frac{\partial w}{\partial x}\right)^2\right] \tag{2.70}$$

$$\varepsilon_y=\frac{1}{1+z/R_2}\left[\frac{1}{A_2}\frac{\partial v}{\partial y}+\frac{w}{R_2}\right]$$
$$+\frac{1}{2(1+z/R_2)^2}\left[\frac{1}{A_2^2}\left(\frac{\partial x}{\partial y}\right)^2+\left(\frac{1}{A_2}\frac{\partial v}{\partial y}+\frac{w}{R_2}\right)^2+\left(\frac{1}{A_2}\frac{\partial w}{\partial y}-\frac{v}{R_2}\right)^2\right] \tag{2.71}$$

$$\gamma_{xy} = \frac{1}{1+z/R_2}\left[\frac{1}{A_2}\frac{\partial u}{\partial y} + \left(1+z/R_2\right)\frac{\partial v}{\partial x}\right] + \frac{1}{1+z/R_2}\left[\frac{\partial v}{\partial x}\left(\frac{1}{A_2}\frac{\partial v}{\partial y} + \frac{w}{R_2}\right) + \frac{\partial w}{\partial x}\left(\frac{1}{A_2}\frac{\partial w}{\partial y} - \frac{v}{R_2}\right) + \frac{1}{A_2}\frac{\partial u}{\partial x}\frac{\partial u}{\partial y}\right] \tag{2.72}$$

$$\gamma_{yz} = \frac{1}{1+z/R_2}\left[\frac{1}{A_2}\frac{\partial w}{\partial y} + \left(1+z/R_2\right)\frac{\partial v}{\partial z} - \frac{v}{R_2}\right] + \frac{1}{1+z/R_2}\left(\frac{1}{A_2}\frac{\partial w}{\partial y}\frac{\partial w}{\partial z} - \frac{v}{R_2}\frac{\partial w}{\partial z} + \frac{1}{A_2}\frac{\partial v}{\partial y}\frac{\partial v}{\partial z} + \frac{w}{R_2}\frac{\partial v}{\partial z} + \frac{1}{A_2}\frac{\partial u}{\partial y}\frac{\partial u}{\partial z}\right) \tag{2.73}$$

$$\gamma_{zx} = \frac{\partial u}{\partial z} + \frac{\partial w}{\partial x} + \frac{\partial w}{\partial x}\frac{\partial w}{\partial z} + \frac{\partial u}{\partial x}\frac{\partial u}{\partial z} + \frac{\partial v}{\partial x}\frac{\partial v}{\partial z} \tag{2.74}$$

Based on first order shear deformation theory [Reddy, 2004a], displacements at a general point (x, y, z) at time t in a super-elliptic shell can be stated as

$$u(x,y,z,t) = u_0(x,y,t) + z\theta_x(x,y,t) \tag{2.75}$$

$$v(x,y,z,t) = v_0(x,y,t) + z\theta_y(x,y,t) \tag{2.76}$$

$$w(x,y,z,t) = w_0(x,y,t) \tag{2.77}$$

where u_0, v_0, w_0 are mid-plane displacements. θ_x and θ_y are the rotations about y and x axes respectively. By substituting displacements into equations (2.70-74) retaining full nonlinear terms in all degree of freedom parameters yields

$$\varepsilon_x = \frac{\partial u_0}{\partial x} + z\frac{\partial \theta_x}{\partial x} + \frac{1}{2}\left[\left(\frac{\partial u_0}{\partial x} + z\frac{\partial \theta_x}{\partial x}\right)^2 + \left(\frac{\partial v_0}{\partial x} + z\frac{\partial \theta_y}{\partial x}\right)^2 + \left(\frac{\partial w_0}{\partial x}\right)^2\right] \tag{2.78}$$

$$\varepsilon_y = \frac{1}{1+z/R_2}\left[\frac{1}{A_2}\left(\frac{\partial v_0}{\partial y}+z\frac{\partial \theta_y}{\partial y}\right)+\frac{w_0}{R_2}\right] + \frac{1}{2(1+z/R_2)^2}\left[\begin{array}{l}\frac{1}{A_2^2}\left(\frac{\partial u_0}{\partial y}+z\frac{\partial \theta_x}{\partial y}\right)^2+\left(\frac{1}{A_2}\frac{\partial v_0}{\partial y}+\frac{z}{A_2}\frac{\partial \theta_y}{\partial y}+\frac{w_0}{R_2}\right)^2 \\ +\left(\frac{1}{A_2}\frac{\partial w_0}{\partial y}-\frac{v_0}{R_2}-\frac{z}{R_2}\theta_y\right)^2\end{array}\right] \tag{2.79}$$

$$\gamma_{xy} = \frac{\partial v_0}{\partial x}+z\frac{\partial \theta_y}{\partial x}+\frac{1}{1+z/R_2}\left[\frac{1}{A_2}\frac{\partial u_0}{\partial y}+\frac{z}{A_2}\frac{\partial \theta_x}{\partial y}\right] + \frac{1}{1+z/R_2}\left[\begin{array}{l}\left(\frac{\partial v_0}{\partial x}+z\frac{\partial \theta_y}{\partial x}\right)\left(\frac{1}{A_2}\frac{\partial v_0}{\partial y}+\frac{z}{A_2}\frac{\partial \theta_y}{\partial y}+\frac{w_0}{R_2}\right) \\ +\frac{\partial w_0}{\partial x}\left(\frac{1}{A_2}\frac{\partial w_0}{\partial y}-\frac{v_0}{R_2}-\frac{z}{R_2}\theta_y\right) \\ +\frac{1}{A_2}\left(\frac{\partial u_0}{\partial x}+z\frac{\partial \theta_x}{\partial x}\right)\left(\frac{\partial u_0}{\partial y}+z\frac{\partial \theta_x}{\partial y}\right)\end{array}\right] \tag{2.80}$$

$$\gamma_{yz} = \theta_y+\frac{1}{1+z/R_2}\left[\frac{1}{A_2}\frac{\partial w_0}{\partial y}-\frac{v_0}{R_2}-\frac{z}{R_2}\theta_y\right] + \frac{1}{1+z/R_2}\left[\frac{\theta_y}{A_2}\left(\frac{\partial v_0}{\partial y}+z\frac{\partial \theta_y}{\partial y}\right)+\frac{w_0}{R_2}\theta_y+\frac{\theta_x}{A_2}\left(\frac{\partial u_0}{\partial y}+z\frac{\partial \theta_x}{\partial y}\right)\right] \tag{2.81}$$

$$\gamma_{zx} = \theta_x+\frac{\partial w_0}{\partial x}+\theta_x\left(\frac{\partial u_0}{\partial x}+z\frac{\partial \theta_x}{\partial x}\right)+\theta_y\left(\frac{\partial v_0}{\partial x}+z\frac{\partial \theta_y}{\partial x}\right) \tag{2.82}$$

By rearranging, equation (2.78-82) can be expressed in the following form

$$\varepsilon_x = \varepsilon_{x1}+z\varepsilon_{x2}+z^2\varepsilon_{x3} \tag{2.83}$$

$$\varepsilon_y = \frac{1}{1+z/R_2}\varepsilon_{y1}+\frac{z}{1+z/R_2}\varepsilon_{y2}+\frac{1}{2(1+z/R_2)^2}\varepsilon_{y3} + \frac{z}{2(1+z/R_2)^2}\varepsilon_{y4}+\frac{z^2}{2(1+z/R_2)^2}\varepsilon_{y5} \tag{2.84}$$

$$\gamma_{xy} = \gamma_{xy1} + z\gamma_{xy2} + \frac{1}{1+z/R_2}\gamma_{xy3} + \frac{z}{1+z/R_2}\gamma_{xy4} + \frac{z^2}{1+z/R_2}\gamma_{xy5} \tag{2.85}$$

$$\gamma_{yz} = \gamma_{yz1} + \frac{1}{1+z/R_2}\gamma_{yz2} + \frac{z}{1+z/R_2}\gamma_{yz3} \tag{2.86}$$

$$\gamma_{zx} = \gamma_{zx1} + z\gamma_{zx2} \tag{2.87}$$

where

$$\varepsilon_{x1} = \frac{\partial u_0}{\partial x} + \frac{1}{2}\left[\left(\frac{\partial u_0}{\partial x}\right)^2 + \left(\frac{\partial v_0}{\partial x}\right)^2 + \left(\frac{\partial w_0}{\partial x}\right)^2\right] \tag{2.88}$$

$$\varepsilon_{x2} = \frac{\partial \theta_x}{\partial x} + \frac{\partial u_0}{\partial x}\frac{\partial \theta_x}{\partial x} + \frac{\partial v_0}{\partial x}\frac{\partial \theta_y}{\partial x} \tag{2.89}$$

$$\varepsilon_{x3} = \frac{1}{2}\left[\left(\frac{\partial \theta_x}{\partial x}\right)^2 + \left(\frac{\partial \theta_y}{\partial x}\right)^2\right] \tag{2.90}$$

$$\varepsilon_{y1} = \frac{1}{A_2}\frac{\partial v_0}{\partial y} + \frac{w_0}{R_2} \tag{2.91}$$

$$\varepsilon_{y2} = \frac{1}{A_2}\frac{\partial \theta_y}{\partial y} \tag{2.92}$$

$$\varepsilon_{y3} = \frac{1}{A_2^2}\left(\frac{\partial u_0}{\partial y}\right)^2 + \left(\frac{1}{A_2}\frac{\partial v_0}{\partial y} + \frac{w_0}{R_2}\right)^2 + \left(\frac{1}{A_2}\frac{\partial w_0}{\partial y} - \frac{v_0}{R_2}\right)^2 \tag{2.93}$$

$$\varepsilon_{y4} = \frac{2}{A_2^2}\frac{\partial u_0}{\partial y}\frac{\partial \theta_x}{\partial y} + \frac{R_2}{A_2}\frac{\partial \theta_y}{\partial y}\left(\frac{2}{A_2 R_2}\frac{\partial v_0}{\partial y} + \frac{2}{R_2^2}w_0\right) + \theta_y\left(\frac{2}{R_2^2}v_0 - \frac{2}{A_2 R_2}\frac{\partial w_0}{\partial y}\right) \tag{2.94}$$

$$\varepsilon_{y5} = \frac{1}{A_2^2}\left(\left(\frac{\partial \theta_x}{\partial y}\right)^2 + \left(\frac{\partial \theta_y}{\partial y}\right)^2\right) + \left(\frac{\theta_y}{R_2}\right)^2 \tag{2.95}$$

$$\gamma_{xy1} = \frac{\partial v_0}{\partial x} \tag{2.96}$$

$$\gamma_{xy2} = \frac{\partial \theta_y}{\partial x} \tag{2.97}$$

$$\gamma_{xy3} = \frac{1}{A_2}\frac{\partial u_0}{\partial y}\left(1+\frac{\partial u_0}{\partial x}\right)+\frac{\partial v_0}{\partial x}\left(\frac{1}{A_2}\frac{\partial v_0}{\partial y}+\frac{w_0}{R_2}\right)+\frac{\partial w_0}{\partial x}\left(\frac{1}{A_2}\frac{\partial w_0}{\partial y}-\frac{v_0}{R_2}\right) \tag{2.98}$$

$$\begin{aligned}\gamma_{xy4} = {} & \frac{1}{A_2}\frac{\partial \theta_x}{\partial y}\left(1+\frac{\partial u_0}{\partial x}\right)+\frac{\partial \theta_y}{\partial x}\left(\frac{1}{A_2}\frac{\partial v_0}{\partial y}+\frac{w_0}{R_2}\right) \\ & +\frac{1}{A_2}\frac{\partial \theta_x}{\partial x}\frac{\partial u_0}{\partial y}+\frac{1}{A_2}\frac{\partial \theta_y}{\partial y}\frac{\partial v_0}{\partial x}-\frac{1}{R_2}\frac{\partial w_0}{\partial x}\theta_y\end{aligned} \tag{2.99}$$

$$\gamma_{xy5} = \frac{1}{A_2}\frac{\partial \theta_y}{\partial x}\frac{\partial \theta_y}{\partial y}+\frac{1}{A_2}\frac{\partial \theta_x}{\partial x}\frac{\partial \theta_x}{\partial y} \tag{2.100}$$

$$\gamma_{yz1} = \theta_y \tag{2.101}$$

$$\gamma_{yz2} = \frac{1}{A_2}\frac{\partial w_0}{\partial y}-\frac{v_0}{R_2}+\theta_y\left(\frac{1}{A_2}\frac{\partial v_0}{\partial y}+\frac{w_0}{R_2}\right)+\frac{1}{A_2}\frac{\partial u_0}{\partial y}\theta_x \tag{2.102}$$

$$\gamma_{yz3} = \theta_y\left(\frac{1}{A_2}\frac{\partial \theta_y}{\partial y}-\frac{1}{R_2}\right)+\frac{1}{A_2}\frac{\partial \theta_x}{\partial y}\theta_x \tag{2.103}$$

$$\gamma_{zx1} = \frac{\partial w_0}{\partial x}+\theta_x\left(1+\frac{\partial u_0}{\partial x}\right)+\theta_y\frac{\partial v_0}{\partial x} \tag{2.104}$$

$$\gamma_{zx2} = \theta_x\frac{\partial \theta_x}{\partial x}+\theta_y\frac{\partial \theta_y}{\partial x} \tag{2.105}$$

The strain-displacement equations given in equations (2.83-87), keeping terms including z^2 and expanding series as

$$\frac{1}{1+z/R_2} \cong 1-\frac{z}{R_2}+\frac{z^2}{R_2^2} \tag{2.106}$$

$$\frac{1}{2(1+z/R_2)^2} \cong \frac{1}{2}-\frac{z}{R_2}+\frac{3}{2}\frac{z^2}{R_2^2} \tag{2.107}$$

can be expressed in terms of membrane and transverse shear parts as following,

$$\begin{Bmatrix} \varepsilon_x \\ \varepsilon_y \\ \gamma_{xy} \end{Bmatrix} = \begin{Bmatrix} \varepsilon_x^{(0)} \\ \varepsilon_y^{(0)} \\ \gamma_{xy}^{(0)} \end{Bmatrix} + z\begin{Bmatrix} k_x^{(0)} \\ k_y^{(0)} \\ k_{xy}^{(0)} \end{Bmatrix} + z^2\begin{Bmatrix} k_x^{(1)} \\ k_y^{(1)} \\ k_{xy}^{(1)} \end{Bmatrix} + z^3\begin{Bmatrix} 0 \\ k_y^{(2)} \\ k_{xy}^{(2)} \end{Bmatrix} + z^4\begin{Bmatrix} 0 \\ k_y^{(3)} \\ k_{xy}^{(3)} \end{Bmatrix} \tag{2.108}$$

$$\begin{Bmatrix} \gamma_{yz} \\ \gamma_{zx} \end{Bmatrix} = \begin{Bmatrix} \gamma_{yz}^{(0)} \\ \gamma_{zx}^{(0)} \end{Bmatrix} + z\begin{Bmatrix} k_{yz}^{(0)} \\ k_{zx}^{(0)} \end{Bmatrix} + z^2\begin{Bmatrix} k_{yz}^{(1)} \\ 0 \end{Bmatrix} + z^3\begin{Bmatrix} k_{yz}^{(2)} \\ 0 \end{Bmatrix} \tag{2.109}$$

respectively. In equations (2.106) and (2.107), the error values due to the series expansion do not exceed % 0.2 and % 0.3 considering super-elliptic shell geometries investigated in this study, respectively. The terms in equations (2.108) and (2.109) can be stated as

$$\varepsilon_x^{(0)} = \varepsilon_{x1} \tag{2.110}$$

$$k_x^{(0)} = \varepsilon_{x2} \tag{2.111}$$

$$k_x^{(1)} = \varepsilon_{x3} \tag{2.112}$$

$$\varepsilon_y^{(0)} = \varepsilon_{y1} + \frac{1}{2}\varepsilon_{y3} \tag{2.113}$$

$$k_y^{(0)} = -\frac{\varepsilon_{y1}}{R_2} + \varepsilon_{y2} - \frac{\varepsilon_{y3}}{R_2} + \frac{\varepsilon_{y4}}{2} \tag{2.114}$$

$$k_y^{(1)} = \frac{1}{R_2}\left(\frac{\varepsilon_{y1}}{R_2} - \varepsilon_{y2} + \frac{3}{2}\frac{\varepsilon_{y3}}{R_2} - \varepsilon_{y4} + \frac{R_2}{2}\varepsilon_{y5}\right) \tag{2.115}$$

$$k_y^{(2)} = \frac{1}{R_2^2}\left(\varepsilon_{y2} - \frac{3}{2}\varepsilon_{y4} - R_2\varepsilon_{y5}\right) \tag{2.116}$$

$$k_y^{(3)} = \frac{3}{2}\frac{\varepsilon_{y5}}{R_2^2} \tag{2.117}$$

$$\gamma_{xy}^{(0)} = \gamma_{xy1} + \gamma_{xy3} \tag{2.118}$$

$$k_{xy}^{(0)} = \gamma_{xy2} - \frac{\gamma_{xy3}}{R_2} + \gamma_{xy4} \tag{2.119}$$

$$\gamma_{xy3} = \frac{1}{A_2}\frac{\partial u_0}{\partial y}\left(1 + \frac{\partial u_0}{\partial x}\right) + \frac{\partial v_0}{\partial x}\left(\frac{1}{A_2}\frac{\partial v_0}{\partial y} + \frac{w_0}{R_2}\right) + \frac{\partial w_0}{\partial x}\left(\frac{1}{A_2}\frac{\partial w_0}{\partial y} - \frac{v_0}{R_2}\right) \tag{2.120}$$

$$k_{xy}^{(1)} = \frac{1}{R_2}\left(\frac{\gamma_{xy3}}{R_2} - \gamma_{xy4} + R_2\gamma_{xy5}\right) \tag{2.121}$$

$$k_{xy}^{(2)} = \frac{1}{R_2^2}\left(\gamma_{xy4} - R_2\gamma_{xy5}\right) \tag{2.122}$$

$$k_{xy}^{(3)} = \frac{\gamma_{xy5}}{R_2^2} \tag{2.123}$$

$$\gamma_{yz}^{(0)} = \gamma_{yz1} + \gamma_{yz2} \tag{2.124}$$

$$k_{yz}^{(0)} = -\frac{\gamma_{yz2}}{R_2} + \gamma_{yz3} \tag{2.125}$$

$$k_{yz}^{(1)} = \frac{1}{R_2}\left(\frac{\gamma_{yz2}}{R_2} - \gamma_{yz3}\right) \tag{2.126}$$

$$k_{yz}^{(2)} = \frac{\gamma_{yz3}}{R_2^2} \tag{2.127}$$

$$k_{yz}^{(3)} = -\frac{\gamma_{yz3}}{R_2^3} \tag{2.128}$$

$$\gamma_{zx}^{(0)} = \gamma_{zx1} \tag{2.129}$$

$$k_{zx}^{(0)} = \gamma_{zx2} \tag{2.130}$$

Equations (2.108) and (2.109) can be expressed in series form of z as:

$$\boldsymbol{\varepsilon}_{\mathbf{b}} = \boldsymbol{\varepsilon}_{\mathbf{0}} + z\boldsymbol{\varepsilon}_{\mathbf{1}} + z^2\boldsymbol{\varepsilon}_{\mathbf{2}} + z^3\boldsymbol{\varepsilon}_{\mathbf{3}} + z^4\boldsymbol{\varepsilon}_{\mathbf{4}} \tag{2.131}$$

$$\boldsymbol{\varepsilon}_{\mathbf{s}} = \boldsymbol{\varepsilon}_{\mathbf{s0}} + z\boldsymbol{\varepsilon}_{\mathbf{s1}} + z^2\boldsymbol{\varepsilon}_{\mathbf{s2}} + z^3\boldsymbol{\varepsilon}_{\mathbf{s3}} \tag{2.132}$$

where $\boldsymbol{\varepsilon}_{\mathbf{b}}$ and $\boldsymbol{\varepsilon}_{\mathbf{s}}$ are in-plane and transverse shear strains, respectively.

2.4. Constitutive Equations and Equation of Motion

Within the scope of this thesis, two material models such that orthotropic composite and functionally graded material (FGM) models are considered in the analysis of super-elliptic shell structures. In the following sections, constitutive equations for orthotropic composite and FGM material models are explained in detail.

2.4.1. Super-Elliptic Shells Made of Laminated Composite Materials

The constitutive equation for a laminated super-elliptic composite shell can be written in terms of in-plane force and moment resultants as

$$\mathbf{N}=\begin{Bmatrix}\mathbf{N_1}\\ \mathbf{N_2}\\ \mathbf{N_3}\\ \mathbf{N_4}\\ \mathbf{N_5}\end{Bmatrix}=\begin{bmatrix}\mathbf{A} & \mathbf{B} & \mathbf{C} & \mathbf{D} & \mathbf{E}\\ \mathbf{B} & \mathbf{C} & \mathbf{D} & \mathbf{E} & \mathbf{F}\\ \mathbf{C} & \mathbf{D} & \mathbf{E} & \mathbf{F} & \mathbf{G}\\ \mathbf{D} & \mathbf{E} & \mathbf{F} & \mathbf{G} & \mathbf{H}\\ \mathbf{E} & \mathbf{F} & \mathbf{G} & \mathbf{H} & \mathbf{I}\end{bmatrix}\begin{Bmatrix}\boldsymbol{\varepsilon_0}\\ \boldsymbol{\varepsilon_1}\\ \boldsymbol{\varepsilon_2}\\ \boldsymbol{\varepsilon_3}\\ \boldsymbol{\varepsilon_4}\end{Bmatrix} \tag{2.133}$$

where

$$\mathbf{N_1}=\begin{Bmatrix}N_{x1}\\ N_{y1}\\ N_{xy1}\end{Bmatrix},\quad \mathbf{N_2}=\begin{Bmatrix}N_{x2}\\ N_{y2}\\ N_{xy2}\end{Bmatrix},\quad \mathbf{N_3}=\begin{Bmatrix}N_{x3}\\ N_{y3}\\ N_{xy3}\end{Bmatrix},\quad \mathbf{N_4}=\begin{Bmatrix}N_{x4}\\ N_{y4}\\ N_{xy4}\end{Bmatrix},\quad \mathbf{N_5}=\begin{Bmatrix}N_{x5}\\ N_{y5}\\ N_{xy5}\end{Bmatrix} \tag{2.134}$$

and

$$\mathbf{A}=\begin{bmatrix}A_{11} & A_{12} & A_{16}\\ A_{21} & A_{22} & A_{26}\\ A_{61} & A_{62} & A_{66}\end{bmatrix},\quad \mathbf{B}=\begin{bmatrix}B_{11} & B_{12} & B_{16}\\ B_{21} & B_{22} & B_{26}\\ B_{61} & B_{62} & B_{66}\end{bmatrix},\quad \mathbf{C}=\begin{bmatrix}C_{11} & C_{12} & C_{16}\\ C_{21} & C_{22} & C_{26}\\ C_{61} & C_{62} & C_{66}\end{bmatrix}$$

$$\mathbf{D}=\begin{bmatrix}D_{11} & D_{12} & D_{16}\\ D_{21} & D_{22} & D_{26}\\ D_{61} & D_{62} & D_{66}\end{bmatrix},\quad \mathbf{E}=\begin{bmatrix}E_{11} & E_{12} & E_{16}\\ E_{21} & E_{22} & E_{26}\\ E_{61} & E_{62} & E_{66}\end{bmatrix},\quad \mathbf{F}=\begin{bmatrix}F_{11} & F_{12} & F_{16}\\ F_{21} & F_{22} & F_{26}\\ F_{61} & F_{62} & F_{66}\end{bmatrix} \tag{2.135}$$

$$\mathbf{G}=\begin{bmatrix}G_{11} & G_{12} & G_{16}\\ G_{21} & G_{22} & G_{26}\\ G_{61} & G_{62} & G_{66}\end{bmatrix},\quad \mathbf{H}=\begin{bmatrix}H_{11} & H_{12} & H_{16}\\ H_{21} & H_{22} & H_{26}\\ H_{61} & H_{62} & H_{66}\end{bmatrix},\quad \mathbf{I}=\begin{bmatrix}I_{11} & I_{12} & I_{16}\\ I_{21} & I_{22} & I_{26}\\ I_{61} & I_{62} & I_{66}\end{bmatrix}$$

For transverse shear, constitutive equation can be stated in terms of shear force resultant as

$$\mathbf{Q}=\begin{Bmatrix}\mathbf{Q_1}\\ \mathbf{Q_2}\\ \mathbf{Q_3}\\ \mathbf{Q_4}\end{Bmatrix}=\begin{bmatrix}\mathbf{A_s} & \mathbf{B_s} & \mathbf{C_s} & \mathbf{D_s}\\ \mathbf{B_s} & \mathbf{C_s} & \mathbf{D_s} & \mathbf{E_s}\\ \mathbf{C_s} & \mathbf{D_s} & \mathbf{E_s} & \mathbf{F_s}\\ \mathbf{D_s} & \mathbf{E_s} & \mathbf{F_s} & \mathbf{G_s}\end{bmatrix}\begin{Bmatrix}\boldsymbol{\varepsilon}_{\mathbf{s0}}\\ \boldsymbol{\varepsilon}_{\mathbf{s1}}\\ \boldsymbol{\varepsilon}_{\mathbf{s2}}\\ \boldsymbol{\varepsilon}_{\mathbf{s3}}\end{Bmatrix} \tag{2.136}$$

where

$$\mathbf{Q_1}=\begin{Bmatrix}Q_{yz1}\\ Q_{zx1}\end{Bmatrix},\ \mathbf{Q_2}=\begin{Bmatrix}Q_{yz2}\\ Q_{zx2}\end{Bmatrix},\ \mathbf{Q_3}=\begin{Bmatrix}Q_{yz3}\\ Q_{zx3}\end{Bmatrix},\ \mathbf{Q_4}=\begin{Bmatrix}Q_{yz4}\\ Q_{zx4}\end{Bmatrix} \tag{2.137}$$

and

$$\begin{gathered}\mathbf{A}_s=\begin{bmatrix}A_{44} & A_{45}\\ A_{45} & A_{55}\end{bmatrix},\ \mathbf{B}_s=\begin{bmatrix}B_{44} & B_{45}\\ B_{45} & B_{55}\end{bmatrix},\ \mathbf{C}_s=\begin{bmatrix}C_{44} & C_{45}\\ C_{45} & C_{55}\end{bmatrix}\\ \mathbf{D}_s=\begin{bmatrix}D_{44} & D_{45}\\ D_{45} & D_{55}\end{bmatrix},\ \mathbf{E}_s=\begin{bmatrix}E_{44} & E_{45}\\ E_{45} & E_{55}\end{bmatrix},\ \mathbf{F}_s=\begin{bmatrix}F_{44} & F_{45}\\ F_{45} & F_{55}\end{bmatrix},\ \mathbf{G}_s=\begin{bmatrix}G_{44} & G_{45}\\ G_{45} & G_{55}\end{bmatrix}\end{gathered} \tag{2.138}$$

A_{ij}, B_{ij}, C_{ij}, D_{ij}, E_{ij}, F_{ij}, G_{ij}, H_{ij} and I_{ij} are laminate stiffness coefficients representing in-plane, bending-stretching coupling, bending and transverse shear stiffnesses. They are obtained as below:

$$\begin{gathered}\left\{A_{ij},B_{ij},C_{ij},D_{ij},E_{ij},F_{ij},G_{ij},H_{ij},I_{ij}\right\}\\ =\sum_{k=1}^{n}\int_{z_{k-1}}^{z_k}\left\{1,z,z^2,z^3,z^4,z^5,z^6,z^7,z^8\right\}\bar{Q}_{ij}^{(k)}A_2(1+z/R_2)dz\ \ (i,j=1,2,6)\end{gathered} \tag{2.139}$$

$$\begin{gathered}\left\{A_{ij},B_{ij},C_{ij},D_{ij},E_{ij},F_{ij},G_{ij}\right\}\\ =\sum_{k=1}^{n}k_ik_j\int_{z_{k-1}}^{z_k}\left\{1,z,z^2,z^3,z^4,z^5,z^6\right\}\bar{Q}_{ij}^{(k)}A_2(1+z/R_2)dz\ \ (i,j=4,5)\end{gathered} \tag{2.140}$$

where $k_i^2 = 5/6$ ($i = 4, 5$) are the shear correction factors according to the first order shear deformation theory [Reddy, 2003]. $\overline{Q}_{ij}^{(k)}$ are transformed stiffness coefficients of k-th layer. Detailed expressions of laminate stiffness coefficients are given in Appendix B.

Laminate mass inertias are expressed as

$$\{I_0, I_1, I_2\} = \sum_{k=1}^{n} \int_{z_{k-1}}^{z_k} \{1, z, z^2\} \, \rho^{(k)} A_2 (1 + z / R_2) dz \tag{2.141}$$

where $\rho^{(k)}$ denotes density of the k-th layer.

Equation of motion for super-elliptic laminated composite shells can be obtained using the dynamic adaptation of the virtual work principle. In this context, the sum of virtual works of internal and inertia forces is equal to the virtual work of external forces. For the super-elliptic laminated composite shells, equation of motion (without damping) can be expressed as

$$\begin{aligned} &\sum_{k=1}^{n} \int_{z_{k-1}}^{z_k} [\int_{\Omega} \{\sigma_x^{(k)} \delta\varepsilon_x + \sigma_y^{(k)} \delta\varepsilon_y + \tau_{xy}^{(k)} \delta\gamma_{xy} + \tau_{yz}^{(k)} \delta\gamma_{yz} + \tau_{zx}^{(k)} \delta\gamma_{zx} \\ &+ \rho^{(k)} \begin{bmatrix} \left(\ddot{u}_0 + z \ddot{\theta}_x \right) \left(\delta u_0 + z \delta\theta_x \right) \\ + \left(\ddot{v}_0 + z \ddot{\theta}_y \right) \left(\delta v_0 + z \delta\theta_y \right) + \ddot{w}_0 \, \delta w_0 \end{bmatrix} \} dxdy] A_2 (1 + z / R_2) dz \\ &= \int_{\Omega} q \delta w_0 A_2 (1 + z / R_2) dxdy \end{aligned} \tag{2.142}$$

where the sum of virtual work of internal forces stemmed from stresses and virtual work of inertia forces stemmed from accelerations is seen on the left-hand side and virtual work of external forces stemmed from distributed load is seen on the right-hand side. In equation (2.142) stresses correspond to 2nd Piola-Kirchhoff stresses. It is assumed as distributed load q is applied on the middle surface of the shell (z=0). Considering this assumption, equation (2.142) can be expressed regarding force and moment resultants and mass inertias as following

$$\int_{\Omega}[\boldsymbol{\delta\varepsilon}_0^{\mathrm{T}}\mathbf{N}_1+\boldsymbol{\delta\varepsilon}_1^{\mathrm{T}}\mathbf{N}_2+\boldsymbol{\delta\varepsilon}_2^{\mathrm{T}}\mathbf{N}_3+\boldsymbol{\delta\varepsilon}_3^{\mathrm{T}}\mathbf{N}_4+\boldsymbol{\delta\varepsilon}_4^{\mathrm{T}}\mathbf{N}_5+\boldsymbol{\delta\varepsilon}_{s0}^{\mathrm{T}}\mathbf{Q}_1+\boldsymbol{\delta\varepsilon}_{s1}^{\mathrm{T}}\mathbf{Q}_2+\boldsymbol{\delta\varepsilon}_{s2}^{\mathrm{T}}\mathbf{Q}_3+\boldsymbol{\delta\varepsilon}_{s3}^{\mathrm{T}}\mathbf{Q}_4$$

$$+(I_0\ddot{u}_0+I_1\ddot{\theta}_x)\delta u_0+(I_0\ddot{v}_0+I_1\ddot{\theta}_y)\delta v_0+I_1\ddot{w}_0\,\delta w_0+(I_1\ddot{u}_0+I_2\ddot{\theta}_x)\delta\theta_x \tag{2.143}$$

$$+(I_1\ddot{v}_0+I_2\ddot{\theta}_y)\delta\theta_y]dxdy=\int_{\Omega}q\delta w_0A_2dxdy$$

2.4.2. Super-Elliptic Shells Made of FGMs

Constitutive equation of a super-elliptic shell made of functionally graded material can be expressed in terms of in-plane force, in-plane moment and shear force resultants as the same given in equations (2.133-138). However, stiffness coefficients (A_{ij}, B_{ij}, C_{ij}, D_{ij}, E_{ij}, F_{ij}, G_{ij}, H_{ij} and I_{ij}) of a FGM super-elliptic shell are expressed as below

$$\left\{A_{ij},B_{ij},C_{ij},D_{ij},E_{ij},F_{ij},G_{ij},H_{ij},I_{ij}\right\}$$
$$=\int_{-h/2}^{h/2}\left\{1,z,z^2,z^3,z^4,z^5,z^6,z^7,z^8\right\}Q_{ij}(z)A_2(1+z/R_2)dz\quad(i,j=1,2,6) \tag{2.144}$$

$$\left\{A_{ij},B_{ij},C_{ij},D_{ij},E_{ij},F_{ij},G_{ij}\right\}$$
$$=k_ik_j\int_{-h/2}^{h/2}\left\{1,z,z^2,z^3,z^4,z^5,z^6\right\}Q_{ij}(z)A_2(1+z/R_2)dz\quad(i,j=4,5) \tag{2.145}$$

where k_i^2 = 5/6 (i = 4, 5) denote shear correction factors. $Q_{ij}(z)$ denote stiffness coefficients of FGM material and can be stated as following:

$$Q_{11}=\frac{E(z)}{1-\nu^2(z)} \tag{2.146}$$

$$Q_{22}=\frac{E(z)}{1-\nu^2(z)} \tag{2.147}$$

$$Q_{12} = \frac{\nu(z)E(z)}{1-\nu^2(z)} \tag{2.148}$$

$$Q_{44} = Q_{55} = Q_{66} = G(z) \tag{2.149}$$

where $\nu(z)$, $E(z)$ and $G(z)$ denote Poisson's ratio, elastic modulus and shear modulus of FGM, respectively. Material specifications of FGMs continuously change throughout the thickness direction of the structure. Considering a functionally graded super-elliptic shell, Poisson's ratio ν, elastic modulus E and density ρ can be expressed using a power law distribution function as following

$$\nu(z) = \left(\nu_T - \nu_B\right)\left(\frac{z}{h} + \frac{1}{2}\right)^k + \nu_B \tag{2.150}$$

$$E(z) = \left(E_T - E_B\right)\left(\frac{z}{h} + \frac{1}{2}\right)^k + E_B \tag{2.151}$$

$$\rho(z) = \left(\rho_T - \rho_B\right)\left(\frac{z}{h} + \frac{1}{2}\right)^k + \rho_B \tag{2.152}$$

where k denotes the volume fraction exponent of FGM, and h is the shell thickness. Sub-indices B and T denote material specifications at the bottom and top surfaces of super-elliptic shell, respectively. In this study, bottom and top surface material is considered as metal and ceramic, respectively. If volume fraction exponent k is equal to 0, then shell material corresponds to fully ceramic. Using equations (2.150) and (2.151) shear modulus $G(z)$ can be stated as

$$G(z) = \frac{E(z)}{2(1+\nu(z))} \tag{2.153}$$

Mass inertias for FGM super-elliptic shell can be stated as

$$\{I_0, I_1, I_2\} = \int_{-h/2}^{h/2} \{1, z, z^2\} \rho(z) A_2 (1 + z / R_2) dz \tag{2.154}$$

where $\rho(z)$ indicates density of the FGM.

For FGM super-elliptic shells, equation of motion can be stated as following

$$\begin{aligned} &\int_{-h/2}^{h/2} [\int_{\Omega} \{\sigma_x \delta\varepsilon_x + \sigma_y \delta\varepsilon_y + \tau_{xy} \delta\gamma_{xy} + \tau_{yz} \delta\gamma_{yz} + \tau_{xz} \delta\gamma_{zx} \\ &+ \rho(z) \begin{bmatrix} \left(\ddot{u}_0 + z \ddot{\theta}_x \right) \left(\delta u_0 + z \delta\theta_x \right) \\ + \left(\ddot{v}_0 + z \ddot{\theta}_y \right) \left(\delta v_0 + z \delta\theta_y \right) + \ddot{w}_0 \, \delta w_0 \end{bmatrix} \} dxdy] \\ &\times A_2 (1 + z / R_2) dz = \int_{\Omega} q \delta w_0 A_2 (1 + z / R_2) dxdy \end{aligned} \tag{2.155}$$

Left-hand side of equation (2.155) demonstrates the virtual work summation of internal forces owing to stresses and inertia forces owing to accelerations. Right-hand side demonstrates virtual work of external forces owing to distributed load. Similarly, in equation (2.155) stresses correspond to 2nd Piola-Kirchhoff stresses. Considering distributed load (q) is applied upon the mid-surface (z=0), equation (2.155) can be stated regarding force, moment and shear resultants and mass inertias as follows

$$\begin{aligned} &\int_{\Omega} [\boldsymbol{\delta\varepsilon}_0^{\mathrm{T}} \mathbf{N}_1 + \boldsymbol{\delta\varepsilon}_1^{\mathrm{T}} \mathbf{N}_2 + \boldsymbol{\delta\varepsilon}_2^{\mathrm{T}} \mathbf{N}_3 + \boldsymbol{\delta\varepsilon}_3^{\mathrm{T}} \mathbf{N}_4 + \boldsymbol{\delta\varepsilon}_4^{\mathrm{T}} \mathbf{N}_5 + \boldsymbol{\delta\varepsilon}_{s0}^{\mathrm{T}} \mathbf{Q}_1 \\ &+ \boldsymbol{\delta\varepsilon}_{s1}^{\mathrm{T}} \mathbf{Q}_2 + \boldsymbol{\delta\varepsilon}_{s2}^{\mathrm{T}} \mathbf{Q}_3 + \boldsymbol{\delta\varepsilon}_{s3}^{\mathrm{T}} \mathbf{Q}_4 \\ &+ (I_0 \ddot{u}_0 + I_1 \ddot{\theta}_x) \delta u_0 + (I_0 \ddot{v}_0 + I_1 \ddot{\theta}_y) \delta v_0 + I_0 \ddot{w}_0 \, \delta w_0 + (I_1 \ddot{u}_0 + I_2 \ddot{\theta}_x) \delta\theta_x \\ &+ (I_1 \ddot{v}_0 + I_2 \ddot{\theta}_y) \delta\theta_y] dxdy = \int_{\Omega} q \delta w_0 A_2 dxdy \end{aligned} \tag{2.156}$$

3. SOLUTION PROCEDURE

In the thesis, generalized differential quadrature (GDQ) method is utilized in the calculation of spatial derivatives. Constant-average acceleration adaptation of Newmark implicit method and Newton-Raphson method are applied to solve equation of motion. Before the solution of the system, a geometric mapping process is applied. In the following sections, these methods are explained in detail.

3.1. Geometric Mapping

When the domain of the shell is irregular, integral terms in the virtual work equation are usually calculated using numerical methods such as Gauss quadrature or Gauss-Lobatto quadrature rules. As shown in Figure 3.1, in numerical integral calculations, cartesian domain is often transformed into a bi-unit square domain by geometric mapping as

$$x(\xi,\eta) = \sum S_k(\xi,\eta) x_k \qquad -1 \le \xi \le 1 \tag{3.1}$$

$$y(\xi,\eta) = \sum S_k(\xi,\eta) y_k \qquad -1 \le \eta \le 1 \tag{3.2}$$

where $S_k(\xi, \eta)$ denote interpolation functions that is utilized in geometric mapping process and ξ, η denote natural coordinates of bi-unit square domain. The interpolation functions can both be found in finite element books and are as follows

$$S_1 = \frac{1}{4}(1-\xi)(1-\eta) \tag{3.3}$$

$$S_2 = \frac{1}{4}(1+\xi)(1-\eta) \tag{3.4}$$

$$S_3 = \frac{1}{4}(1+\xi)(1+\eta) \tag{3.5}$$

$$S_4 = \frac{1}{4}(1-\xi)(1+\eta) \tag{3.6}$$

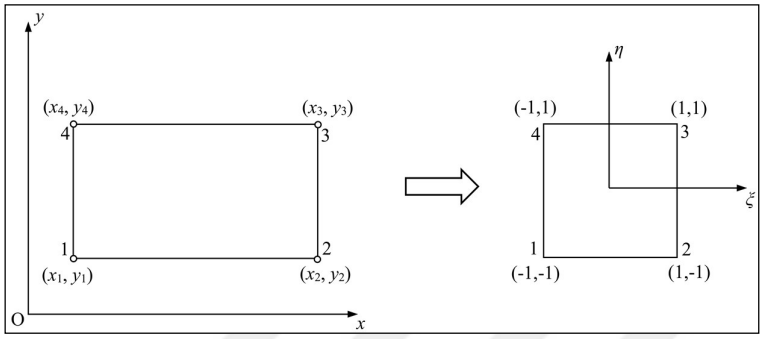

Figure 3.1**:** Geometric mapping process (transformation from Cartesian to natural coordinates).

Spatial derivatives of a function *f*(*x*,*y*) in cartesian domain can be expressed in terms of natural coordinates as below:

$$\frac{\partial f}{\partial x} = \frac{1}{J}\left(\frac{\partial y}{\partial \eta}\frac{\partial f}{\partial \xi} - \frac{\partial y}{\partial \xi}\frac{\partial f}{\partial \eta}\right) \tag{3.7}$$

$$\frac{\partial f}{\partial y} = \frac{1}{J}\left(\frac{\partial x}{\partial \xi}\frac{\partial f}{\partial \eta} - \frac{\partial x}{\partial \eta}\frac{\partial f}{\partial \xi}\right) \tag{3.8}$$

where *J* indicates the determinant of the Jacobian and given as following

$$J = \frac{\partial x}{\partial \xi}\frac{\partial y}{\partial \eta} - \frac{\partial y}{\partial \xi}\frac{\partial x}{\partial \eta} \tag{3.9}$$

3.2. Generalized Differential Quadrature (GDQ) Method

In early 1970s, [Bellman and Casti, 1971], [Bellman et al., 1972] proposed an efficient numerical method called differential quadrature method (DQM). They extended well-known integral quadrature method for the derivative calculation of a function [Tornabene and Bacciocchi, 2018]. The advantage of this method is to obtain

accurate results using less grid points than the well-known finite element method [Tornabene and Bacciocchi, 2018]. However, first applications of DQM allows the use of a limited number of grids and it is not appropriate to calculate higher order derivatives. The key point of DQM is the evaluation of weighting coefficients as in integral quadrature method. In DQM, weighting coefficients are calculated by solving an algebraic system of equations which becomes ill-conditioned in case of using more than 13 grid points. However, DQM was used most in calculation of first order derivatives, since it allows to choose the grid points arbitrarily. Then, an improved version of DQM was proposed by Bellman and his colleagues. In this version, weighting coefficients are calculated without solving an algebraic system of equations. But, the distribution of grid points is restricted to the roots of the shifted Legendre polynomials.

Later, [Shu, 2000] suggested a new technique which is the improved form of DQM called generalized differential quadrature (GDQ) method. The advantage of GDQ method to DQM is that it is appropriate for arbitrary number and distribution of grid points. In addition, higher order derivatives can easily be calculated by using recursive formulations. Followings are the details of GDQ method.

Spatial derivatives of field variables existing in the equation of motion are calculated using GDQ method. Discretization of shell domain with grid points is shown in Figure 3.2. In GDQ method, r-th order derivative of a function $f(\xi)$ at a discrete point can be stated via linear weighted summation of the function values at each grid point in the domain [Kurtaran, 2015a] and can be written as following

$$\left(\frac{\partial f^r(x)}{\partial \xi^r} \right)_{\xi_i} = \sum_{j=1}^{n} \overline{C}_{ij}^{(r)} f_j \tag{3.10}$$

where n and ξ_i denote total number of grid points and corresponding discrete points, respectively. f_j are the function values at grid points and $\overline{C}_{ij}^{(r)}$ are the weighting coefficients which are determined using Lagrange polynomial functions. Considering first-order derivative ($r = 1$), weight coefficients can be expressed as following

$$\bar{C}_{ij}^{(1)} = \frac{\Psi(\xi_i)}{(\xi_i - \xi_j)\Psi(\xi_j)} \qquad (i \neq j) \tag{3.11}$$

where

$$\Psi(\xi_i) = \prod_{j=1}^{n} (\xi_i - \xi_j) \qquad (i \neq j) \tag{3.12}$$

Higher-order derivatives can be calculated using recursive relations given below:

$$\bar{C}_{ij}^{(r)} = r\left[\bar{C}_{ii}^{(r-1)}\bar{C}_{ij}^{(1)} - \frac{\bar{C}_{ij}^{(r-1)}}{(\xi_i - \xi_j)}\right] \qquad (i \neq j) \tag{3.13}$$

$$\bar{C}_{ii}^{(r)} = -\sum_{\substack{j=1 \\ i \neq j}}^{n} \bar{C}_{ij}^{(r)} \tag{3.14}$$

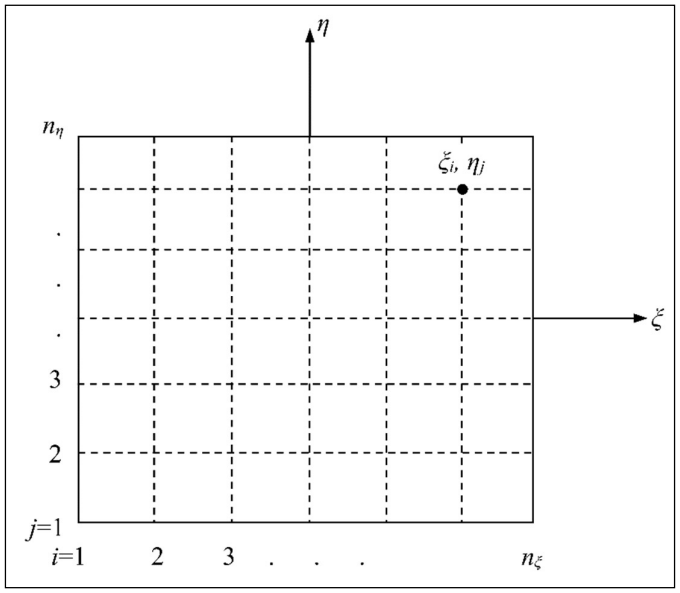

Figure 3.2**:** Discretized shell domain in natural coordinate system.

Partial derivatives can be calculated with GDQ method by extending one dimensional derivatives into two-dimensional case. Partial derivatives at an arbitrary grid point (ξ_i, η_j) on a discretized domain (Figure 3.2) can be calculated as following

$$\left(\frac{\partial f^r(\xi,\eta)}{\partial \xi^r}\right)_{\xi_i,\eta_j} = \sum_{k=1}^{n_x} \bar{C}_{ik}^{(r)} f_{kj} \tag{3.15}$$

$$\left(\frac{\partial f^s(\xi,\eta)}{\partial \eta^s}\right)_{\xi_i,\eta_j} = \sum_{m=1}^{n_y} \bar{C}_{jm}^{(s)} f_{im} \tag{3.16}$$

$$\left(\frac{\partial f^{(r+s)}(\xi,\eta)}{\partial \xi^r \partial \eta^s}\right)_{\xi_i,y_j} = \frac{\partial^r}{\partial \xi^r}\left(\frac{\partial^s f}{\partial \eta^s}\right) = \sum_{k=1}^{n_x} \bar{C}_{ik}^{(r)} \sum_{m=1}^{n_y} \bar{C}_{jm}^{(s)} f_{km} \tag{3.17}$$

where r and s denote order of partial derivatives, n_ξ and n_η represent number of grids in ξ and η directions, respectively.

The derivatives in Cartesian coordinates can be calculated in terms of derivatives in natural coordinates as

$$\left(\frac{\partial f}{\partial x}\right)_{ij} = \frac{1}{J_{ij}}\left[\left(\frac{\partial y}{\partial \eta}\right)_{ij}\left(\sum_{k=1}^{n_x} \bar{C}_{ik}^{(1)} f_{kj}\right) - \left(\frac{\partial y}{\partial \xi}\right)_{ij}\left(\sum_{m=1}^{n_y} \bar{C}_{jm}^{(1)} f_{im}\right)\right] \tag{3.18}$$

$$\left(\frac{\partial f}{\partial y}\right)_{ij} = \frac{1}{J_{ij}}\left[\left(\frac{\partial x}{\partial \xi}\right)_{ij}\left(\sum_{m=1}^{n_y} \bar{C}_{jm}^{(1)} f_{im}\right) - \left(\frac{\partial x}{\partial \eta}\right)_{ij}\left(\sum_{k=1}^{n_x} \bar{C}_{ik}^{(1)} f_{kj}\right)\right] \tag{3.19}$$

In this thesis, Gauss-Lobatto distribution is utilized in the distribution of points since Lobatto rule creates grid points with non-uniform intervals which provide more accuracy in the calculation of derivatives in GDQ method. For instance, considering n integration points in x direction, Gauss-Lobatto points x_i can be calculated between the interval [-1,1] by computing the roots of

$$\frac{d}{dx}\left(P_{n-1}(x)\right)=0 \qquad \textbf{for } i=2,...,n-1 \tag{3.20}$$

where $P(x)$ denote Legendre polynomials. End points are $x_1 = -1$ and $x_n = 1$. In equation (3.20), Legendre polynomials $P_n(x)$ can be expressed explicitly by Rodrigue's formula as follows

$$P_n(x)=\frac{1}{2^n n!}\frac{d^n}{dx^n}\left(\left(x^2-1\right)^n\right) \tag{3.21}$$

and first few Legendre polynomials can be calculated as:

$$P_0(x)=1 \tag{3.22}$$

$$P_1(x)=x \tag{3.23}$$

$$P_2(x)=\frac{1}{2}\left(3x^2-1\right) \tag{3.24}$$

$$P_3(x)=\frac{1}{2}\left(5x^3-3x\right) \tag{3.25}$$

$$P_4(x)=\frac{1}{8}\left(35x^4-30x^2+3\right) \tag{3.26}$$

$$P_5(x)=\frac{1}{8}\left(63x^5-70x^3+15x\right) \tag{3.27}$$

In addition, the application of boundary conditions becomes easy since grid points can be located on the boundaries with Lobatto rule. These points are also utilized in numerical integration of equations (2.143) and (2.156).

3.3. Solution of Equations of Motion

The equations of motion of the discretized shell domain can be stated in matrix form as following

$$\bar{\mathbf{M}}\,\ddot{\mathbf{U}} + \bar{\mathbf{P}} = \bar{\mathbf{F}} \tag{3.28}$$

where $\bar{\mathbf{M}}$, $\ddot{\mathbf{U}}$, $\bar{\mathbf{P}}$, $\bar{\mathbf{F}}$ indicate mass matrix, acceleration vector, internal and external force vectors, respectively.

Time integration of equation of motion can be calculated using constant-average acceleration version of Newmark implicit method. In this method, at (n+1)-th time step (at time (n+1)Δt or t_{n+1}) equation of motion can be stated as

$$\bar{\mathbf{M}}\ddot{\mathbf{U}}_{n+1} + \bar{\mathbf{P}}_{n+1} = \bar{\mathbf{F}}_{n+1} \tag{3.29}$$

Substituting following acceleration and velocity expressions (at time t_{n+1}) into equation (3.29)

$$\ddot{\mathbf{U}}_{n+1} = C_0\left(\mathbf{U}_{n+1} - \mathbf{U}_n\right) - C_1\dot{\mathbf{U}}_n - \ddot{\mathbf{U}}_n \tag{3.30}$$

$$\dot{\mathbf{U}}_{n+1} = \dot{\mathbf{U}}_n + \Delta t\ddot{\mathbf{U}}_n + \frac{\Delta t}{2}\left(\dot{\mathbf{U}}_{n+1} - \ddot{\mathbf{U}}_n\right) \tag{3.31}$$

following algebraic equation system is obtained

$$C_0\bar{\mathbf{M}}\mathbf{U}_{n+1} + \bar{\mathbf{P}}_{n+1} = \bar{\mathbf{F}}_{n+1} + \bar{\mathbf{M}}(C_0\mathbf{U}_n + C_1\dot{\mathbf{U}}_n + \ddot{\mathbf{U}}_n) \tag{3.32}$$

where $\mathbf{U}_n$ denote the displacements at n-th time step and C_0=4/Δt^2, C_1=4/Δt can be utilized according to the implicit Newmark constant average acceleration time integration scheme.

Equation (3.32) is nonlinear since internal force $\bar{\mathbf{P}}_{n+1}$ is nonlinear function of unknown displacements $\mathbf{U}_{n+1}$. To obtain the solution of equation (3.32) an iterative approach can be employed such as Newton-Raphson method. In this method, equation (3.32) is expressed in residual form as

$$\bar{\mathbf{R}}_{n+1} = \bar{\mathbf{F}}_{n+1} + \bar{\mathbf{M}}\left(C_0\mathbf{U}_n + C_1\dot{\mathbf{U}}_n + \ddot{\mathbf{U}}_n\right) - C_0\bar{\mathbf{M}}\mathbf{U}_{n+1} - \bar{\mathbf{P}}_{n+1} \tag{3.33}$$

Let $\mathbf{U}_{n+1}^{i}$ and $\bar{\mathbf{R}}_{n+1}^{i}$ be an approximate solution and its error function at the i-th iteration, respectively. By equating Taylor series expansion of error function $\bar{\mathbf{R}}_{n+1}^{i+1}$ to zero, an improved solution at (i+1)-th iteration $\mathbf{U}_{n+1}^{i+1}$ can be obtained as following

$$\bar{\mathbf{R}}_{n+1}^{i+1} \approx \bar{\mathbf{R}}_{n+1}^{i} + \mathbf{K}_{n+1}^{i}(\mathbf{U}_{n+1}^{i+1} - \mathbf{U}_{n+1}^{i}) = 0 \tag{3.34}$$

where $\mathbf{K}_{n+1}^{i}$ corresponds to tangent stiffness matrix. Incremental form of equation (3.34) can be stated as

$$\mathbf{K}_{n+1}^{i}\Delta\mathbf{U}_{n+1}^{i} = -\bar{\mathbf{R}}_{n+1}^{i} \tag{3.35}$$

where $\Delta\mathbf{U}_{n+1}^{i}$ denotes the displacement increment at the i-th iteration and can be written as

$$\Delta\mathbf{U}_{n+1}^{i} = \mathbf{U}_{n+1}^{i+1} - \mathbf{U}_{n+1}^{i} \tag{3.36}$$

Improved solution at (i+1)-th iteration can be stated as

$$\mathbf{U}_{n+1}^{i+1} = \mathbf{U}_{n+1}^{i} + \Delta\mathbf{U}_{n+1}^{i} \tag{3.37}$$

For the first iteration, initial accelerations $\ddot{\mathbf{U}}_0$ can be obtained by using initial displacements $\mathbf{U}_0$ and velocities $\dot{\mathbf{U}}_0$ at time $t = 0$. Solution steps are iterated until the error function $\overline{\mathbf{R}}_{n+1}^{i+1}$ is proximate enough to zero.

4. NUMERICAL RESULTS

This section consists of two main parts where non-linear transient behavior of laminated composite and FGM super-elliptic shells are investigated. Effects of composite and FGM material properties, geometrical properties and boundary conditions on the dynamic behavior are examined.

In order to obtain the results, two MATLAB programs were developed to implement GDQ technique in the solution of the equations of motion for laminated composite and FGM shells. Validation of GDQ codes with analysis results from the literature and those obtained using the finite element method are presented in the following relevant chapters.

4.1. Validation Examples

4.1.1. Validation Example for Laminated Composite Super-Elliptic Shell

A cylindrical laminated composite shell (panel) from the literature (Figure 4.1) is considered [Isoldi et al., 2008] to validate the GDQ code for laminated composite super-elliptic shells. In this validation example, nonlinear transient response of the panel is examined under uniform internal pressure. Geometric characteristics of the cylindrical panel are considered as R=2.54 m, l_1=0.508 m, l_2=0.508 m, φ=0.10 rad and panel thickness h=1.27x10^{-3} m. Stacking scheme of symmetric composite layers is considered as $[0°/-45°/90°/45°]_s$ where all layers have equal thicknesses. The laminated composite material properties are: E_1=137.90 GPa, E_2=9.86 GPa, G_{12}=5.24 GPa, ρ=1562.20 kg/m^3, ν_{12}=0.30 [Isoldi et al., 2008]. Fully clamped boundary condition at all edges of cylindrical panel is considered where

- $u_0 = v_0 = w_0 = \theta_x = \theta_y = 0$ **at** $x = 0, l_1$ **and** $y = 0, l_2$

Internal pressure is applied suddenly in the form of step time pulse and its magnitude is q=6895 Pa. Time step value is taken as Δt=0.05 ms.

Figure 4.2 illustrates the comparison of transverse displacement histories at the panel center with the results of [To and Wang, 1998], [Wu et al., 1987] and [Isoldi et

al., 2008]. In this validation example, 9x9 grids are utilized to obtain the converged results with GDQ method. Good agreement is obtained with the results in reference [Isoldi et al., 2008].

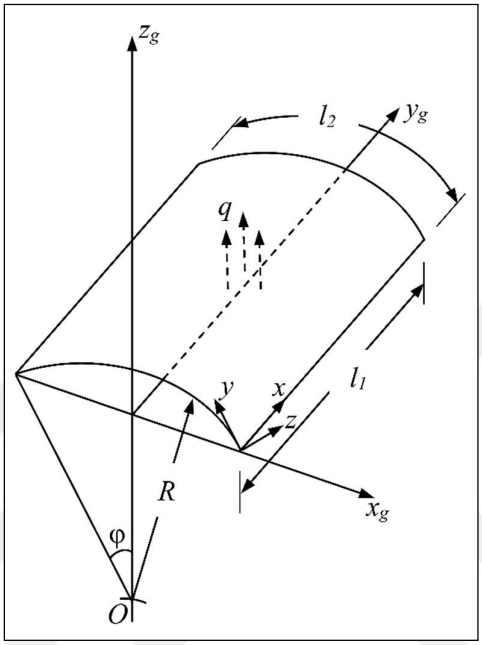

Figure 4.1**:** Representation of the laminated composite cylindrical panel subjected to uniform internal pressure.

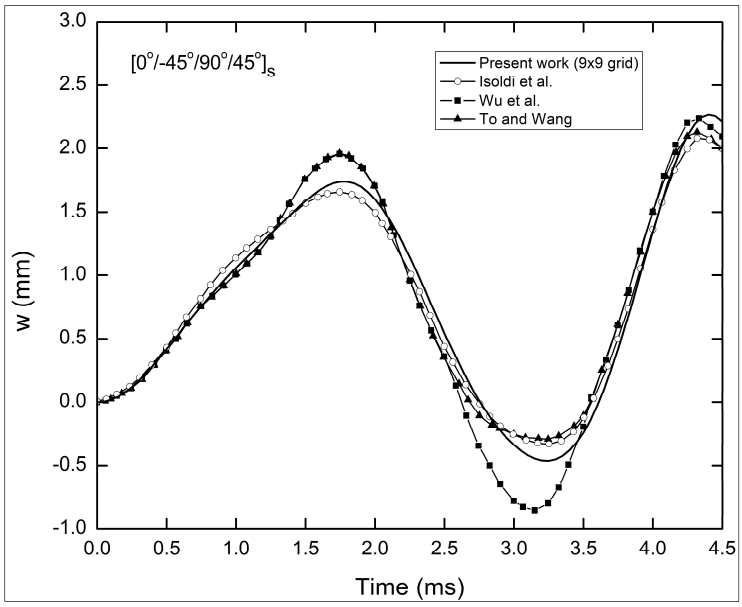

Figure 4.2**:** Time history of transverse displacement at the center of laminated composite cylindrical panel.

4.1.2. Validation Example for FGM Super-Elliptic Shell

Validation of the GDQ code for FGM super-elliptic shells was made through transient analysis results of a FGM plate problem that is available in the literature [Yang and Shen, 2002].

In this validation example, dynamic response of FGM plate is examined under suddenly applied uniformly distributed pressure (Figure 4.3). FGM plate dimensions are given as l_1=0.2 m, l_2=0.2 m (l_1/l_2=1) and plate thickness h=0.02 m (l_2/h=10). FGM material properties are taken as: E_m=208.16 GPa, ρ_m=8166 kg/m^3, ν_m=0.31 for steel (SUS304) and E_c=322.27 GPa, ρ_m=2370 kg/m^3, ν_m=0.24 for silicon nitride (Si_3N_4) [Yang and Shen, 2002]. FGM plate is fully clamped along its edges where

- $u_0 = v_0 = w_0 = \theta_x = \theta_y = 0$ **at** $x = 0, l_1$ **and** $y = 0, l_2$

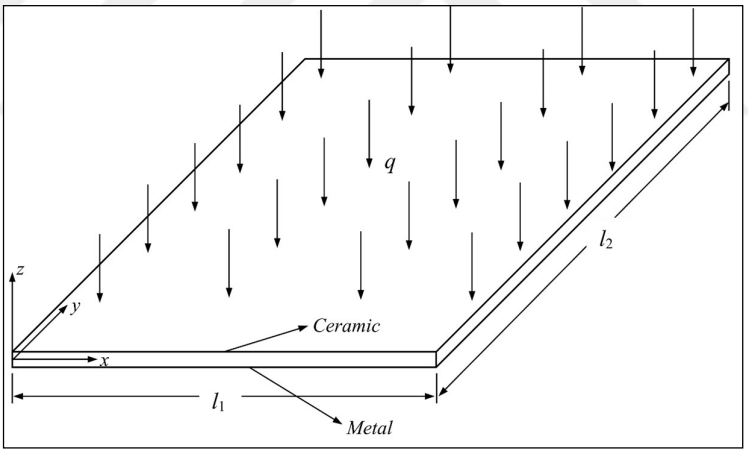

Figure 4.3**:** FGM plate under suddenly applied uniformly distributed pressure.

and uniformly distributed pressure with step pulse is taken as q = -1 Pa. Results are given in non-dimensional form of

$$w_0 = \frac{wE_m h^3}{ql_1^4} \tag{4.1}$$

$$t^* = t\sqrt{\frac{E_m}{\rho_m l_1^2}} \tag{4.2}$$

where w and t indicate transverse displacement at the plate center and time, respectively.

In Figure 4.4, a comparison of non-dimensional transverse displacements at the plate center for volume fraction exponents of k=0.2 and k=2 with the results of [Yang and Shen, 2002] is presented. [Yang and Shen, 2002] used one-dimensional DQM, Galerkin method and modal superposition method to examine transient behavior of FGM plate. Good agreement is achieved with the results in reference [Yang and Shen, 2002]. In this example, 9x9 grids are utilized to obtain converged results.

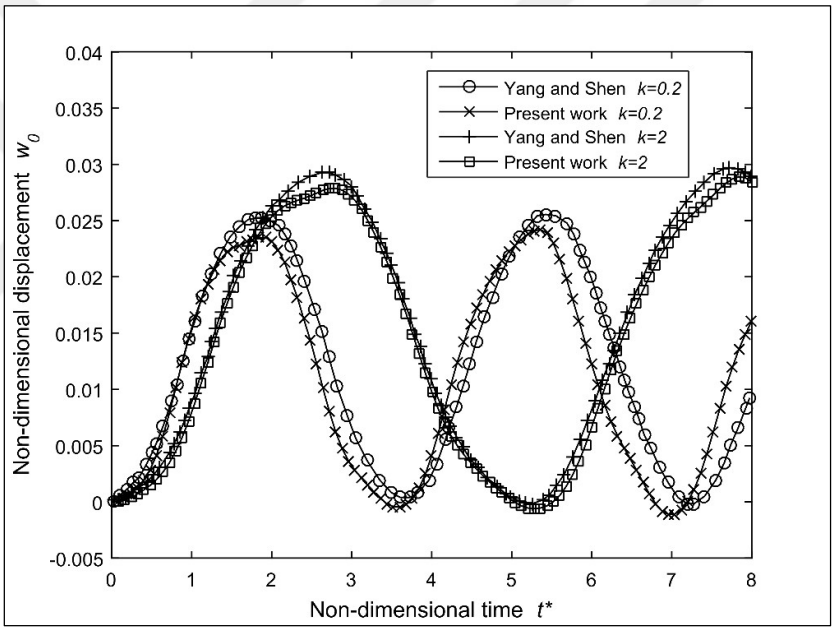

Figure 4.4**:** Time history of non-dimensional transverse displacement at FGM plate center considering fully-clamped boundary condition.

4.2. Examples for Laminated Composite Super-Elliptic Shells

In this section, several super-elliptic composite shell problems are solved with the GDQ method. In the solved examples, different ovality (n) and ellipticity (a/b) values, layer orientations and boundary conditions are used. Uniformly distributed load is applied suddenly in the form of step time pulse.

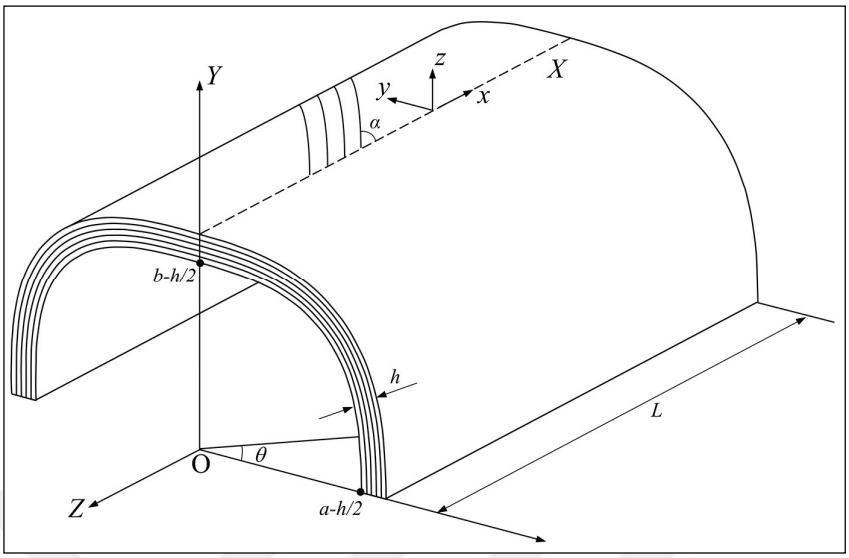

Figure 4.5**:** Super-elliptic shell parameters and fiber orientation angle (α) for laminated composite.

Composite material properties used in the analyses are: E_1=137.90 GPa, E_2=9.86 GPa, G_{12}=5.24 GPa, ρ=1562.20 kg/m^3 and ν_{12}=0.30 (graphite/epoxy, [Wu et al., 1987]). Three different composite layer schemes are used in the analyses: [0º/90º/0º/90º/0º], [30º/-30º/30º/-30º/30º] and [60º/-60º/60º/-60º/60º]. All layers have equal thicknesses. Thickness of the shell (h) is considered as h=0.01 m, a/h=100 and L/h=200 are utilized in all the analyses (Figure 4.5). In Figure 4.5, θ is taken as $\theta = \pi$ radian for super-elliptic panel and $\theta = 2\pi$ radian for super-elliptic tube. As shown in Figure 4.6, three types of boundary conditions are considered: all edges are clamped (CCCC); two edges are clamped, two edges are free (CFCF); two edges clamped for tube version (CC). Details of boundary conditions are as follows

- **CCCC** : $u_0 = v_0 = w_0 = \theta_x = \theta_y = 0$ **at** $x = 0, L$ **and** $y = 0, \theta$
- **CFCF** : $u_0 = v_0 = w_0 = \theta_x = \theta_y = 0$ **at** $y = 0, \theta$
- **CC** : $u_0 = v_0 = w_0 = \theta_x = \theta_y = 0$ **at** $x = 0, L$

Uniformly distributed pressure with step pulse (normal to the surface) is taken as: q = -10 kPa for CCCC boundary condition and q = -1 kPa for CFCF and CC boundary condition. In all the analyses, time step value is taken as Δt=0.5 ms.

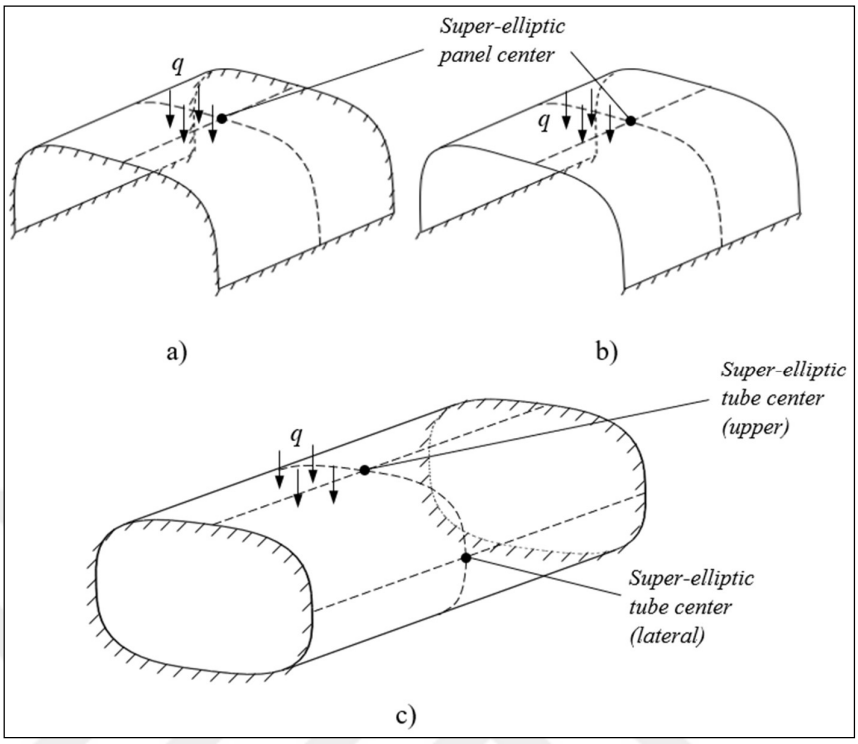

Figure 4.6**:** Boundary and loading conditions of super-elliptic shell: a) CCCC b) CFCF c) CC boundary condition.

In this thesis, GDQ method is employed in element form such as long-familiar finite element method (FEM) which is sometimes called as differential quadrature finite element method. Laminated composite super-elliptic shell is discretized into GDQ elements along *x* and *y* directions. GDQ method is utilized to compute spatial derivatives in GDQ elements. In this study, C^0 and C^1 continuities are imposed at element boundaries. Details of the method are given in reference [Xing,Liu,and Liu, 2010].

4.2.1. Effect of Ovality Value (*n*) on Non-Linear Dynamic Behavior

In the first example, nonlinear transient response of two super-elliptic composite shells (panels) subjected to uniformly distributed load (q = -10 kPa for CCCC boundary condition and q = -1 kPa for CFCF boundary condition) is analyzed. Super-elliptic shell dimensions are: a=1 m, b=0.5 m (a/b=2). Ovality values are taken as n=4 and n=8. Stacking schemes for composite layers are considered as [0°/90°/0°/90°/0°] and [30°/-30°/30°/-30°/30°]. Transverse displacement, strain and stress time histories

at super-elliptic shell (panel) center (strain and stress values are taken from top surface) are obtained with GDQ method and compared with finite element solution as shown in Figures 4.7-10 (for n=4 and n=8). In GDQ solution, a mesh of 1x8 GDQ elements (1 element in x direction, 8 elements in y direction, total 8 elements) and 11x9 grids (11 grids in x direction, 9 grids in y direction) in each element is used to converge the results. The finite element solution is obtained using commercial software ANSYS Workbench. A mesh convergence study is performed to determine appropriate mesh number to be used in finite element analysis (Table 4.1 and Table 4.2). In this context, 50x60 elements of four-noded quadrilaterals are used in finite element analysis (for n=4 and n=8). Good agreement is obtained between the results of GDQ method and finite element solution. With GDQ method, solution is obtained using almost a quarter element number than those used in finite element analysis.

Table 4.1: First three natural frequencies (Hz) of super-elliptic shell (n=4, a/b=2, CCCC, [0°/90°/0°/90°/0°]) according to different mesh numbers.

	15x20 elements	30x40 elements	50x60 elements	60x80 elements
Mode 1	40.179	39.058	38.833	38.766
Mode 2	69.036	66.312	65.768	65.601
Mode 3	77.249	74.769	74.204	74.065

Table 4.2: First three natural frequencies (Hz) of super-elliptic shell (n=8, a/b=2, CCCC, [0°/90°/0°/90°/0°]) according to different mesh numbers.

	15x20 elements	30x40 elements	50x60 elements	60x80 elements
Mode 1	28.838	28.116	27.985	27.948
Mode 2	50.775	48.105	47.65	47.492
Mode 3	66.682	64.733	64.298	64.234

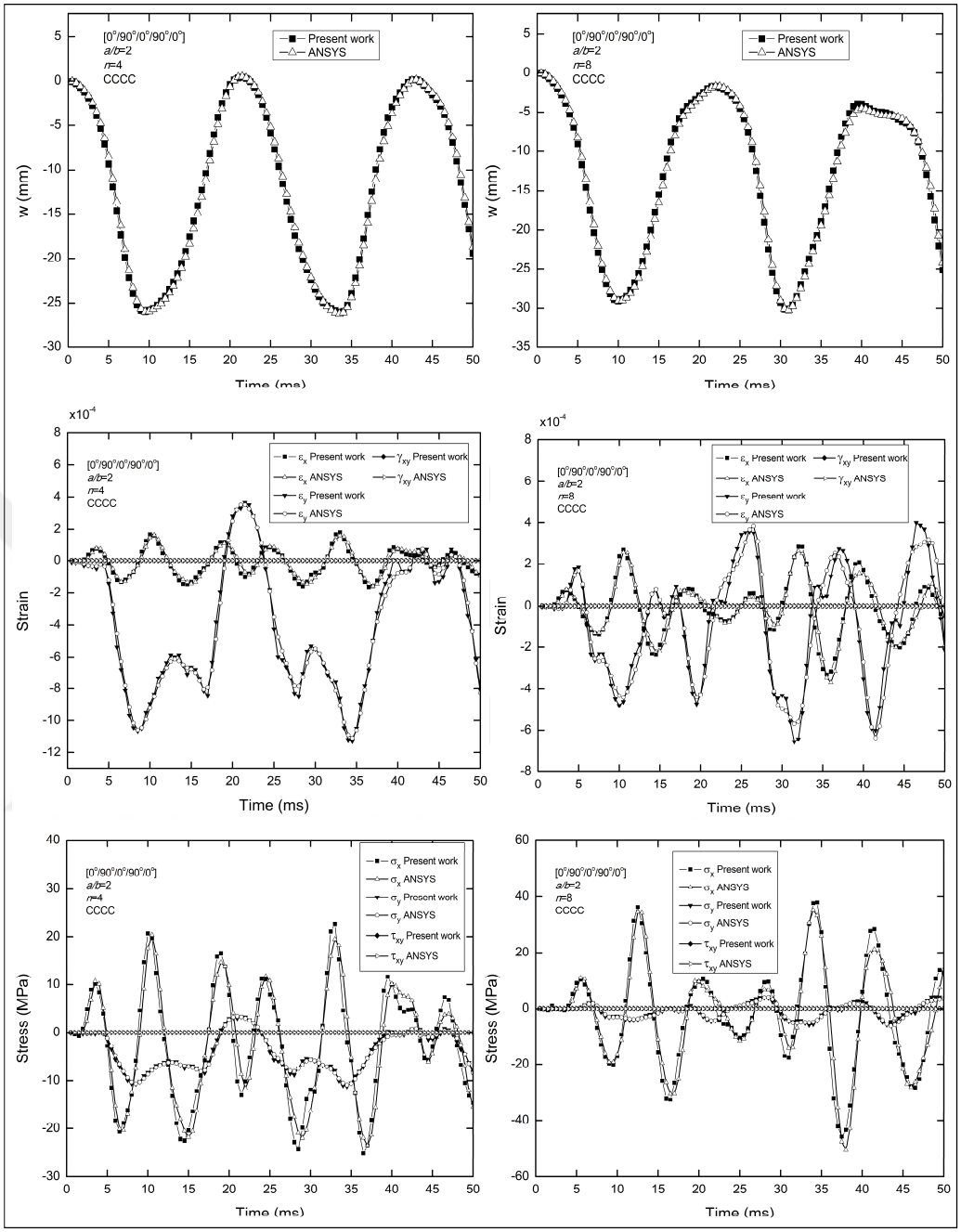

Figure 4.7**:** Transverse displacement, strain and stress history at super-elliptic shell center for CCCC boundary condition for *n*=4 (left) and *n*=8 (right) ([0°/90°/0°/90°/0°]).

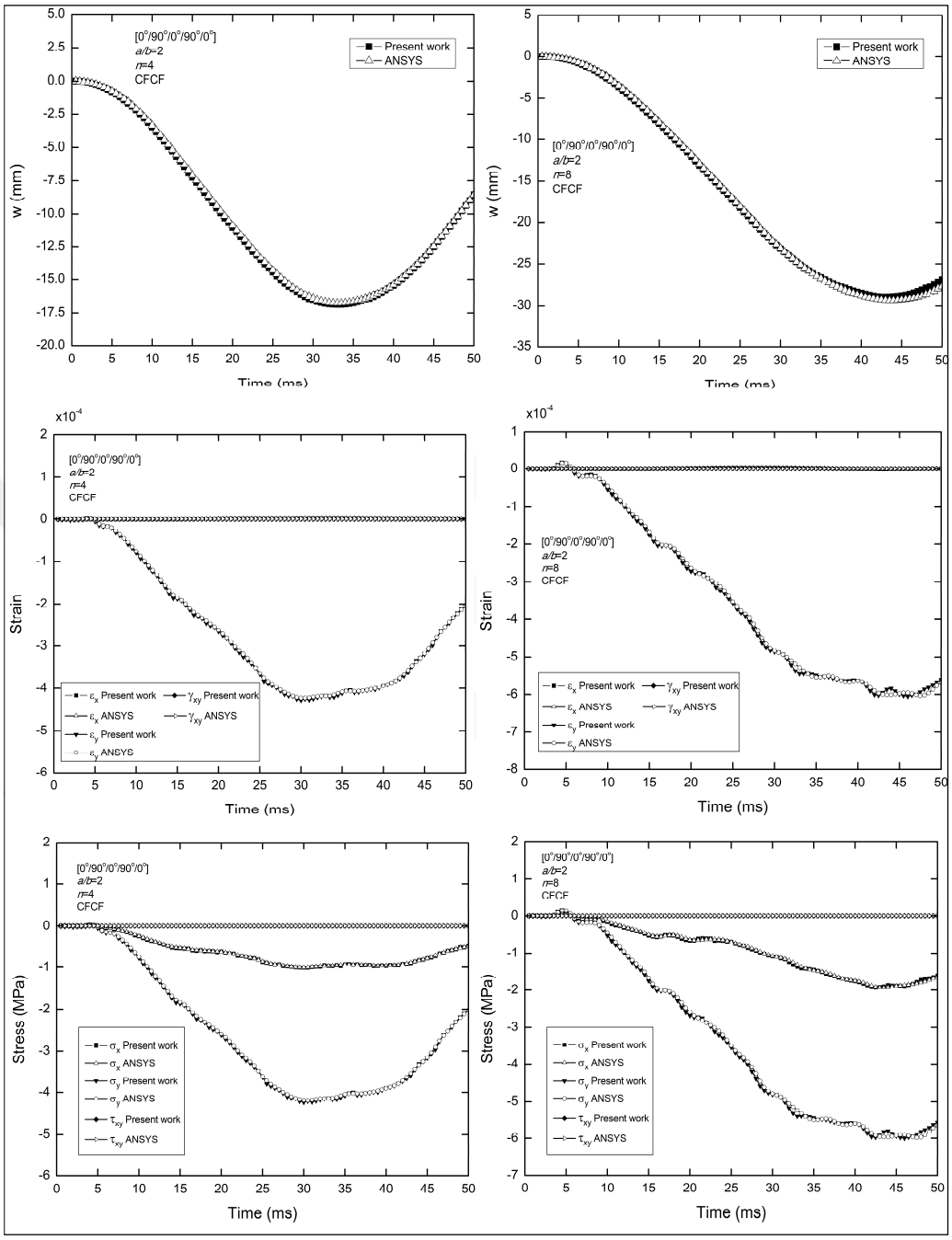

Figure 4.8**:** Transverse displacement, strain and stress history at super-elliptic shell center for CFCF boundary condition for *n*=4 (left) and *n*=8 (right) ([0°/90°/0°/90°/0°]).

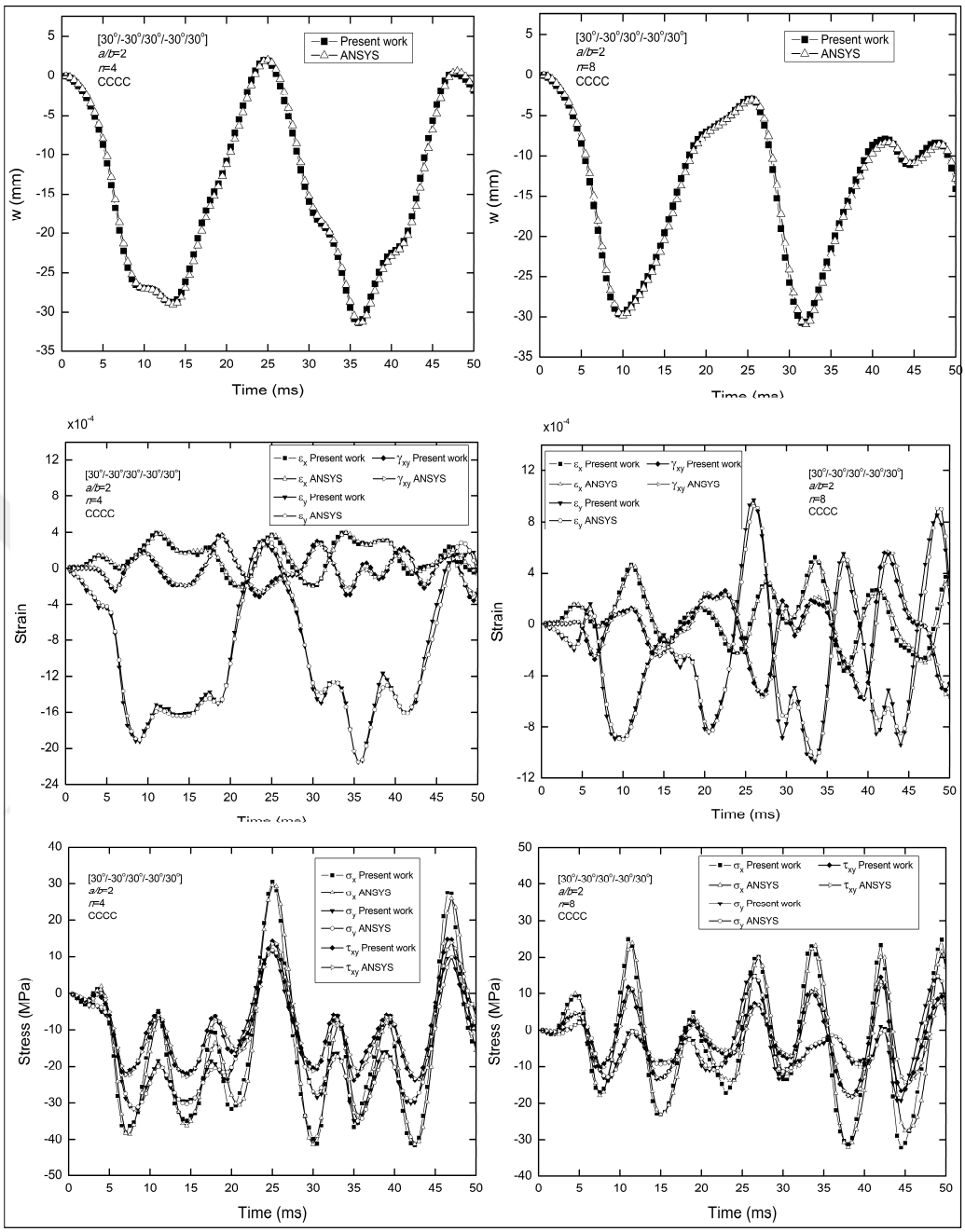

Figure 4.9**:** Transverse displacement, strain and stress history at super-elliptic shell center for CCCC boundary condition for *n*=4 (left) and *n*=8 (right) ([30°/-30°/30°/-30º/30º]).

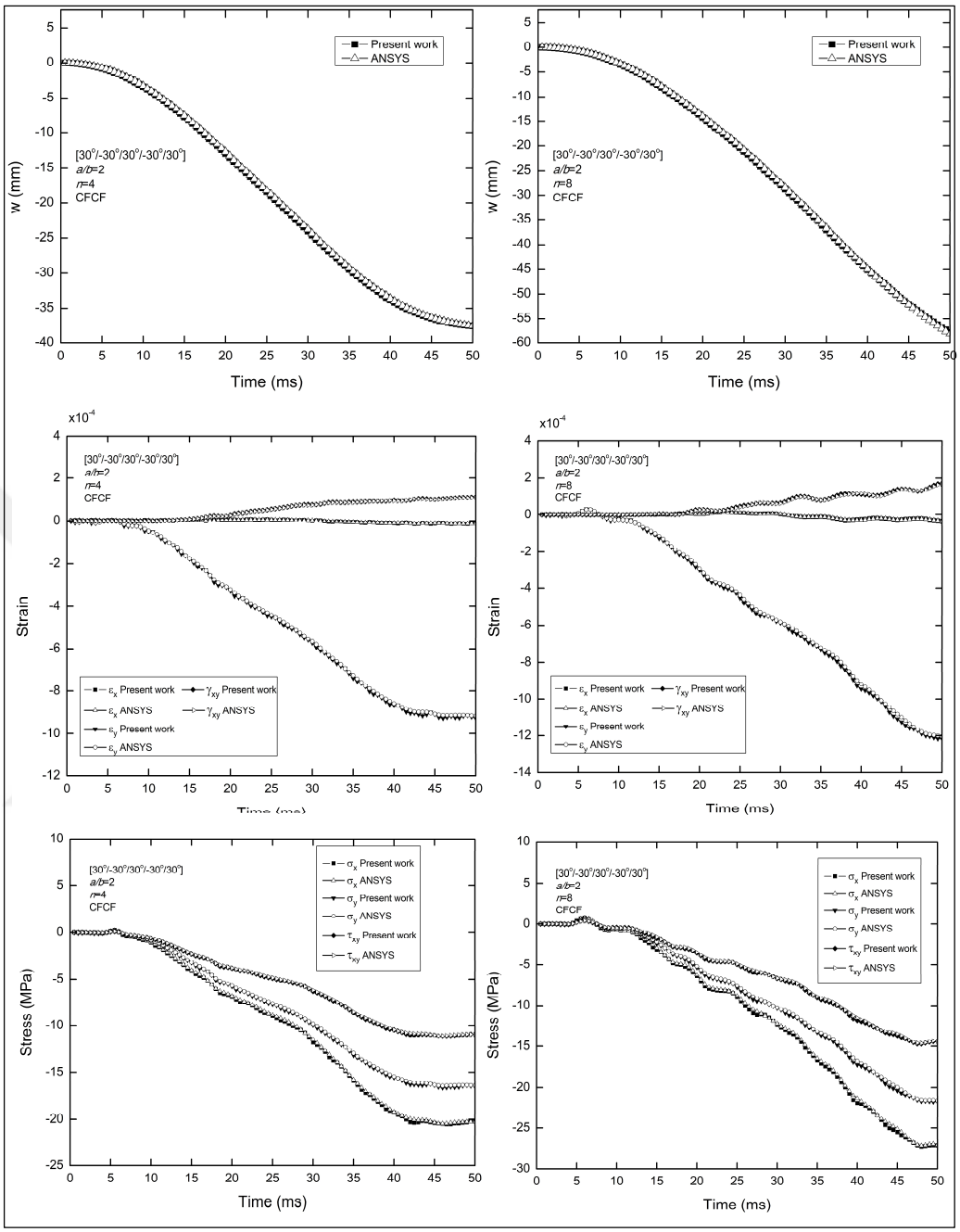

Figure 4.10**:** Transverse displacement, strain and stress history at super-elliptic shell center for CFCF boundary condition for *n*=4 (left) and *n*=8 (right) ([30°/-30°/30°/-30°/30°]).

In the second example, nonlinear transient responses of super-elliptic composite shells (panels) with different ovalities under uniformly distributed load are compared. Super-elliptic shell dimensions are: *a*=1 m, *b*=0.5 m (*a*/*b*=2). Stacking schemes for composite layers are [0°/90°/0°/90°/0°], [30°/-30°/30°/-30°/30°] and [60°/-60°/60°/-60°/60°]. Ovality values are taken as *n*=2,3,4,…,8. In Figures 4.11-19, non-linear

transient responses at the shell (panel) center (transverse displacement, strain in x direction and strain in y direction) are plotted for CCCC boundary condition for [0°/90°/0°/90°/0°], [30°/-30°/30°/-30°/30°] and [60°/-60°/60°/-60°/60°] stacking schemes, respectively. Similarly, In Figures 4.20-28, non-linear transient responses at the shell (panel) center (transverse displacement, strain in x direction and strain in y direction) are presented for CFCF boundary condition for [0°/90°/0°/90°/0°], [30°/-30°/30°/-30°/30°] and [60°/-60°/60°/-60°/60°] stacking schemes, respectively. Since in-plane shear stresses (τ_{xy}) are significant in angle-ply laminated composites, in Figures 4.29-32 shear stress results are given for [30°/-30°/30°/-30°/30°] and [60°/-60°/60°/-60°/60°] stacking schemes. A mesh of 1x4 GDQ elements and 11x9 grids in each element was used for the ovality value n=2. However, as the ovality increases, great changes occur in the principal radii of curvature. Therefore, 4 elements in y direction is not enough to obtain converged results. In this context, 1x8 elements and 11x9 grids in each element were used for the ovality values n=3,4,…,8.

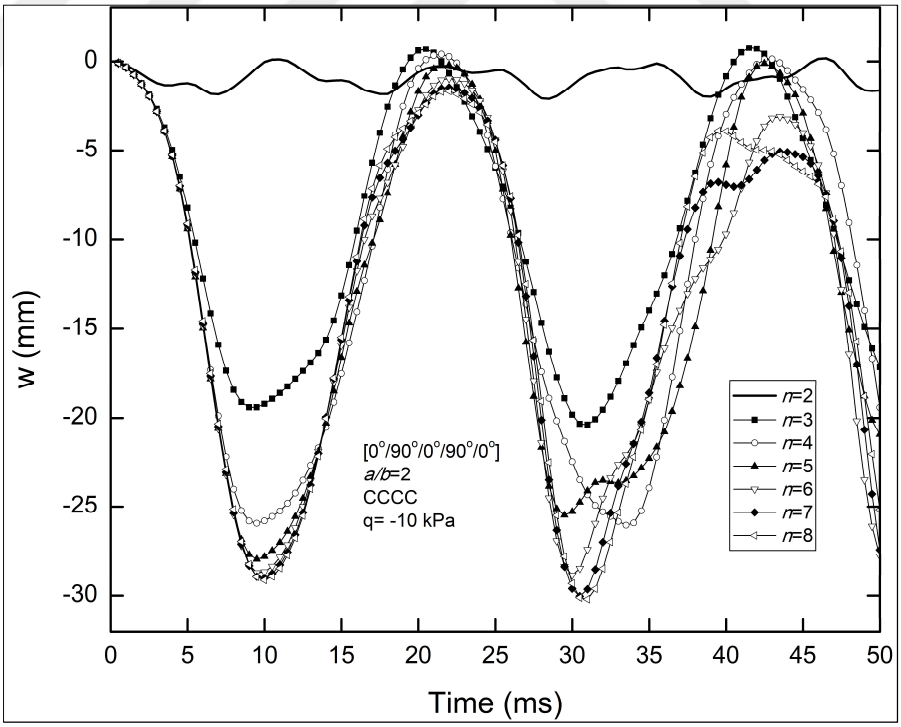

Figure 4.11: Transverse displacement history of super-elliptic shells with different ovalities for CCCC boundary condition ([0°/90°/0°/90°/0°]).

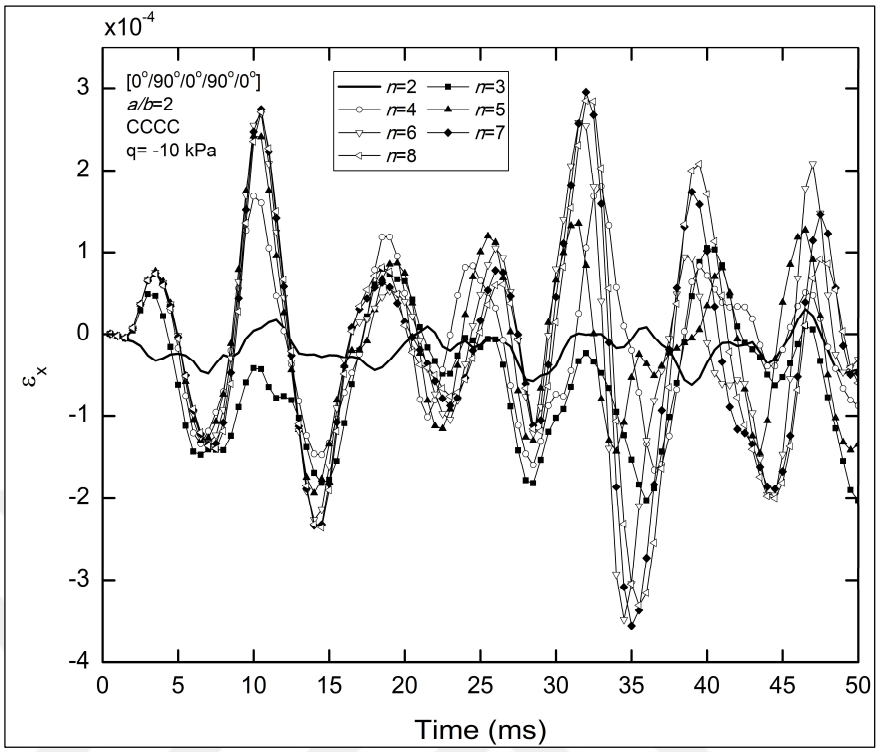

Figure 4.12**:** Strain (in *x* direction) history of super-elliptic shells with different ovalities for CCCC boundary condition ([0°/90°/0°/90°/0°]).

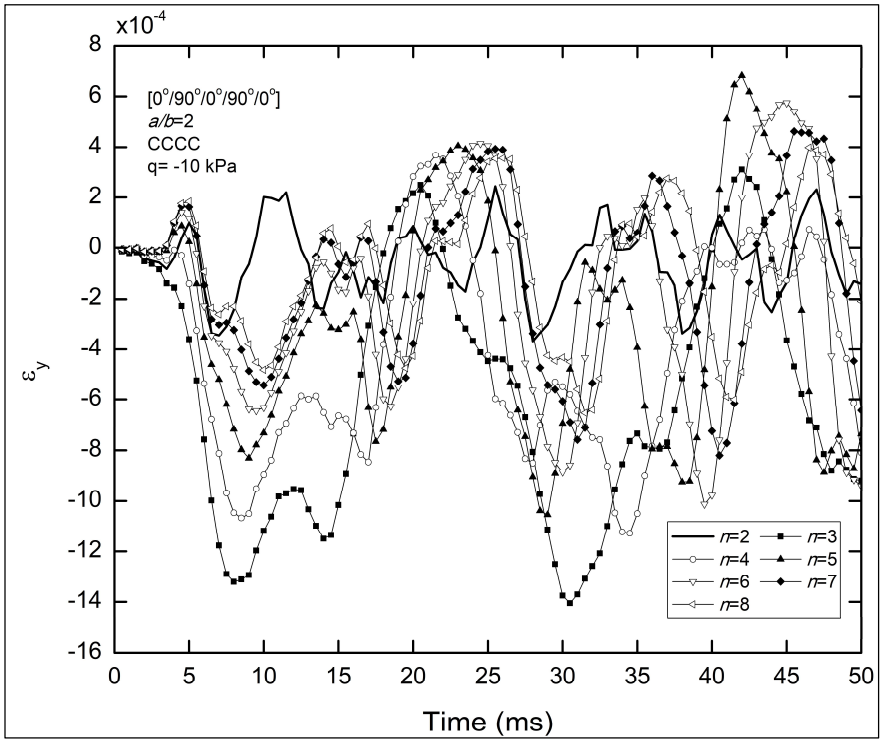

Figure 4.13**:** Strain (in *y* direction) history of super-elliptic shells with different ovalities for CCCC boundary condition ([0°/90°/0°/90°/0°]).

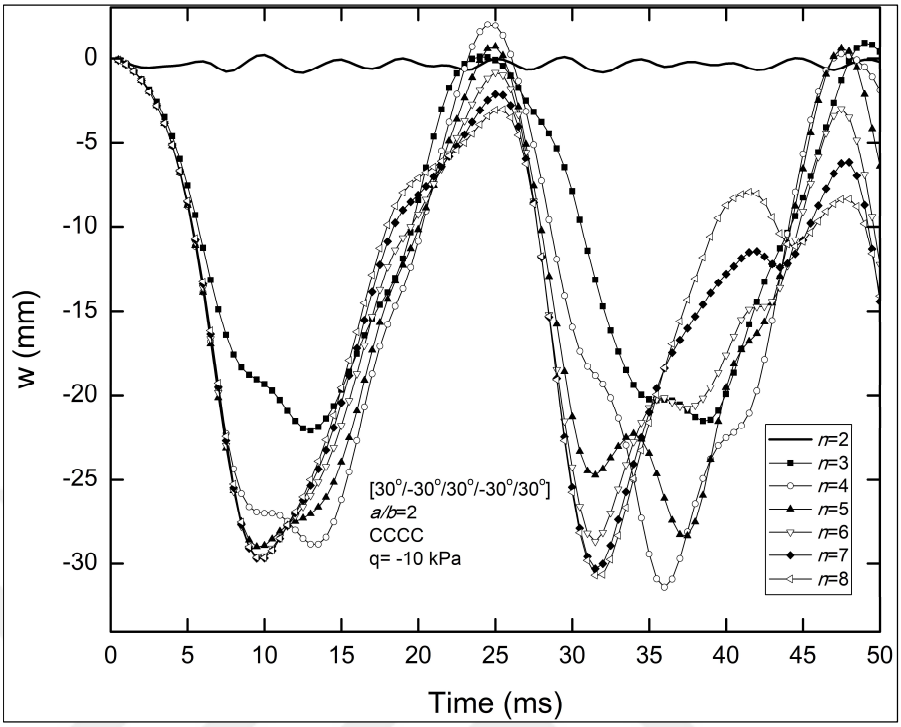

Figure 4.14**:** Transverse displacement history of super-elliptic shells with different ovalities for CCCC boundary condition ([30º/-30º/30º/-30º/30º]).

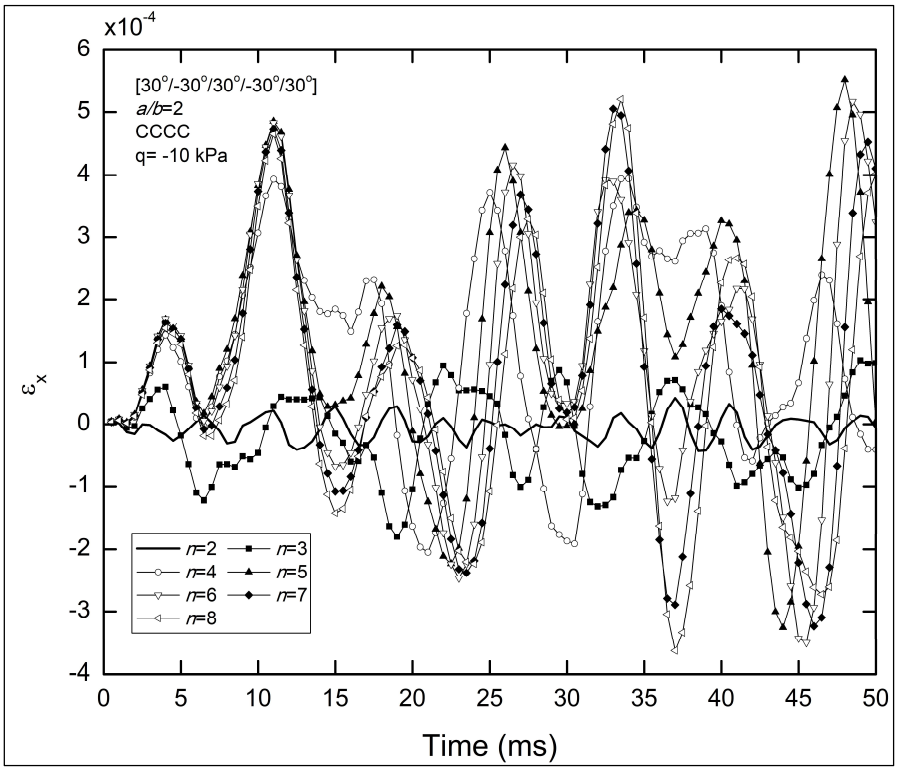

Figure 4.15**:** Strain (in *x* direction) history of super-elliptic shells with different ovalities for CCCC boundary condition ([30º/-30º/30º/-30º/30º]).

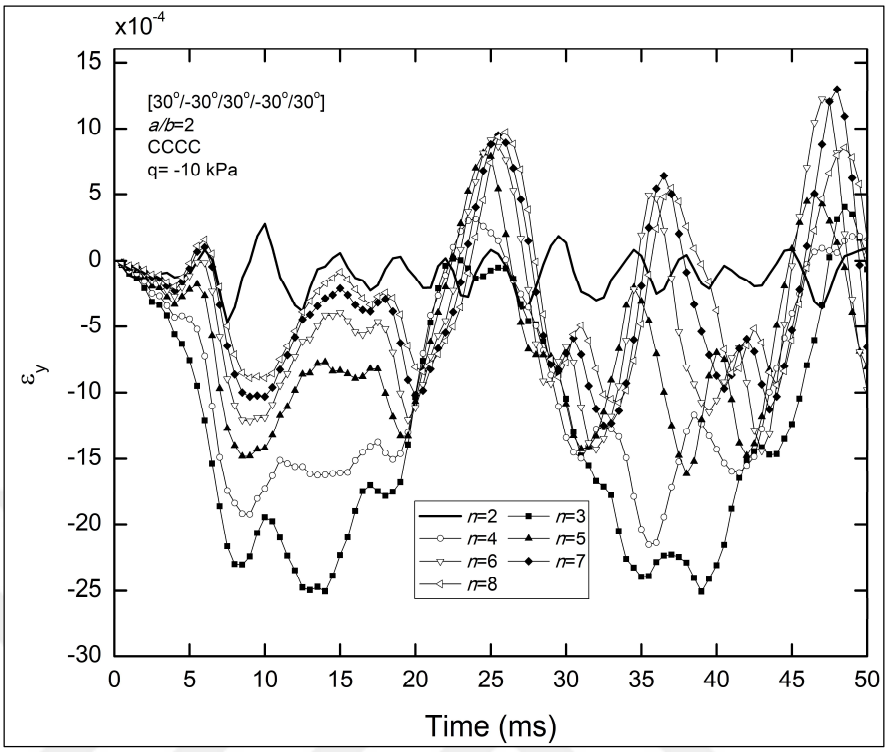

Figure 4.16**:** Strain (in *y* direction) history of super-elliptic shells with different ovalities for CCCC boundary condition ([30º/-30º/30º/-30º/30º]).

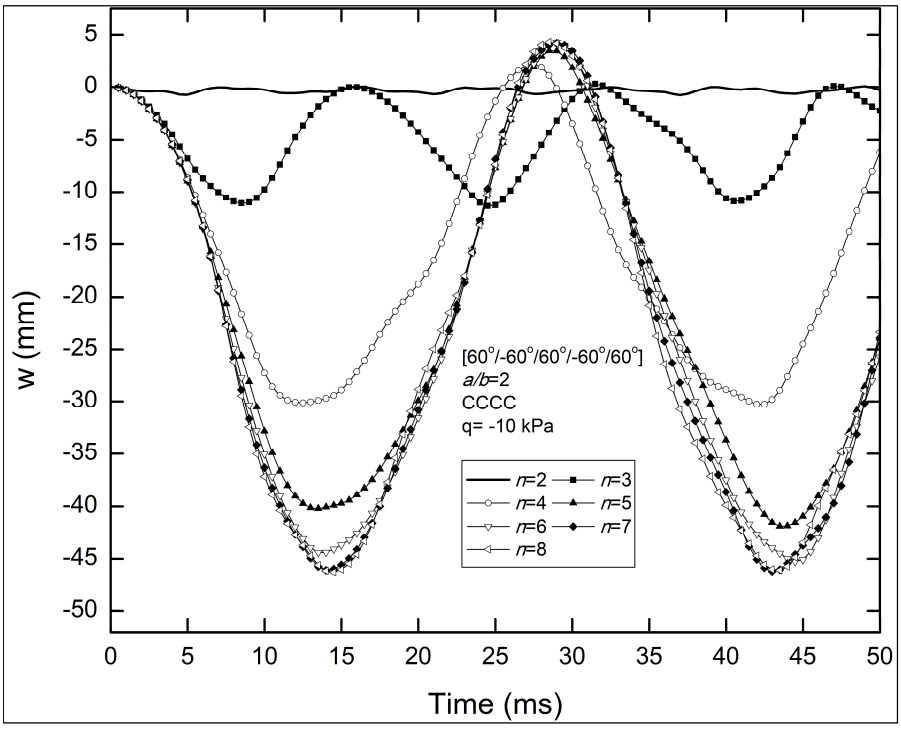

Figure 4.17**:** Transverse displacement history of super-elliptic shells with different ovalities for CCCC boundary condition ([60º/-60º/60º/-60º/60º]).

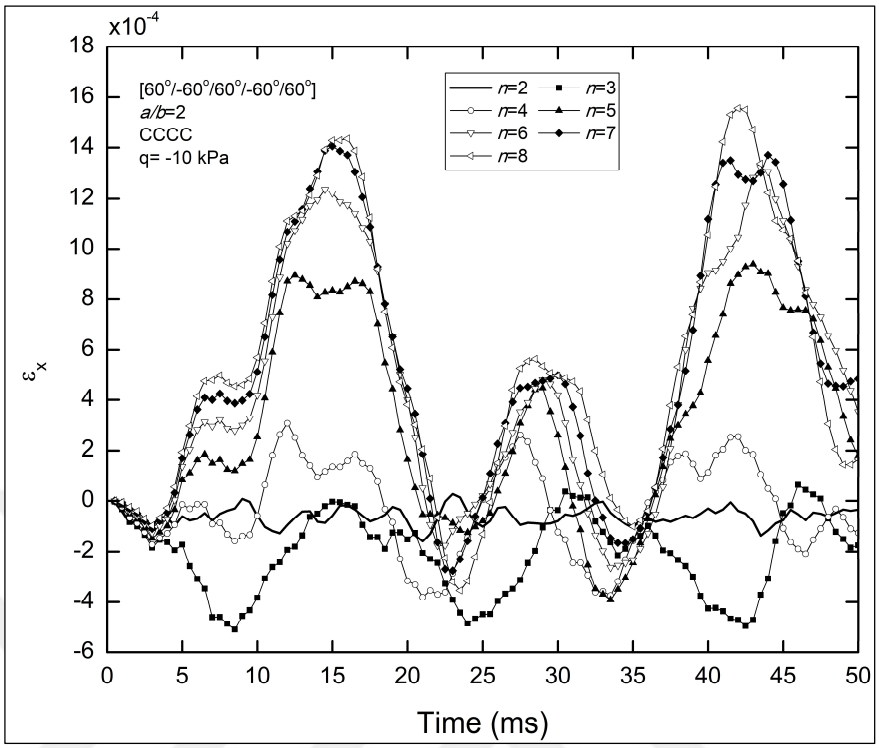

Figure 4.18**:** Strain (in *x* direction) history of super-elliptic shells with different ovalities for CCCC boundary condition ([60º/-60º/60º/-60º/60º]).

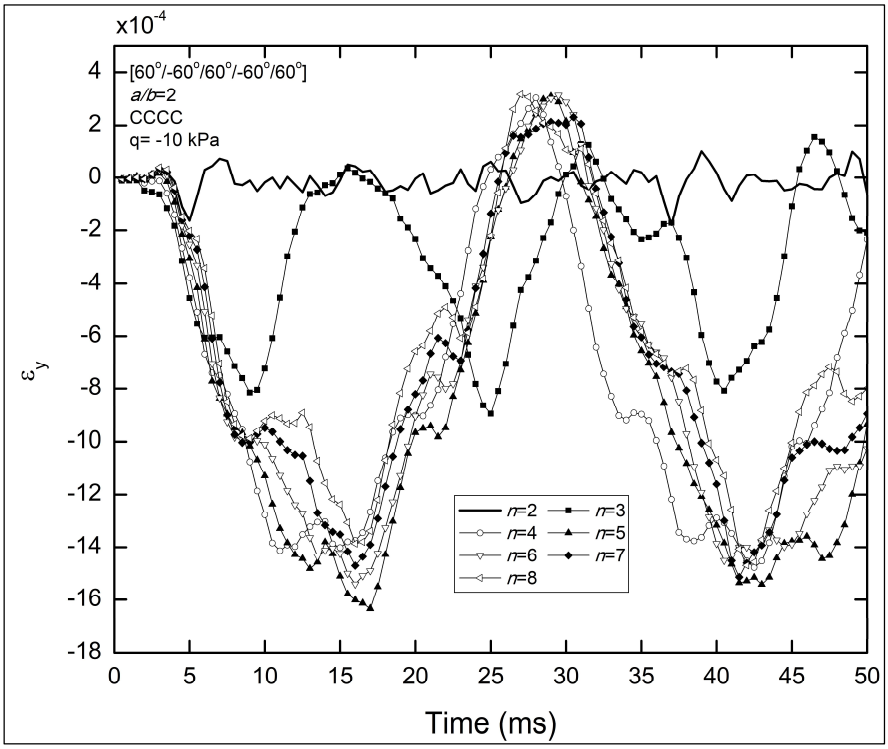

Figure 4.19**:** Strain (in *y* direction) history of super-elliptic shells with different ovalities for CCCC boundary condition ([60º/-60º/60º/-60º/60º]).

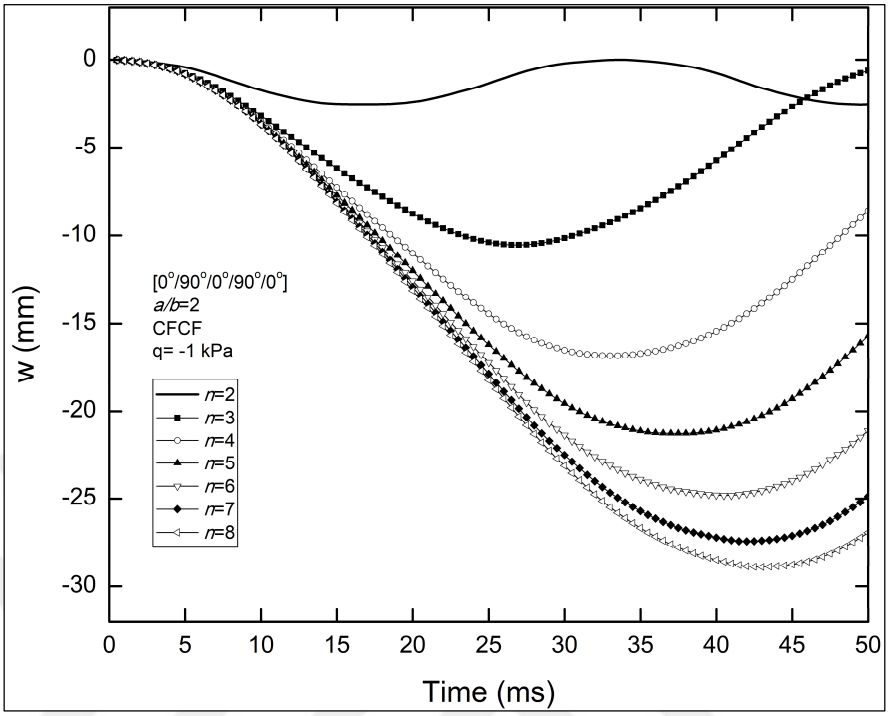

Figure 4.20**:** Transverse displacement history of super-elliptic shells with different ovalities for CFCF boundary condition ([0°/90°/0°/90°/0°]).

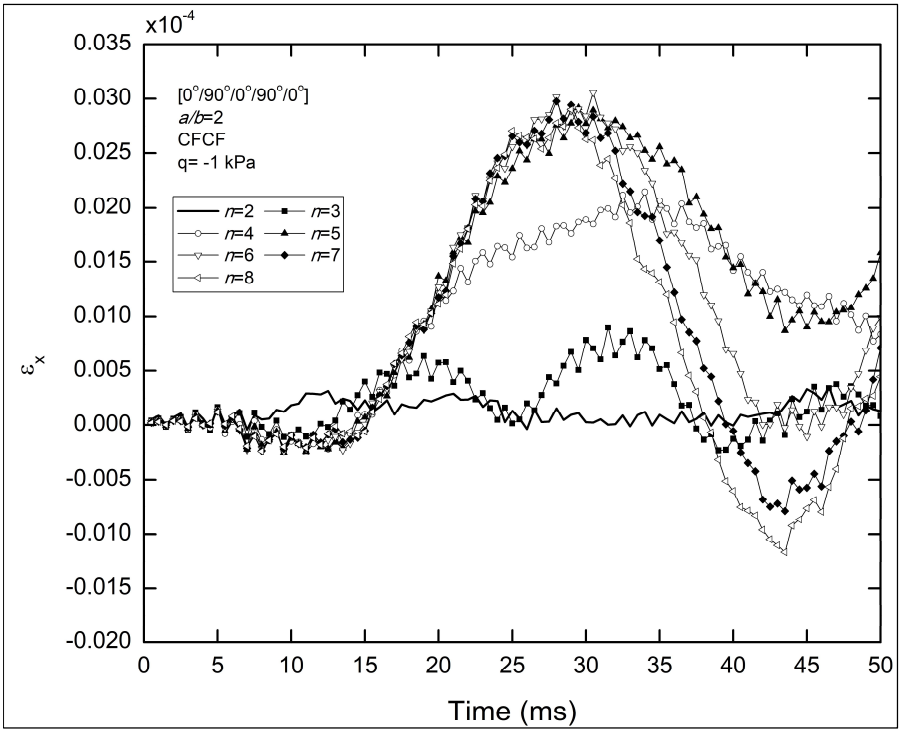

Figure 4.21**:** Strain (in *x* direction) history of super-elliptic shells with different ovalities for CFCF boundary condition ([0°/90°/0°/90°/0°]).

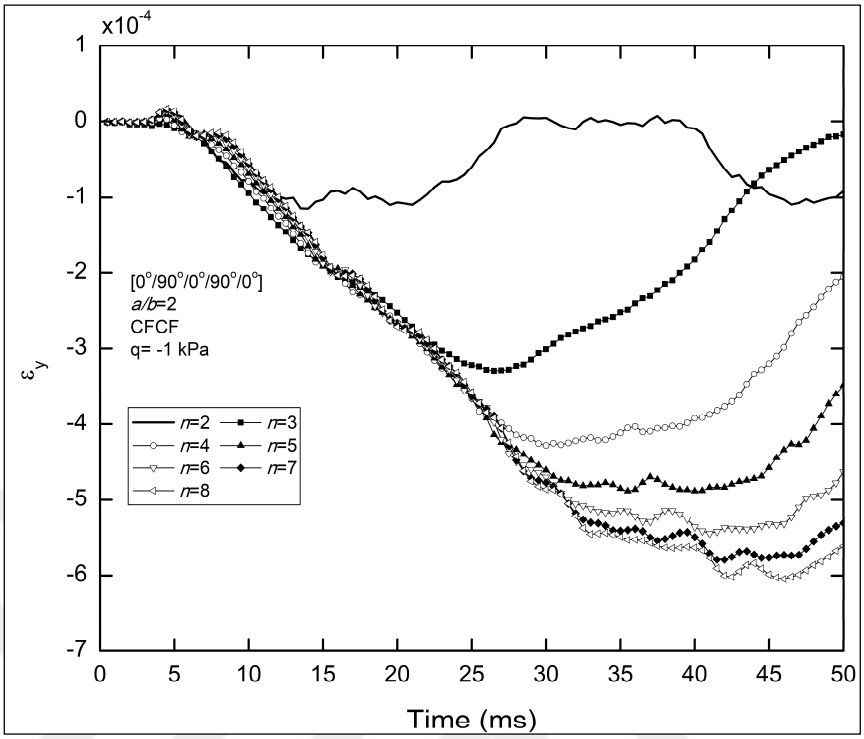

Figure 4.22**:** Strain (in *y* direction) history of super-elliptic shells with different ovalities for CFCF boundary condition ([0°/90°/0°/90°/0°]).

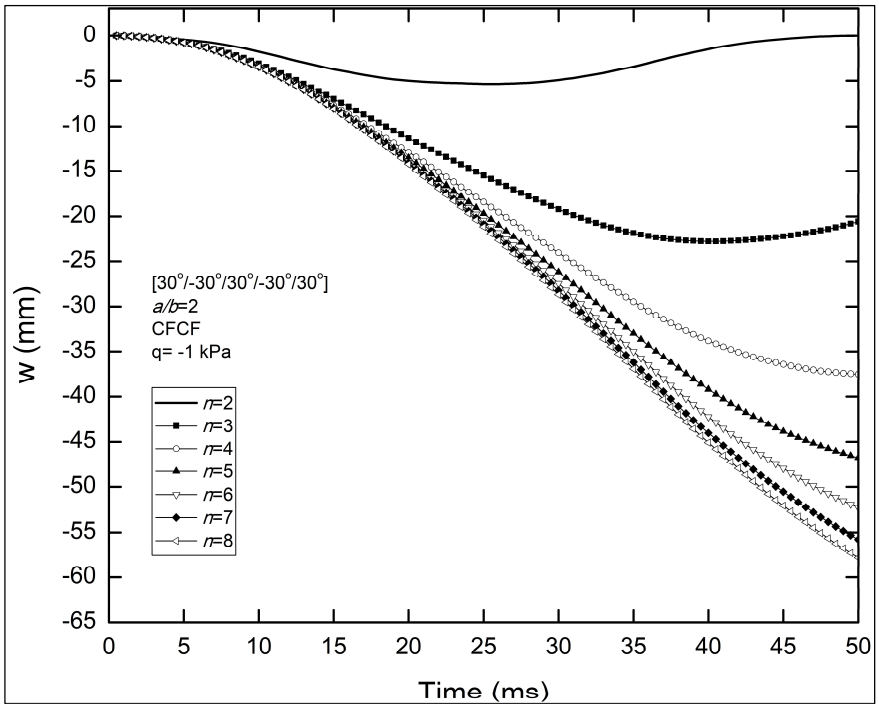

Figure 4.23**:** Transverse displacement history of super-elliptic shells with different ovalities for CFCF boundary condition ([30°/-30°/30°/-30°/30°]).

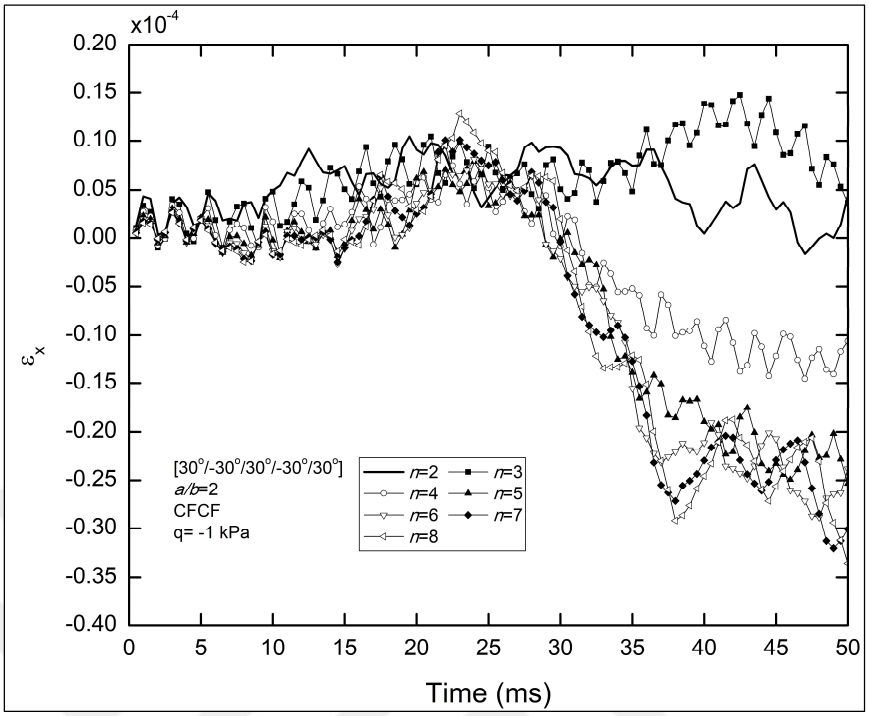

Figure 4.24**:** Strain (in *x* direction) history of super-elliptic shells with different ovalities for CFCF boundary condition ([30º/-30º/30º/-30º/30º]).

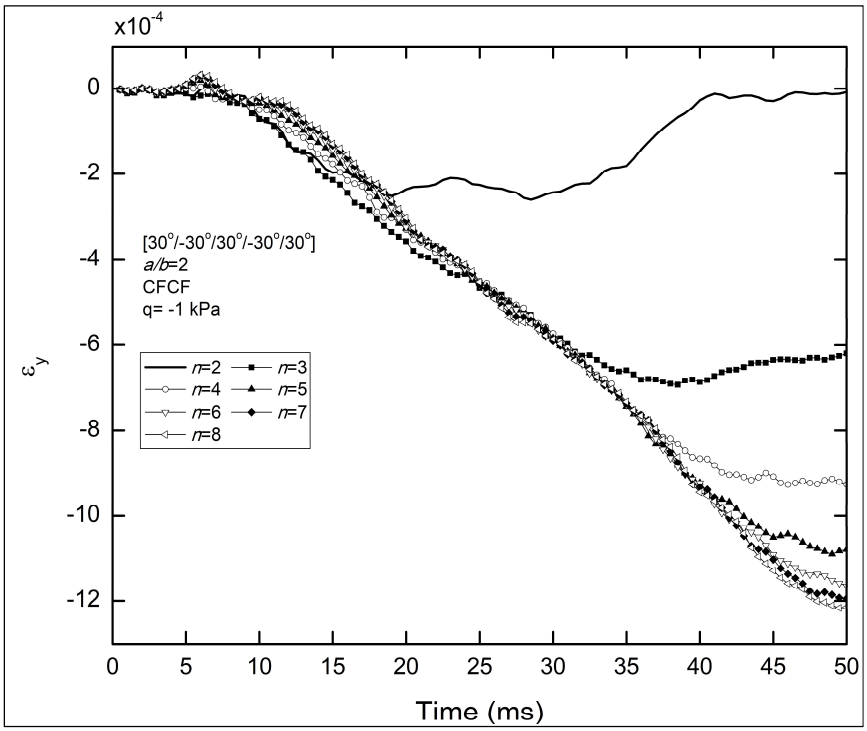

Figure 4.25**:** Strain (in *y* direction) history of super-elliptic shells with different ovalities for CFCF boundary condition ([30º/-30º/30º/-30º/30º]).

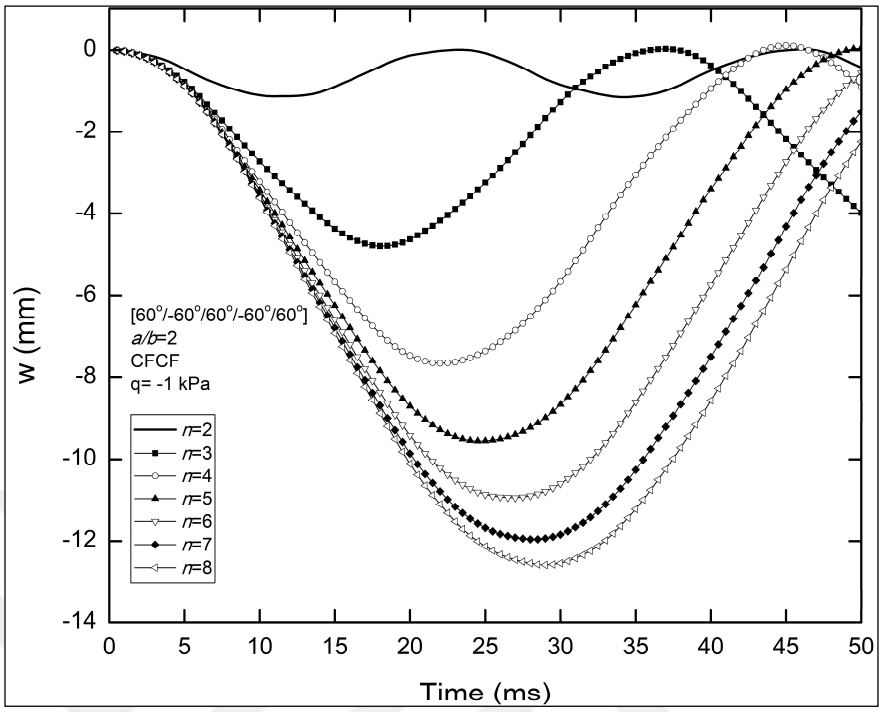

Figure 4.26**:** Transverse displacement history of super-elliptic shells with different ovalities for CFCF boundary condition ([60º/-60º/60º/-60º/60º]).

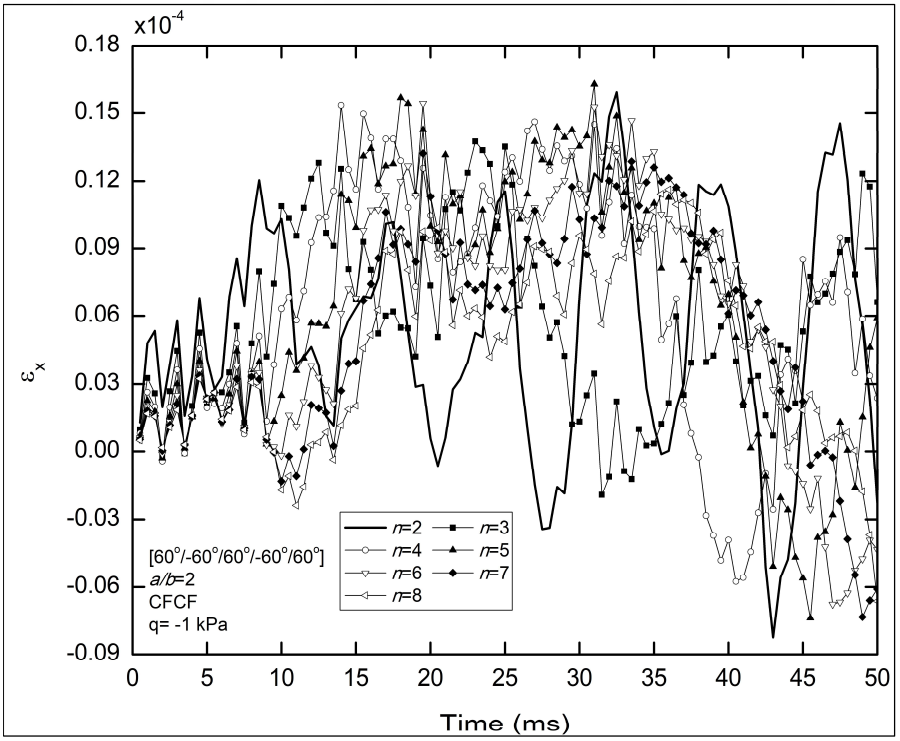

Figure 4.27**:** Strain (in *x* direction) history of super-elliptic shells with different ovalities for CFCF boundary condition ([60º/-60º/60º/-60º/60º]).

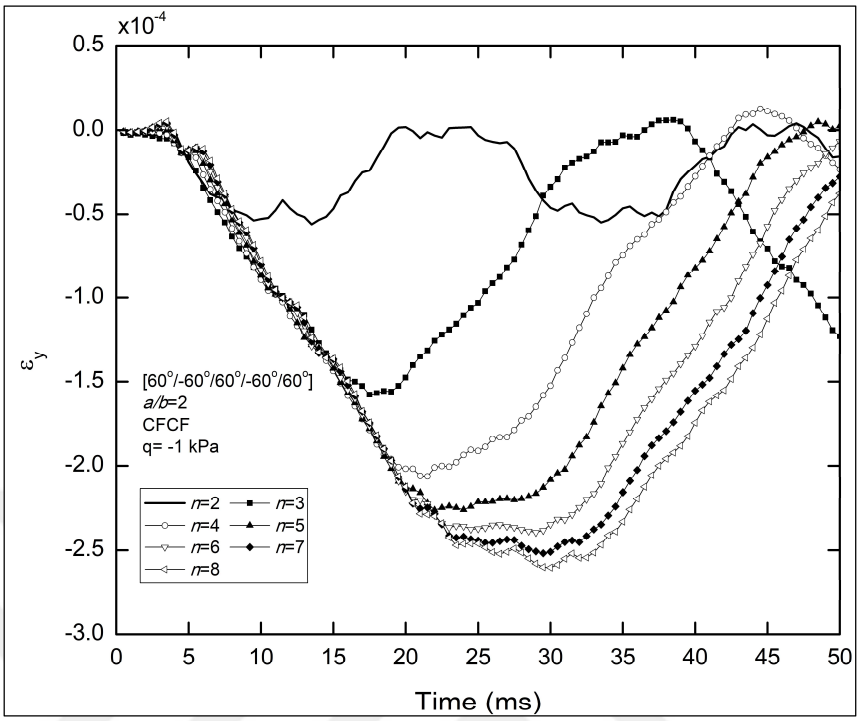

Figure 4.28**:** Strain (in *y* direction) history of super-elliptic shells with different ovalities for CFCF boundary condition ([60º/-60º/60º/-60º/60º]).

As seen in Figures 4.11, 4.14 and 4.17 as the ovality value increases transverse displacement values increase in magnitude for CCCC boundary condition for [0°/90°/0°/90º/0º], [30º/-30º/30º/-30º/30º] and [60º/-60º/60º/-60º/60º] stacking schemes. In Figures 4.12, 4.15 and 4.18, it is seen that ε_x values of elliptical shell (n=2) are much lower than ε_x values for n>2. Similarly, this interpretation is also valid for ε_y values. As shown in Figures 4.13, 4.16 and 4.19, ε_y values of elliptical shell (n=2) are remarkably lower than ε_y values for n>2. Elliptical shell (n=2) is the stiffest structure for all stacking schemes prescribed above leading to least displacement values for CCCC boundary condition.

As seen in Figures 4.20, 4.23 and 4.26 as the ovality value increases transverse displacement values increase in magnitude for CFCF boundary condition for [0°/90°/0°/90º/0º], [30º/-30º/30º/-30º/30º] and [60º/-60º/60º/-60º/60º] stacking schemes. Similarly, as seen in Figures 4.22, 4.25 and 4.28, ε_y values increase in magnitude as the ovality value increases for [0°/90°/0°/90º/0º], [30º/-30º/30º/-30º/30º] and [60º/-60º/60º/-60º/60º] stacking schemes. ε_x and ε_y values of elliptical shell (n=2) are significantly lower than those for n>2 (Figures 4.21, 4.22, 4.24, 4.25, 4.27 and 4.28). For CFCF boundary condition, ε_x values are quite smaller than ε_y values for all

stacking schemes prescribed above. Likewise, elliptical shell (n=2) is the stiffest structure for all stacking schemes leading to least displacement values for CFCF boundary condition.

In-plane shear stress results of super-elliptic shells (panels) with different ovalities for angle-ply laminated composites ([30°/-30°/30°/-30°/30°] and [60°/-60°/60°/-60°/60°]) are given in Figures 4.29-32. For CCCC and CFCF boundary conditions, magnitude of shear stress values for elliptical shell (n=2) are lower than those for n>2. Shear stress values increase in magnitude as the ovality value increases for CFCF boundary condition (Figures 4.31 and 4.32). However, this behavior is not valid for CCCC boundary condition (Figures 4.29 and 4.30).

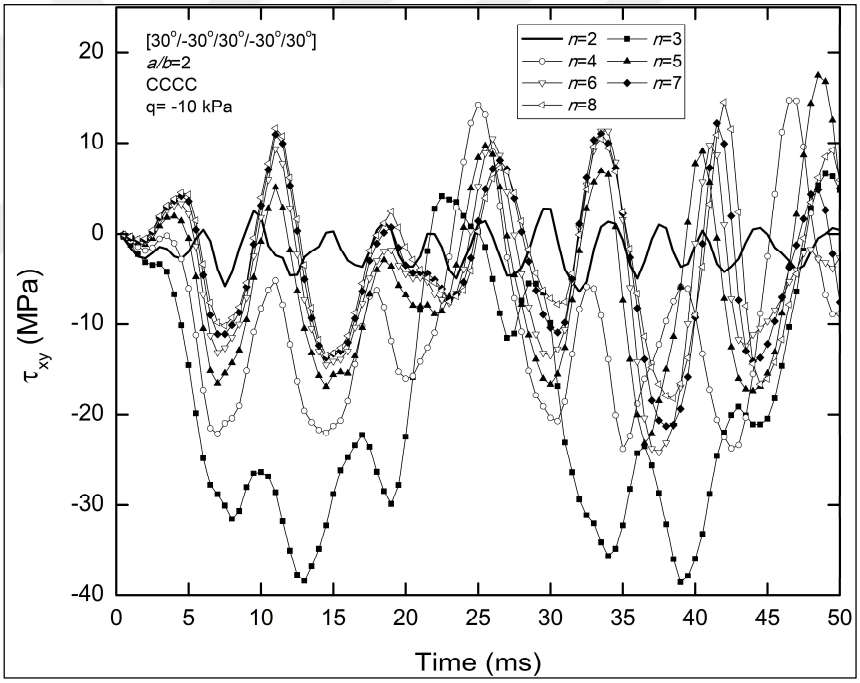

Figure 4.29**:** Shear stress history of super-elliptic shells with different ovalities for CCCC boundary condition ([30°/-30°/30°/-30°/30°]).

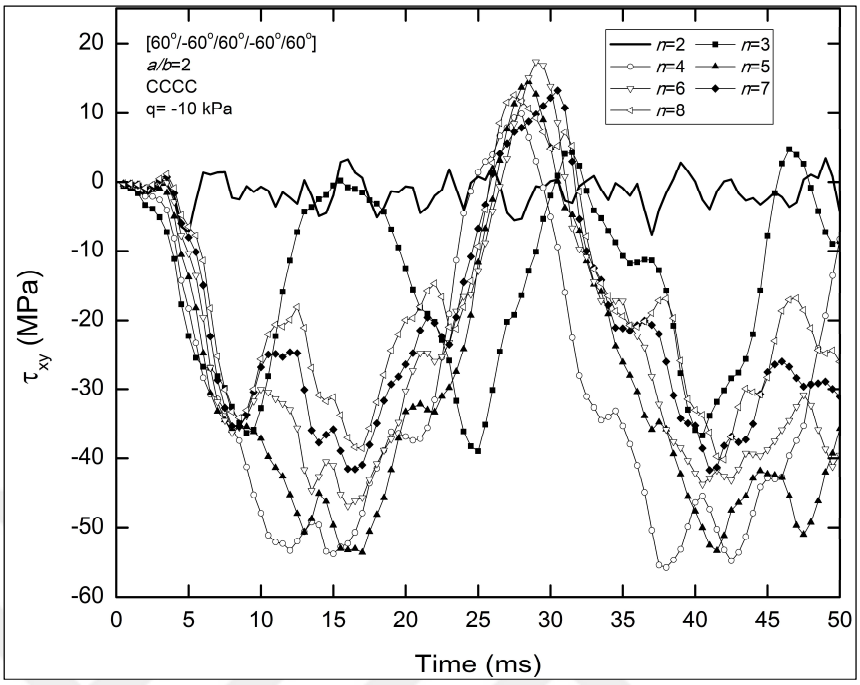

Figure 4.30**:** Shear stress history of super-elliptic shells with different ovalities for CCCC boundary condition ([60º/-60º/60º/-60º/60º]).

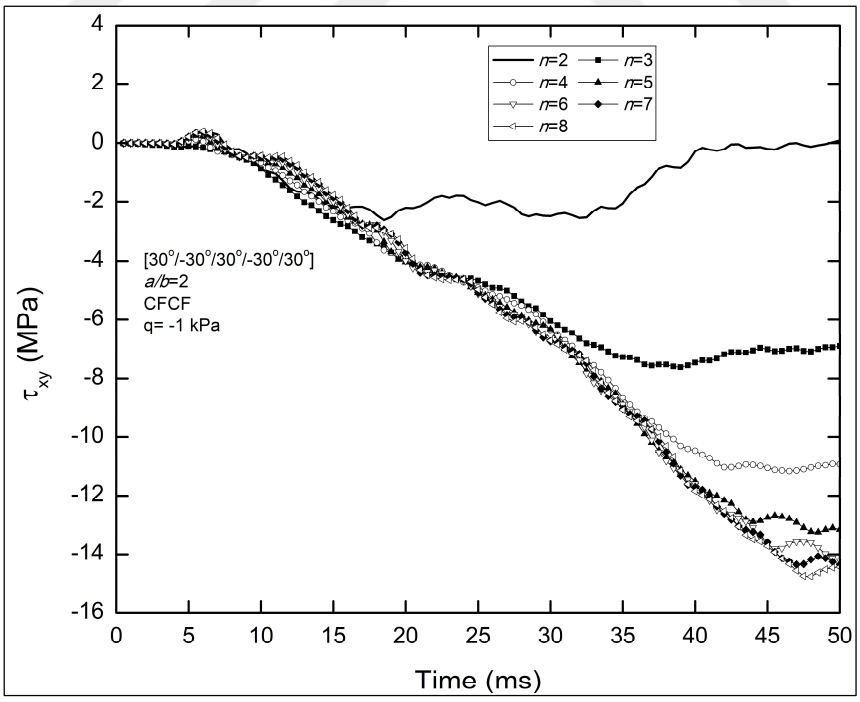

Figure 4.31**:** Shear stress history of super-elliptic shells with different ovalities for CFCF boundary condition ([30º/-30º/30º/-30º/30º]).

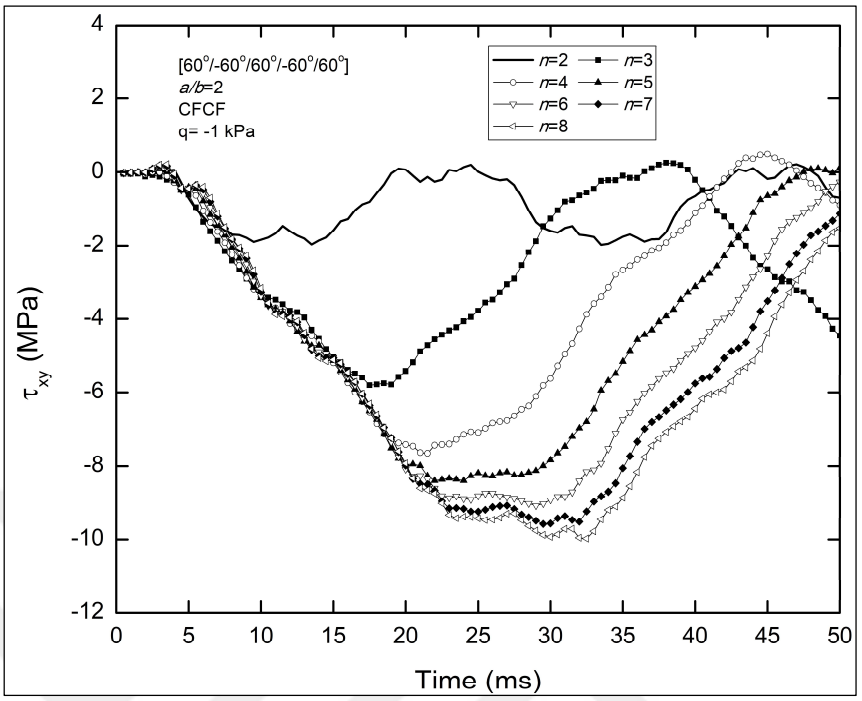

Figure 4.32**:** Shear stress history of super-elliptic shells with different ovalities for CFCF boundary condition ([60º/-60º/60º/-60º/60º]).

In the third example, non-linear transient behavior of super-elliptic shells (tubes) with different ovalities under uniformly distributed load is investigated. Transient responses at the shell (tube) upper center (transverse displacement, strain in *x* direction and strain in *y* direction) are presented in Figures 4.33-35 for CC boundary condition considering [0°/90°/0°/90º/0º] stacking scheme. Similarly, in Figures 4.36-38 results at the shell (tube) lateral center are presented. Super-elliptic shell dimensions remain the same as in the second example (a=1 m, b=0.5 m, a/b=2). In the analyses, 1x16 elements and 11x9 grids in each element were used to obtain converged results for CC boundary condition.

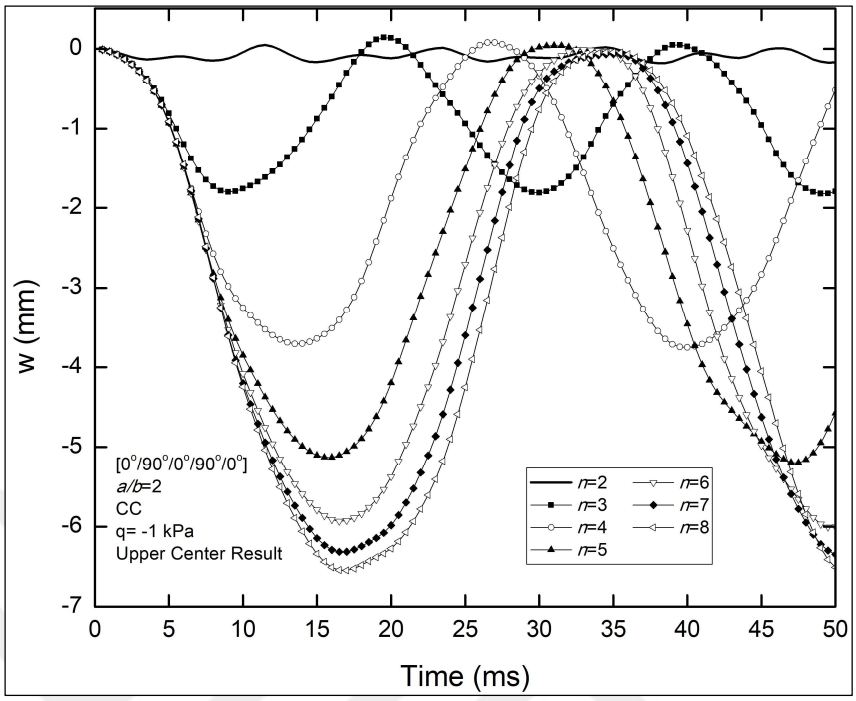

Figure 4.33**:** Transverse displacement history of super-elliptic shells with different ovalities for CC boundary condition ([0°/90°/0°/90°/0°], at the upper center of tube).

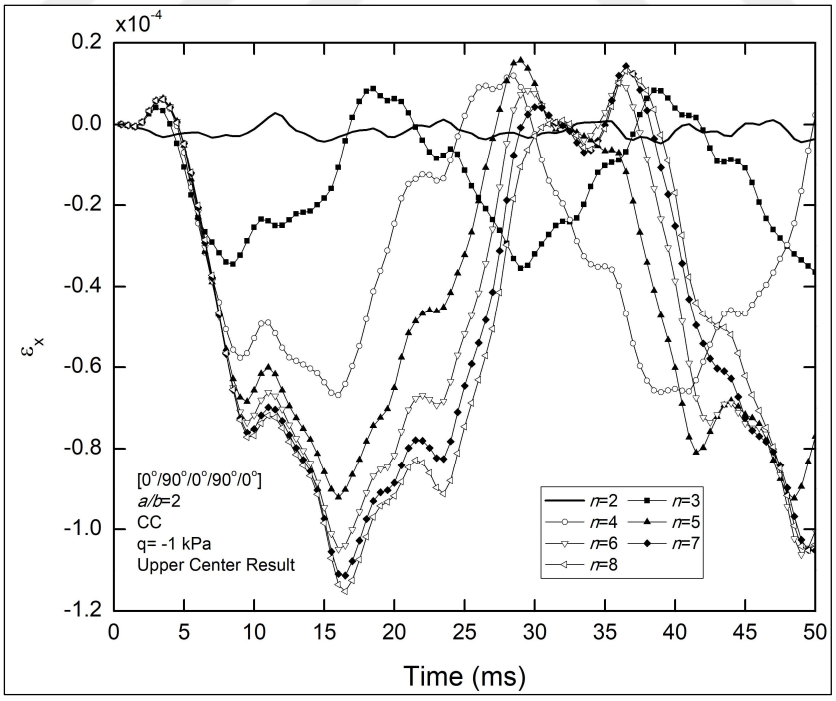

Figure 4.34**:** Strain (in *x* direction) history of super-elliptic shells with different ovalities for CC boundary condition ([0°/90°/0°/90°/0°], at the upper center of tube).

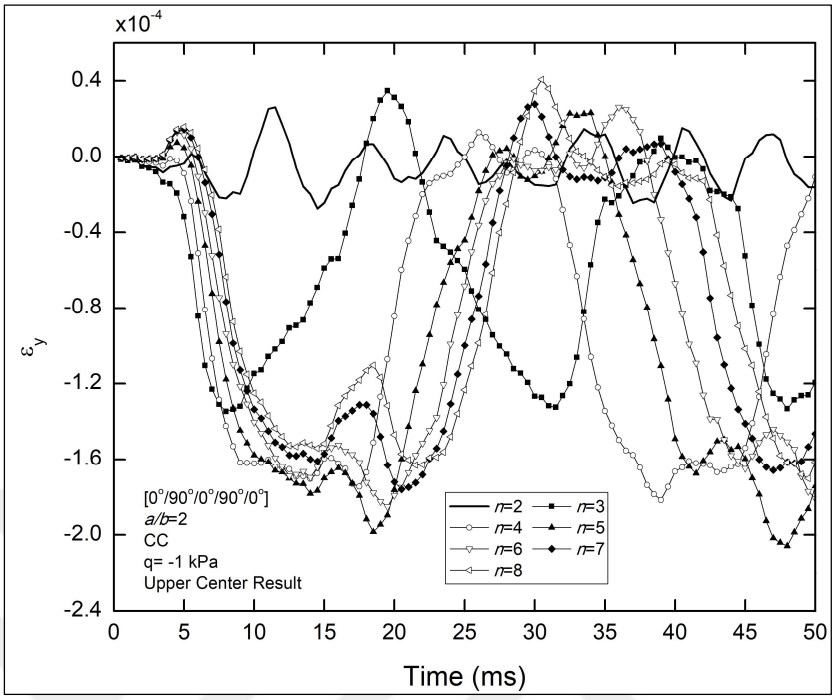

Figure 4.35**:** Strain (in *y* direction) history of super-elliptic shells with different ovalities for CC boundary condition ([0°/90°/0°/90°/0°], at the upper center of tube).

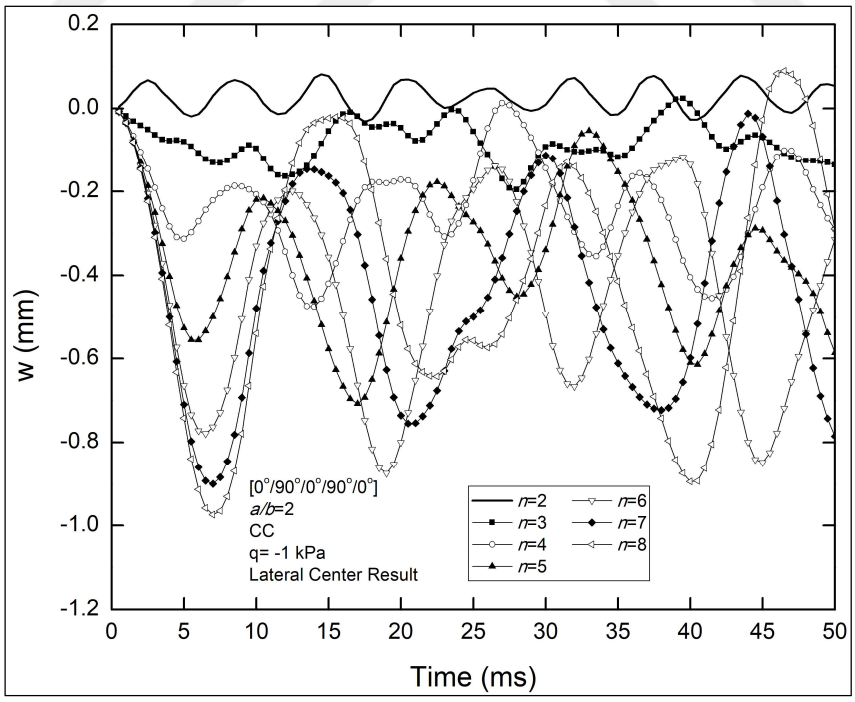

Figure 4.36**:** Transverse displacement history of super-elliptic shells with different ovalities for CC boundary condition ([0°/90°/0°/90°/0°], at the lateral center of tube).

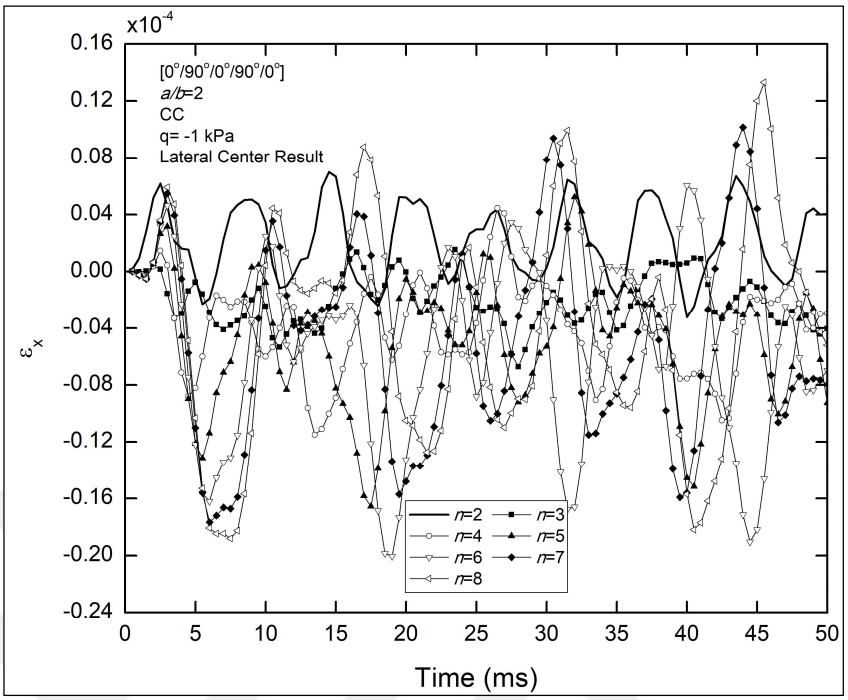

Figure 4.37**:** Strain (in *x* direction) history of super-elliptic shells with different ovalities for CC boundary condition ([0°/90°/0°/90°/0°], at the lateral center of tube).

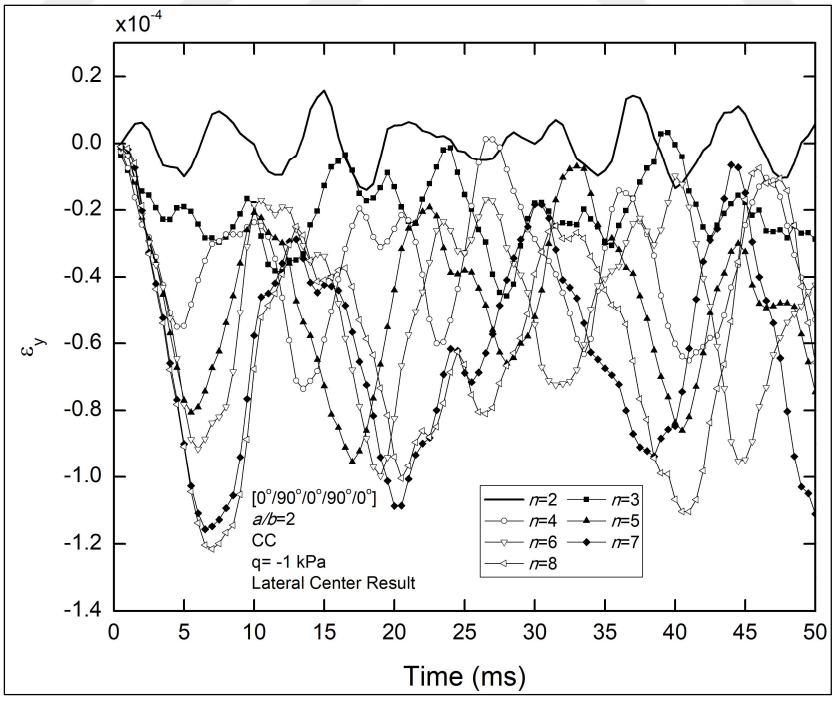

Figure 4.38**:** Strain (in *y* direction) history of super-elliptic shells with different ovalities for CC boundary condition ([0°/90°/0°/90°/0°], at the lateral center of tube).

Figures 4.33 and 4.36 illustrate that displacements increase with increasing values of the ovality for both upper and lateral centers of super-elliptic tube considering CC boundary condition and [0°/90°/0°/90°/0°] stacking scheme. Lowest displacement values are obtained for elliptical tube (n=2). In Figures 4.34 and 4.37, it is seen that ε_x values of elliptical shell (n=2) are remarkably lower than ε_x values for n>2. This interpretation is also valid for ε_y values as can be seen in Figures 4.35 and 4.38. Elliptical shell (n=2) is the stiffest structure for [0°/90°/0°/90°/0°] stacking scheme leading to least displacement values for CC boundary condition. Figures 4.33-38 show that displacement and strain values at the upper center of super-elliptic tube are higher than those at the lateral center.

4.2.2. Effect of Different Stacking Schemes on Non-Linear Dynamic Behavior

In this example, nonlinear transient responses of super-elliptic composite shells for different layer orientation schemes subjected to uniformly distributed load are compared. The effects of cross-ply and angle-ply stacking schemes for composite layers on non-linear transient response are investigated. Layer orientation schemes are considered as [0°/90°/0°/90°/0°], [30°/-30°/30°/-30°/30°] and [60°/-60°/60°/-60°/60°]. Super-elliptic shell dimensions are: a=1 m, b=0.5 m (a/b=2). Ovality values are taken as n=2, 4 and 8. In Figures 4.39-44, non-linear transient responses (transverse displacement at the shell center) of super-elliptic shells (panels) with different stacking schemes are shown for CCCC and CFCF boundary conditions considering ovality values 2, 4 and 8, respectively. In Figures 4.45 and 4.46, non-linear transient responses (transverse displacement at the shell upper and lateral center, respectively) of super-elliptic tubes with different stacking schemes are presented for CC boundary condition considering ovality value n=4. For panel version, 1x8 GDQ elements and 11x9 grids in each element were used in this example. For tube version, 1x16 GDQ elements and 11x9 grids in each element were utilized.

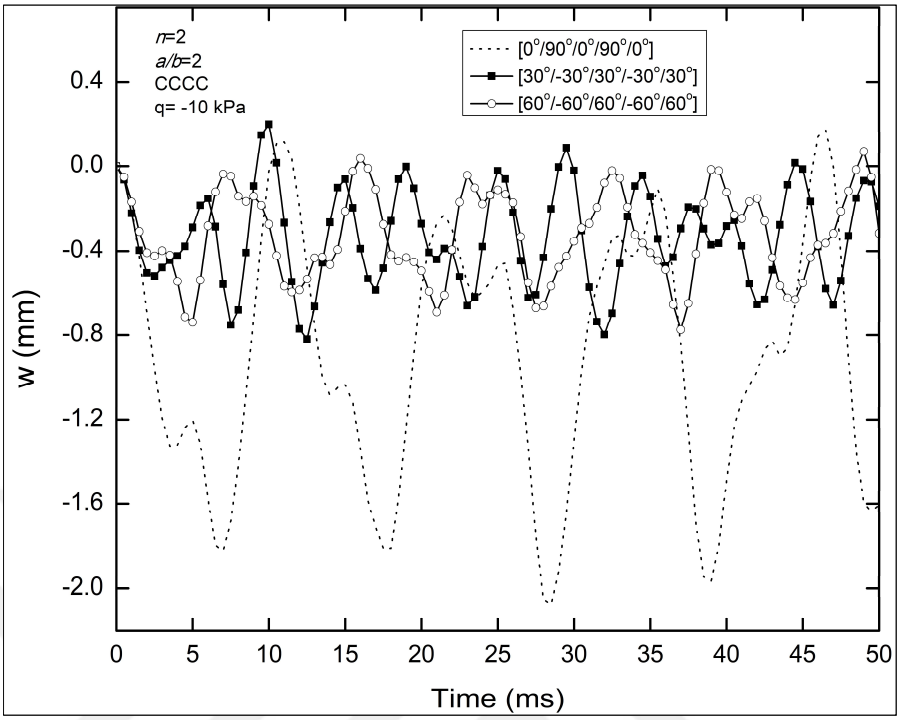

Figure 4.39**:** Transverse displacement history of super-elliptic shells with different layer orientations for CCCC boundary condition (*n*=2).

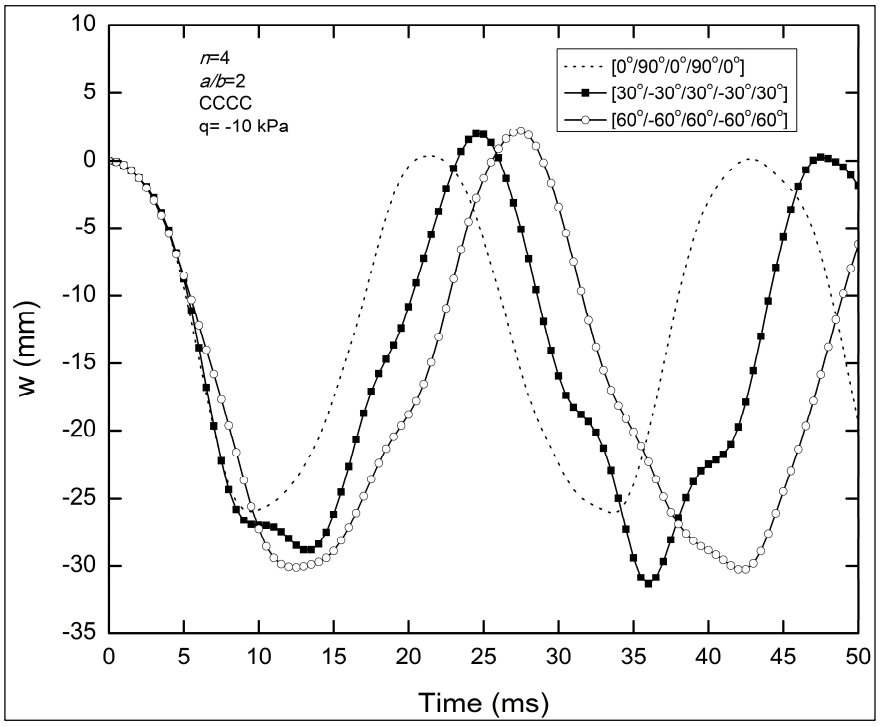

Figure 4.40**:** Transverse displacement history of super-elliptic shells with different layer orientations for CCCC boundary condition (*n*=4).

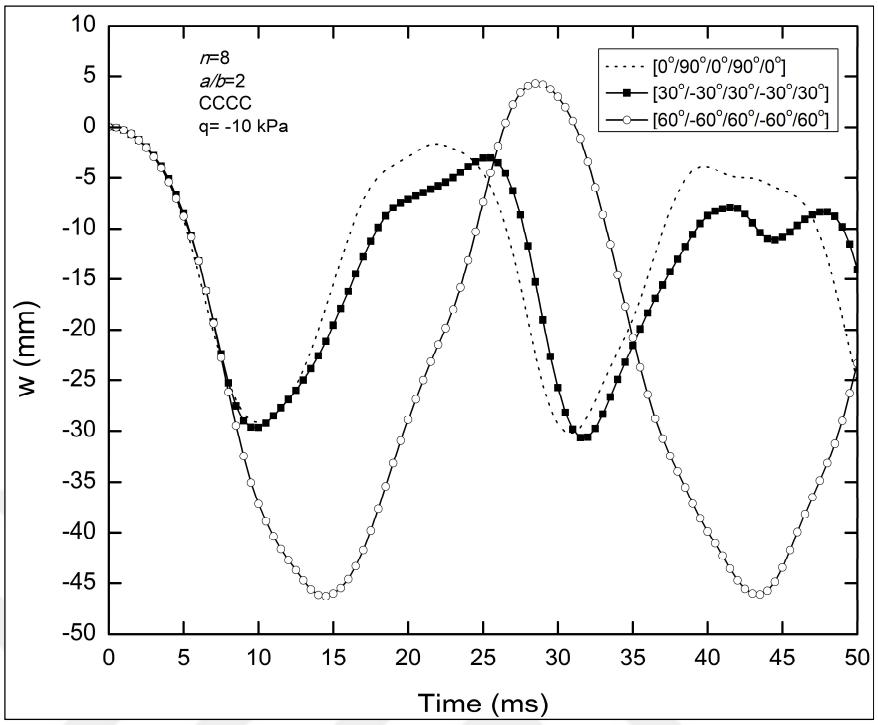

Figure 4.41: Transverse displacement history of super-elliptic shells with different layer orientations for CCCC boundary condition (n=8).

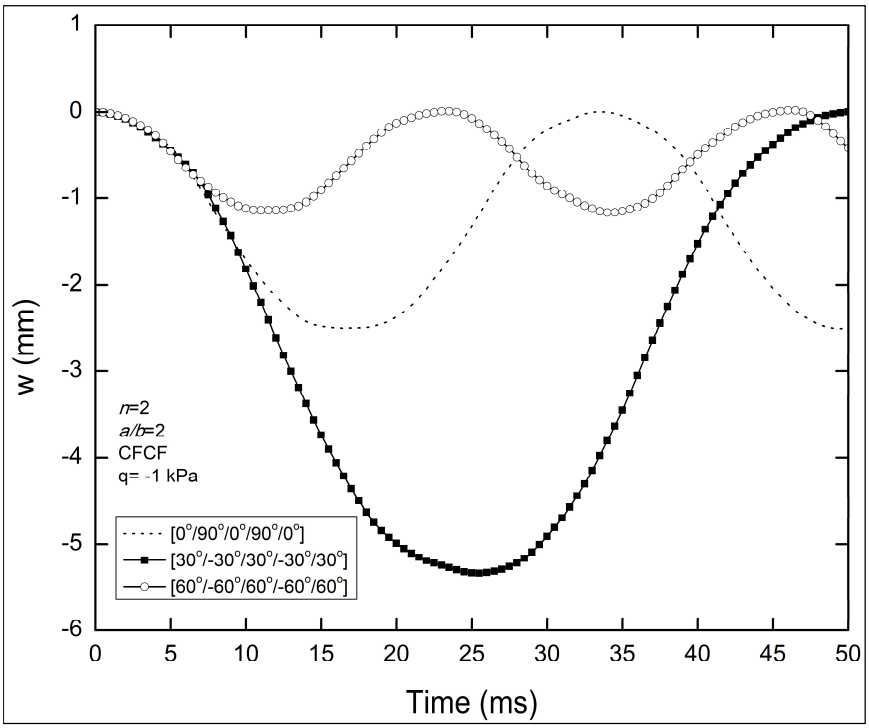

Figure 4.42: Transverse displacement history of super-elliptic shells with different layer orientations for CFCF boundary condition (n=2).

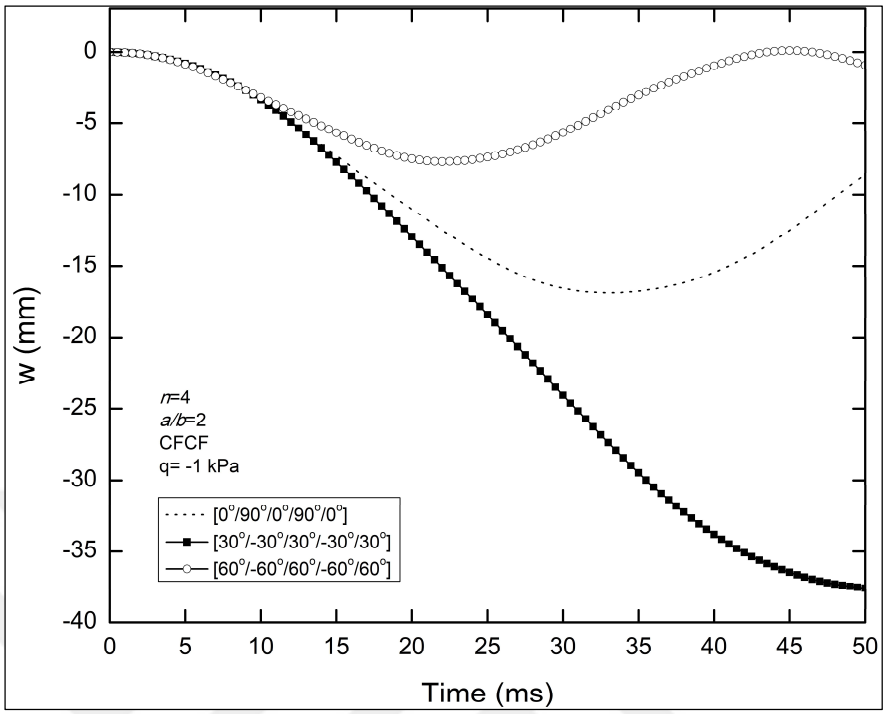

Figure 4.43: Transverse displacement history of super-elliptic shells with different layer orientations for CFCF boundary condition (n=4).

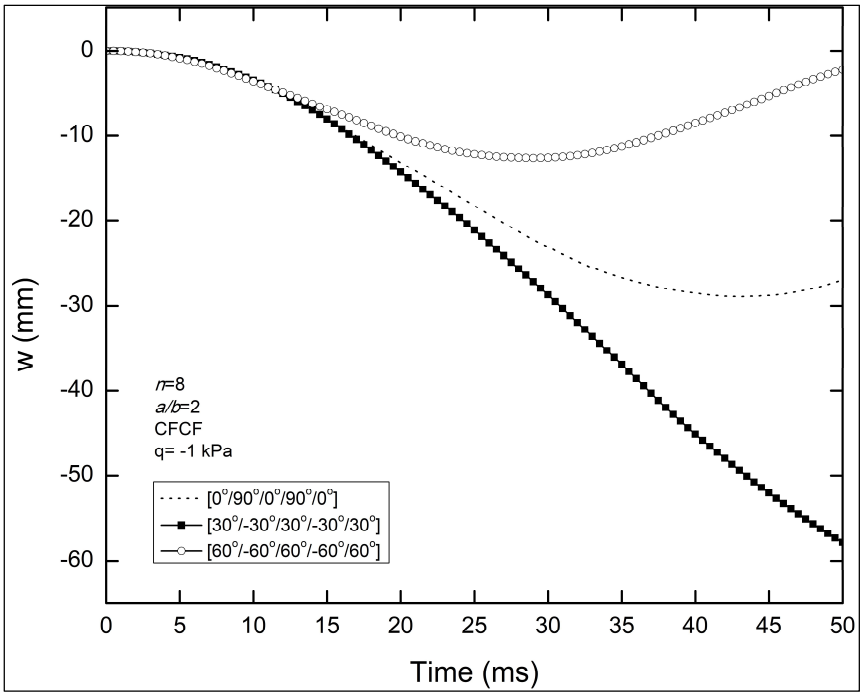

Figure 4.44: Transverse displacement history of super-elliptic shells with different layer orientations for CFCF boundary condition (n=8).

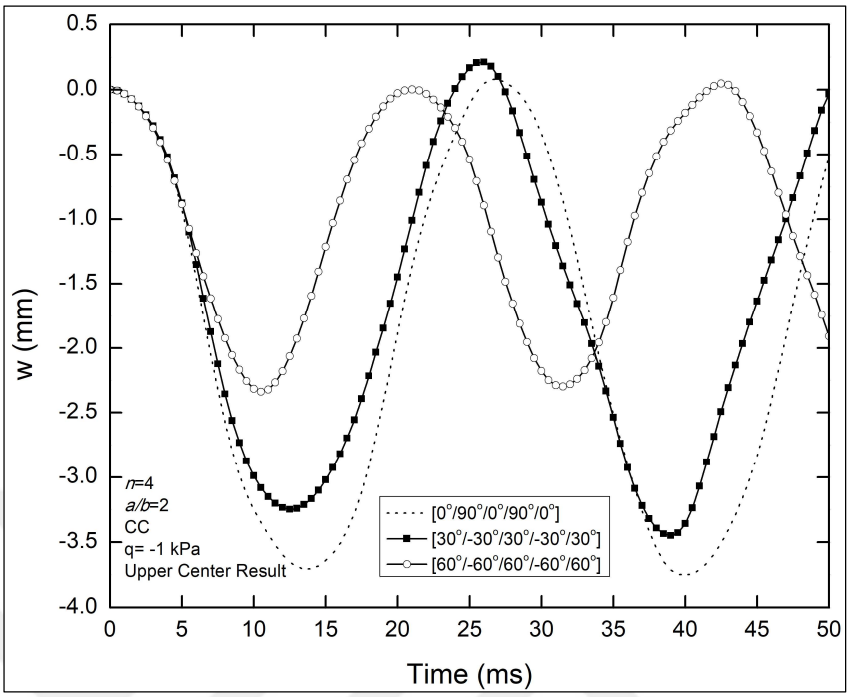

Figure 4.45**:** Transverse displacement history of super-elliptic tubes with different layer orientations for CC boundary condition (*n*=4, at the upper center of tube).

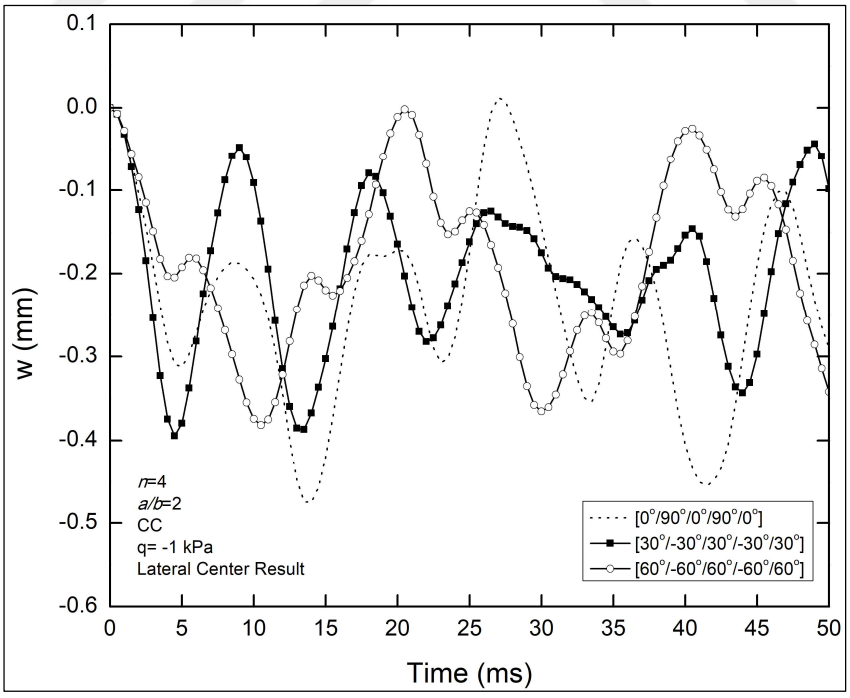

Figure 4.46**:** Transverse displacement history of super-elliptic tubes with different layer orientations for CC boundary condition (*n*=4, at the lateral center of tube).

As seen in Figure 4.39, for CCCC boundary condition, [0°/90°/0°/90°/0°] stacking scheme gives the highest displacement values in magnitude for n=2 and [30°/-30°/30°/-30°/30°] and [60°/-60°/60°/-60°/60°] stacking schemes give similar displacement values. For n=4, [0°/90°/0°/90°/0°] stacking scheme gives the lowest displacement values in magnitude (Figure 4.40). For n=8, [60°/-60°/60°/-60°/60°] stacking scheme gives the highest displacement values in magnitude (Figure 4.41).

In Figures 4.42-44, it is seen that super-elliptic shell (panel) with [60°/-60°/60°/-60°/60°] stacking scheme is the stiffest structure leading to least displacement values for CFCF boundary condition for n=2, 4 and 8.

Regarding CC boundary condition, Figure 4.45 illustrates that super-elliptic tube with ovality n=4 and [60°/-60°/60°/-60°/60°] stacking scheme has the lowest displacements at the upper center of tube. However, at the lateral center of tube, displacements are closer to each other for [30°/-30°/30°/-30°/30°] and [60°/-60°/60°/-60°/60°] stacking schemes (Figure 4.46). For both upper and lateral centers of tube, [0°/90°/0°/90°/0°] stacking scheme leads highest displacement values.

4.2.3. Effect of Ellipticity (a/b) on Non-Linear Dynamic Behavior

In this example, nonlinear transient responses of super-elliptic composite shells (panels) with different ellipticities (a/b) under uniformly distributed load are compared. Super-elliptic shell major radius is taken as a=1 m and ovality values are taken as n=2, 4 and 8. Ellipticity values are taken as a/b=1, 3/2 and 2. Stacking scheme for composite layers is [60°/-60°/60°/-60°/60°]. In Figures 4.47-52, non-linear transient responses (transverse displacement at the shell center) of super-elliptic shells with different ellipticity are shown for CCCC and CFCF boundary conditions for ovality values 2, 4 and 8, respectively. In this example, a mesh of 1x4 GDQ elements and 11x17 grids in each element was used for a/b=1 and a mesh of 1x6 GDQ elements and 11x15 grids in each element was used for a/b=3/2. In other cases, 1x8 GDQ elements and 11x9 grids in each element were used. These element and grid numbers were selected by trial to converge results.

As seen in Figures 4.47 and 4.48, for CCCC boundary condition, there is an increase in transverse displacement values with increasing ellipticity for [60°/-60°/60°/-60°/60°] stacking scheme for n=2 and 4. For n=8, displacement values are

close to each other (Figure 4.49). For CFCF boundary condition (Figure 4.50), displacement values increase in magnitude with increasing ellipticity for n=2. For n=4 and 8, displacement values are close to each other (Figures 4.51 and 4.52). Cylindrical shell (a/b=1 and n=2) leads to lowest displacement values for CCCC and CFCF boundary conditions among the ellipticity and ovality values considered (Figures 4.47 and 4.50).

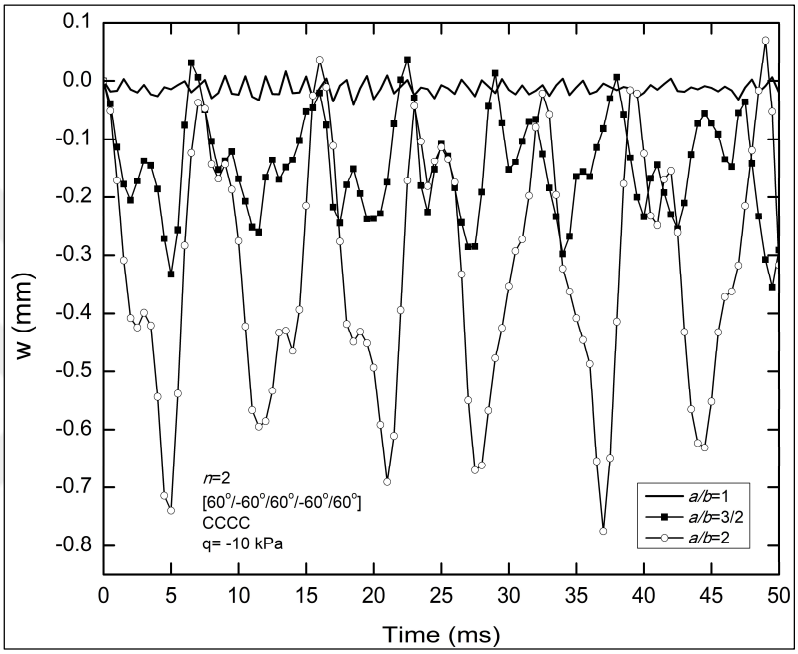

Figure 4.47**:** Transverse displacement history of super-elliptic shells with different ellipticity for CCCC boundary condition (n=2, [60º/-60º/60º/-60º/60º]).

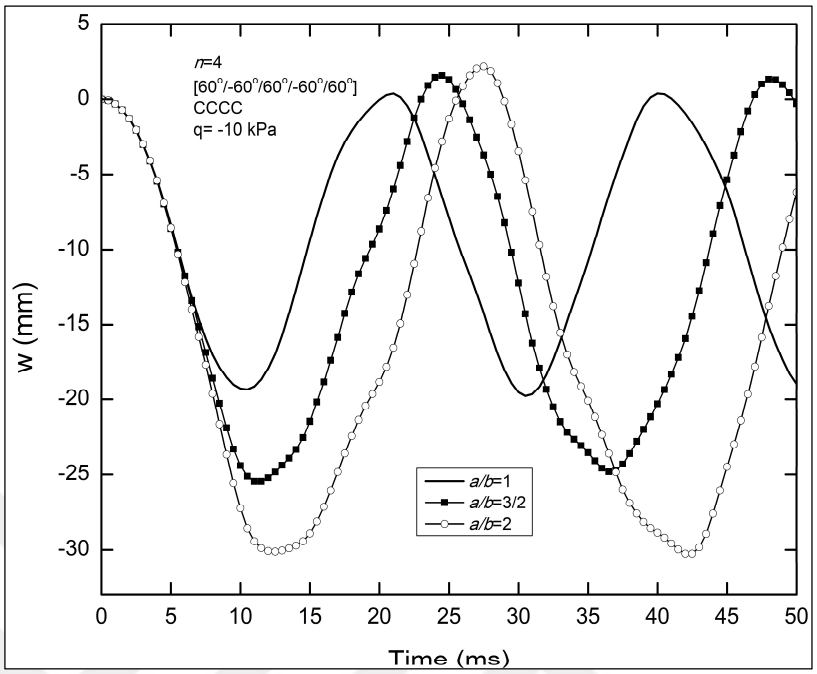

Figure 4.48**:** Transverse displacement history of super-elliptic shells with different ellipticity for CCCC boundary condition (n=4, [60º/-60º/60º/-60º/60º]).

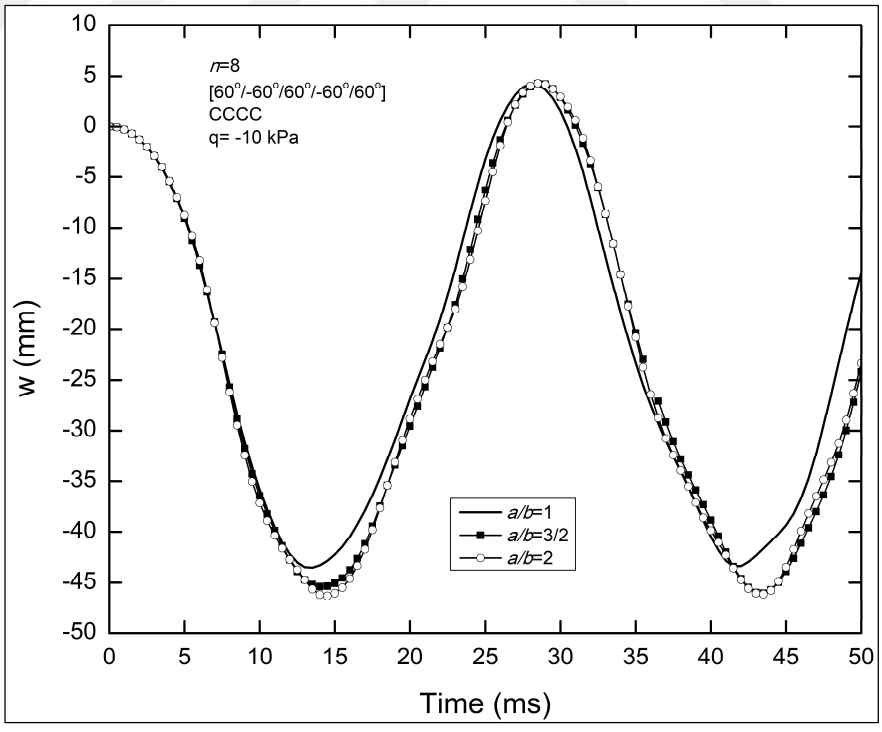

Figure 4.49**:** Transverse displacement history of super-elliptic shells with different ellipticity for CCCC boundary condition (n=8, [60º/-60º/60º/-60º/60º]).

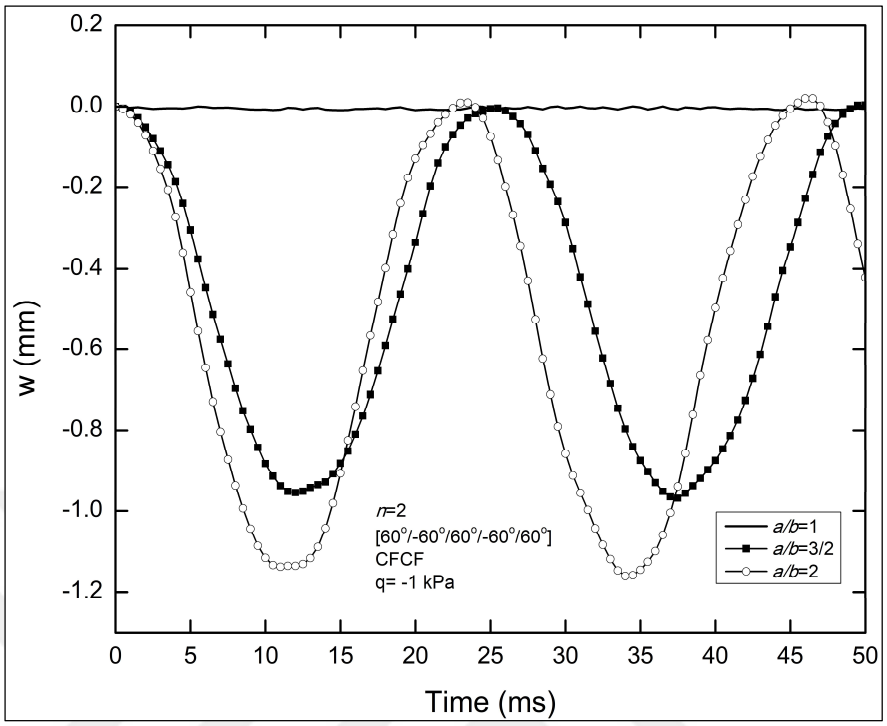

Figure 4.50**:** Transverse displacement history of super-elliptic shells with different ellipticity for CFCF boundary condition (*n*=2, [60º/-60º/60º/-60º/60º]).

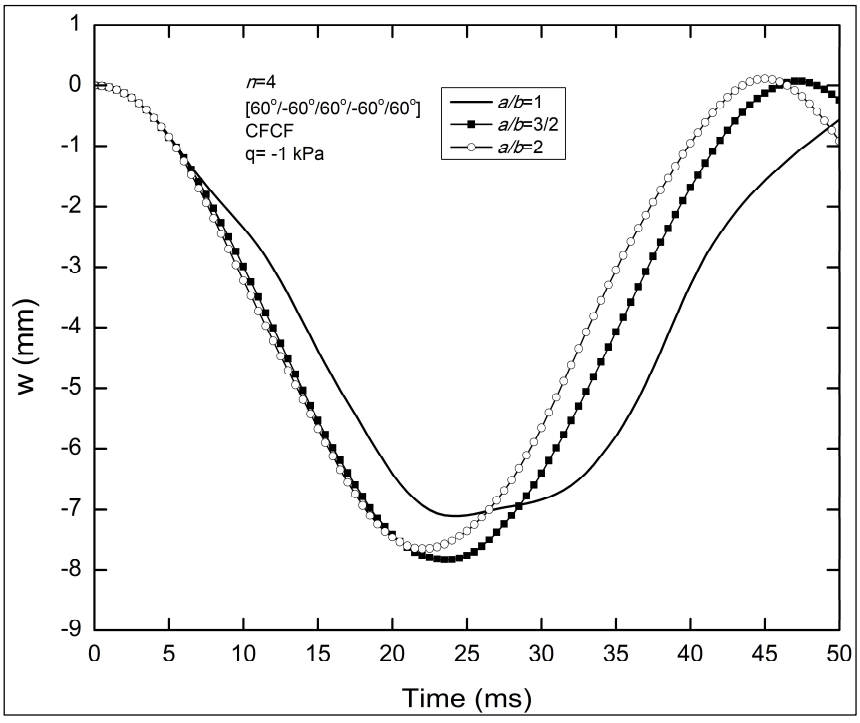

Figure 4.51**:** Transverse displacement history of super-elliptic shells with different ellipticity for CFCF boundary condition (*n*=4, [60º/-60º/60º/-60º/60º]).

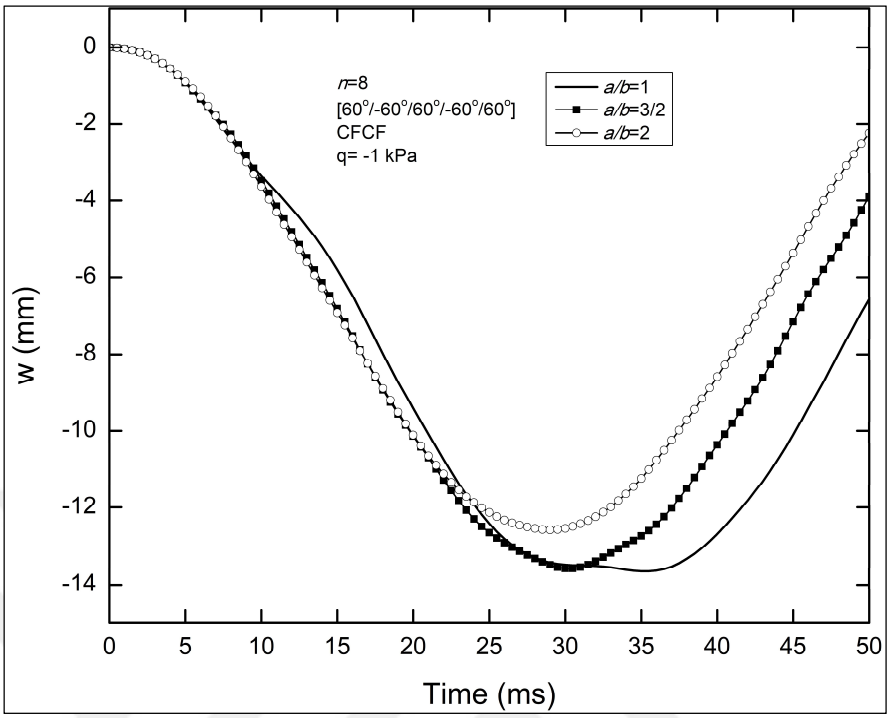

Figure 4.52**:** Transverse displacement history of super-elliptic shells with different ellipticity for CFCF boundary condition (n=8, [60°/-60°/60°/-60°/60°]).

4.3. Examples for FGM Super-Elliptic Shells

Here, effects of ovality (n), FGM material properties, ellipticity (a/b) and boundary conditions on dynamic behavior of FGM super-elliptic shells are examined by solving various examples utilizing GDQ method. In examples, aforementioned material combinations with various volume fraction coefficients (k) are considered.

FGM material specifications utilized in analyses are shown in Table 4.3 [Uysal, 2013]. Five different volume fraction coefficients are considered in the analyses: k=0, 1, 5, 20 and 50 where k=0 represents the case when the structure is completely ceramic. Shell thickness (h) is h=0.025 m and a/h=80, L/h=160 are considered in all the analyses (see Figure 4.53). In Figure 4.53, θ is considered as $\theta = \pi$ radian. However, $\theta = 2\pi$ radian is considered for super-elliptic tube. As illustrated in Figure 4.6, three different boundary conditions are taken into consideration as in section 4.2. Uniformly distributed pressure with step pulse (normal to the surface) is considered as: q=-50 kPa for the cases of CCCC boundary condition and q=-10 kPa for the cases of CFCF and CC boundary conditions. Time step (Δt) is considered as 0.5 ms for all analyses. Transverse displacement results are given in non-dimensional form as w/h.

Table 4.3: Material specifications of FGM.

	Material	E (GPa)	ρ (kg/m^3)	v
Metals	Steel (SUS304)	207	3750	0.26
	Aluminum	70	3000	0.29
	Monel (Ni-Cu)	179.4	2370	0.24
Ceramics	Alumina (Al_2O_3)	320.24	8166	0.31
	Zirconia (ZrO_2)	151	2707	0.26
	Silicon Nitride (Si_3N_4)	322.27	8940	0.368

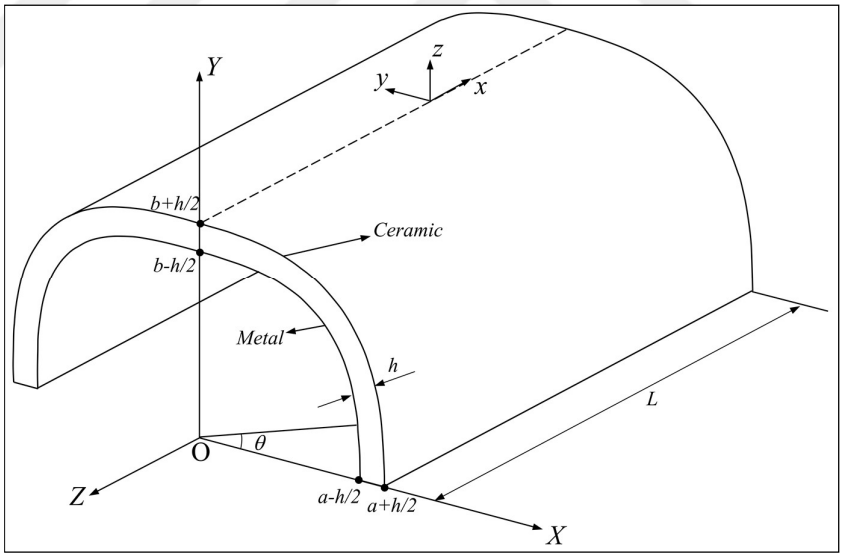

Figure 4.53**:** FGM super-elliptic shell parameters.

4.3.1. Effect of Ovality Value (*n*) on Non-Linear Dynamic Behavior

As a first step, nonlinear dynamic behavior of two different FGM super-elliptic shells (panels) under uniformly distributed pressure is investigated. Geometric characteristics are taken as a=2 m, b=1 m (a/b=2) and ovality values are considered as n=4 and n=8. In this example, Zirconia/Aluminum material with volume fraction

coefficient k=20 is considered. Non-dimensional transverse displacement, stress and strain time histories at FGM super-elliptic shell center (strain and stress values are taken from top surface) are obtained considering CCCC and CFCF cases. Comparisons of present results with finite element solutions are illustrated in Figures 4.55 and 4.56. A grid convergence study is performed for GDQ analysis. In Figure 4.54, it is seen that for the same element number (1x8 element in x and y directions, respectively) 11x9 grids are found to be sufficient, therefore these element and grid numbers are adopted in the cases unless otherwise specified. A script is written using ANSYS Parametric Design Language (APDL) to obtain finite element solution. FGM material is modeled using four-noded quadrilateral shell elements which have 100 layers in z direction. 50x60 elements are utilized in the finite element solution after performing a mesh convergence study as shown in Tables 4.4 and 4.5. Results of GDQ and finite element solutions are very close to each other. In addition, GDQ solution is more advantageous than finite element solution in terms of the number of grids utilized in the analyses.

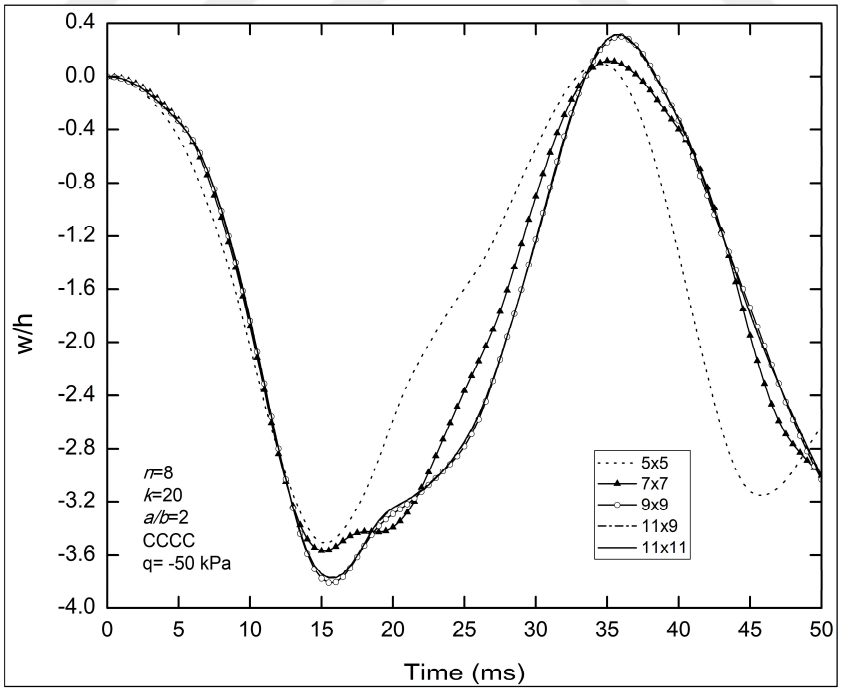

Figure 4.54**:** Time history of non-dimensional displacement at FGM super-elliptic shell center for different grid numbers (1x8 elements).

Table 4.4: Natural frequency values (Hz) of FGM super-elliptic shell (CCCC, a/b=2, n=4, Zirconia/Aluminum, k=20) considering different mesh numbers.

	15x20 elements	30x40 elements	50x60 elements	60x80 elements
Mode 1	27.197	26.439	26.303	26.257
Mode 2	44.378	43.144	42.909	42.845
Mode 3	49.992	48.147	47.818	47.706

Table 4.5: Natural frequency values (Hz) of FGM super-elliptic shell (CCCC, a/b=2, n=8, Zirconia/Aluminum, k=20) considering different mesh numbers.

	15x20 elements	30x40 elements	50x60 elements	60x80 elements
Mode 1	17.274	16.753	16.661	16.631
Mode 2	33.291	32.338	32.156	32.114
Mode 3	35.818	33.996	33.674	33.563

Secondly, the effect of ovality value on nonlinear dynamic response of FGM super-elliptic shells (panels) under uniformly distributed pressure is investigated. In this context, seven different ovality values n=2, 3, 4, 5, 6, 7, and 8 are considered. Geometric characteristics of super-elliptic shells are taken as: a=2 m, b=1 m (a/b=2). In this example, analyses are performed for Alumina/Steel (Al_2O_3/Steel), Zirconia/Aluminum (ZrO_2/Al), Alumina/Aluminum (Al_2O_3/Al), Zirconia/Monel (ZrO_2/Ni-Cu) and Silicon Nitride/Steel (Si_3N_4/Steel) materials and volume fraction coefficient k=1 for each material is considered. Time histories of non-dimensional transverse displacement at FGM super-elliptic shell centers are plotted in Figures 4.57-61 and Figures 4.62-66 considering CCCC and CFCF cases, respectively. In the analyses, 1x8 GDQ elements and 11x9 grids in each element were utilized to obtain converged results.

Figures 4.57-66 show that the increase in the ovality values led to an increase in displacement values for both boundary conditions considering all material combinations. Lowest displacement values are obtained in the elliptical shell case (n=2) for all FGMs prescribed above and FGM super-elliptic shells made of Zirconia/Aluminum have highest displacement values for both boundary conditions. From the Figures 4.57-61, one can see that nonlinear transient responses get closer to

each other for ovality values $n>4$ for material combinations except Zirconia/Aluminum. FGM super-elliptic shells made of Zirconia/Aluminum have closer transient responses for ovality values $n>3$.

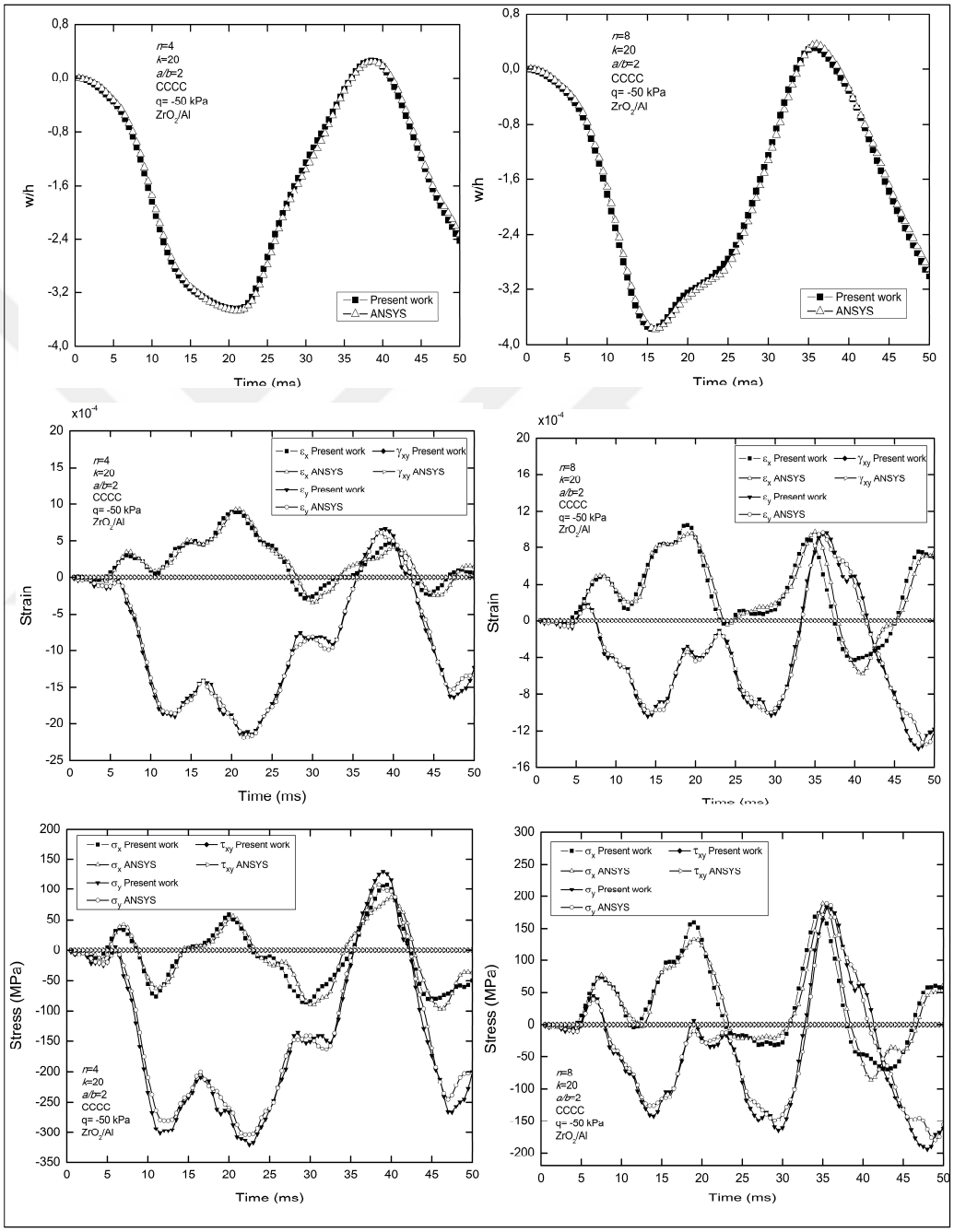

Figure 4.55**:** Time histories of non-dimensional transverse displacement, strain and stress at FGM super-elliptic shell center (CCCC, n=4 (left) and n=8 (right), Zirconia/Aluminum, k=20).

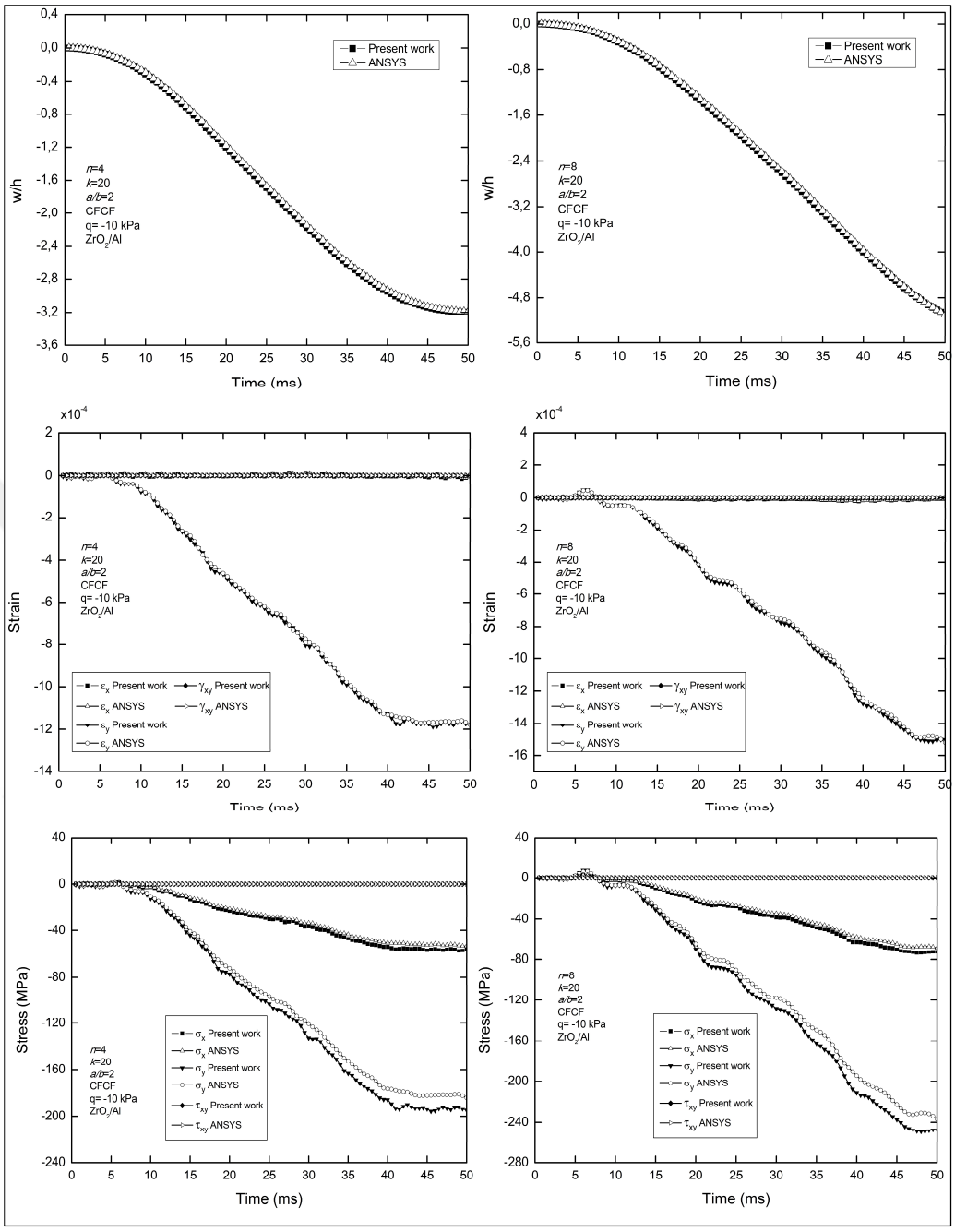

Figure 4.56**:** Time histories of non-dimensional transverse displacement, strain and stress at FGM super-elliptic shell center (CFCF, *n*=4 (left) and *n*=8 (right), Zirconia/Aluminum, *k*=20).

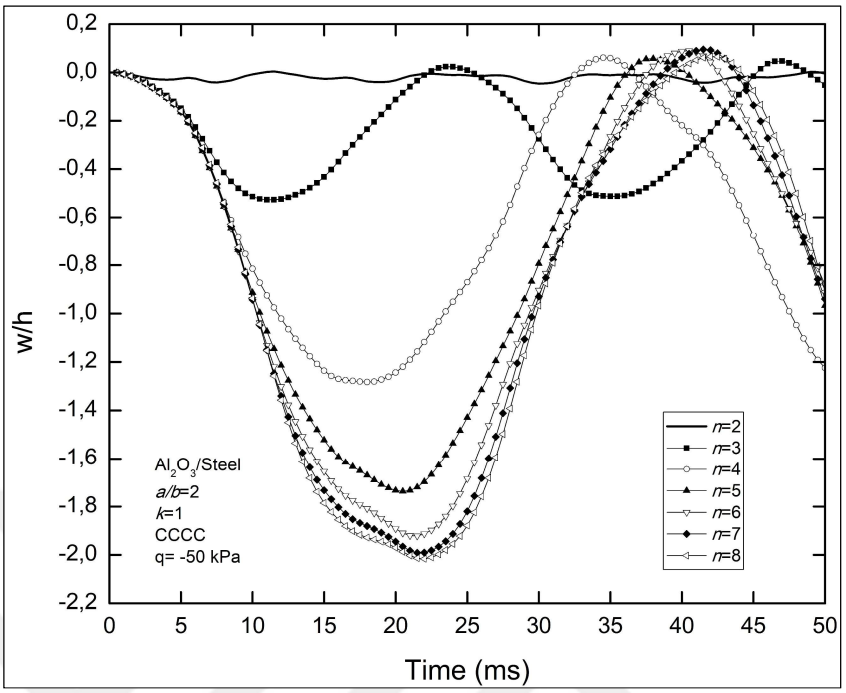

Figure 4.57**:** The effect of ovality value (*n*) on transverse displacement time history (CCCC, Aluminum/Steel, *k*=1).

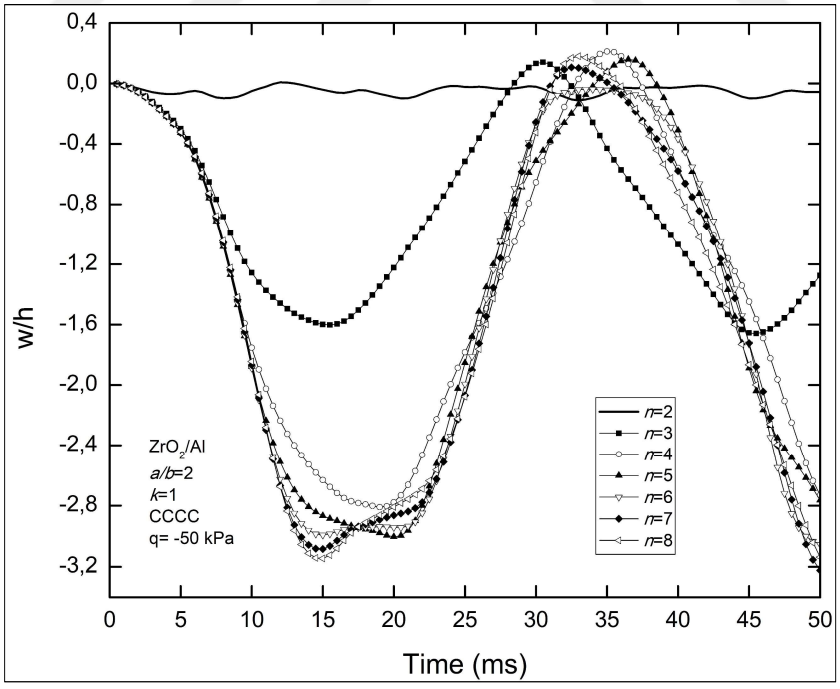

Figure 4.58**:** The effect of ovality value (*n*) on transverse displacement time history (CCCC, Zirconia/Aluminum, *k*=1).

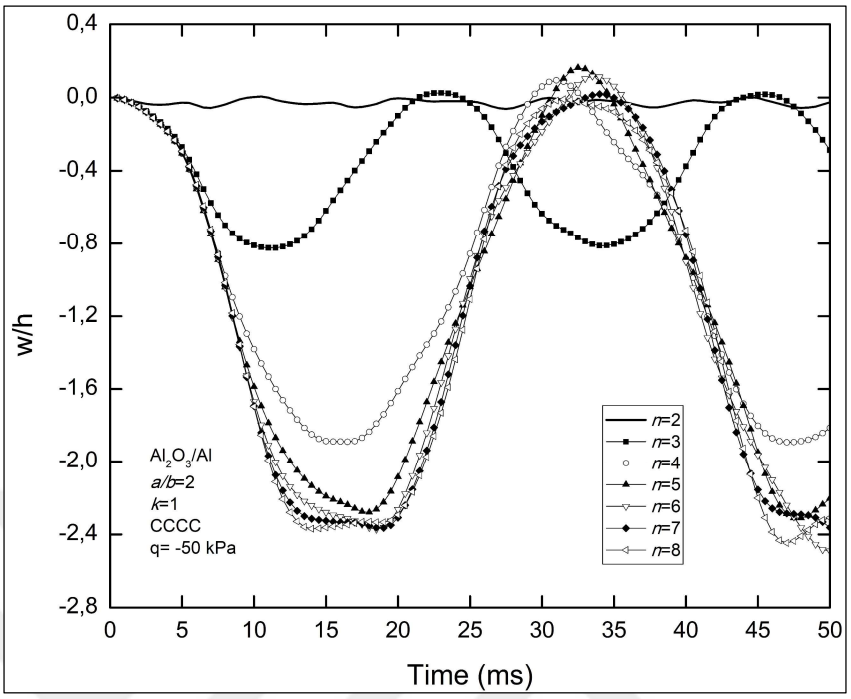

Figure 4.59**:** The effect of ovality value (*n*) on transverse displacement time history (CCCC, Aluminum/Alumina, *k*=1).

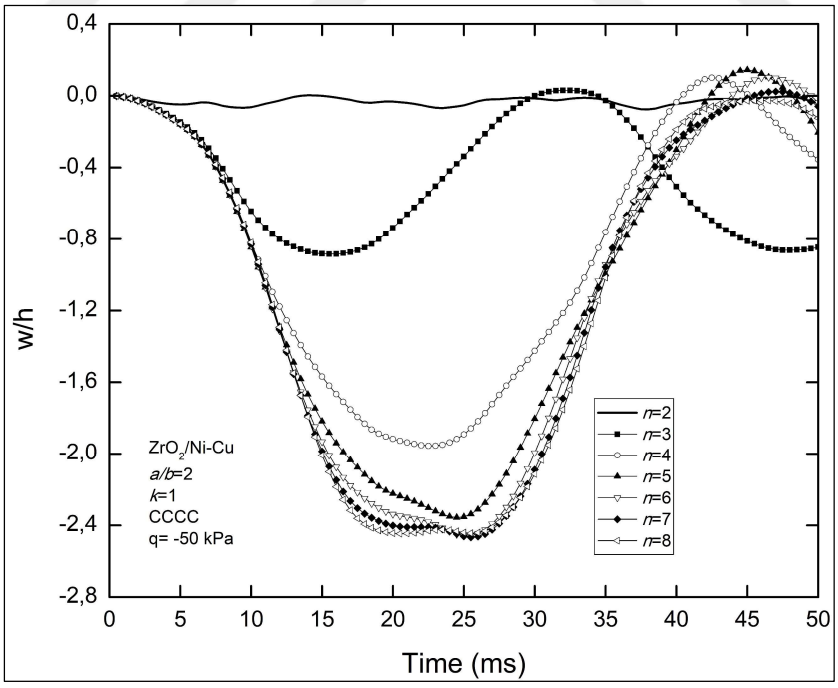

Figure 4.60**:** The effect of ovality value (*n*) on transverse displacement time history (CCCC, Zirconia/Monel, *k*=1).

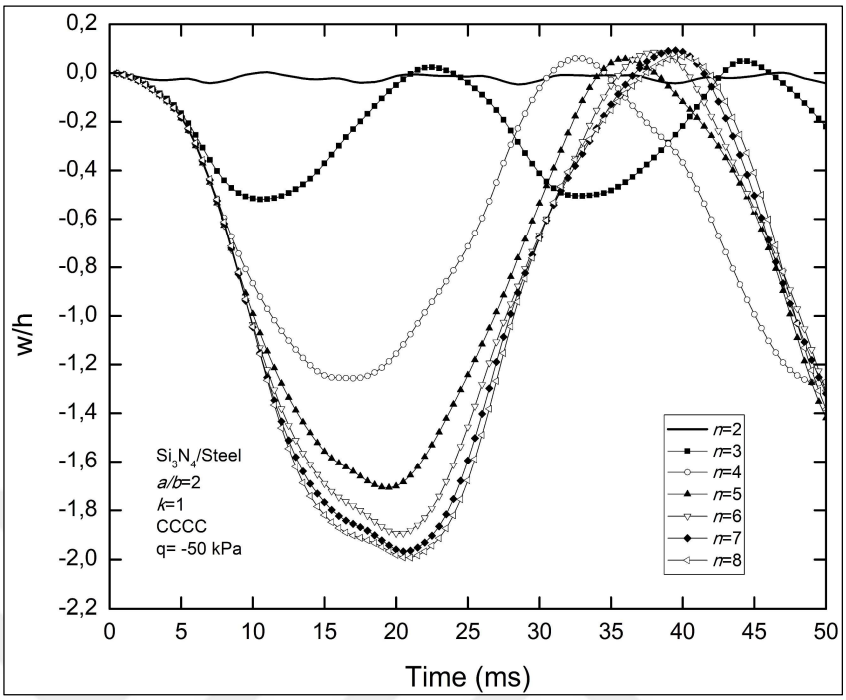

Figure 4.61**:** The effect of ovality value (*n*) on transverse displacement time history (CCCC, Silicon Nitride/Steel, *k*=1).

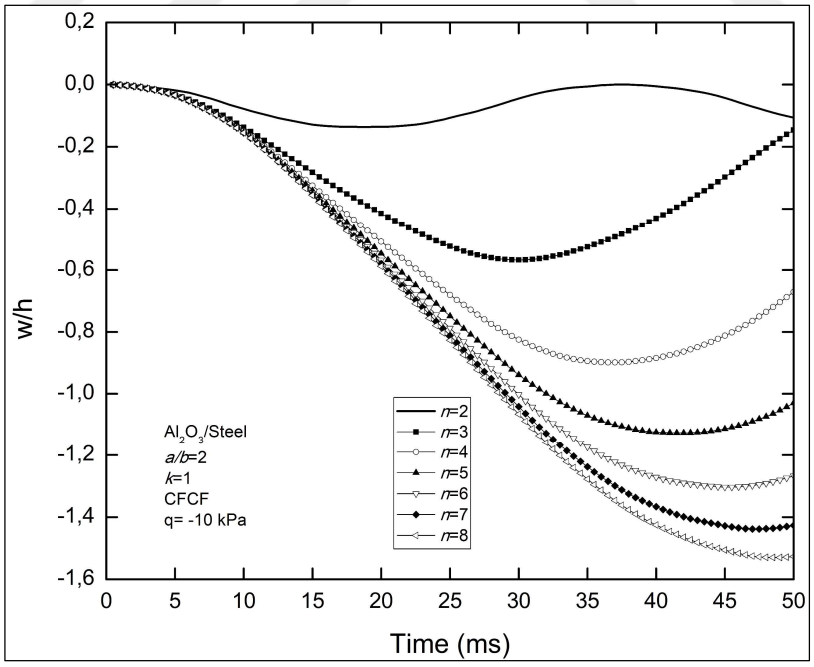

Figure 4.62**:** The effect of ovality value (*n*) on transverse displacement time history (CFCF, Aluminum/Steel, *k*=1).

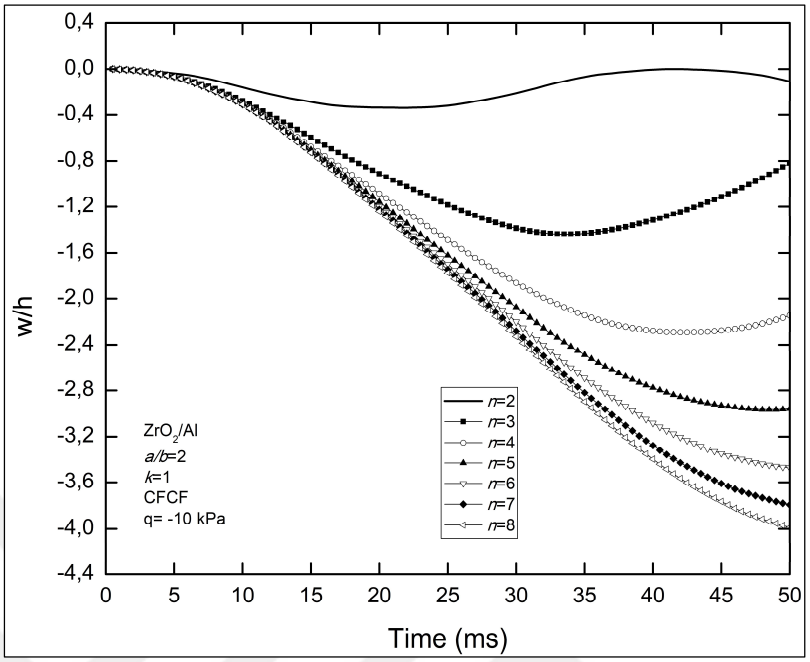

Figure 4.63**:** The effect of ovality value (*n*) on transverse displacement time history (CFCF, Zirconia/Aluminum, *k*=1).

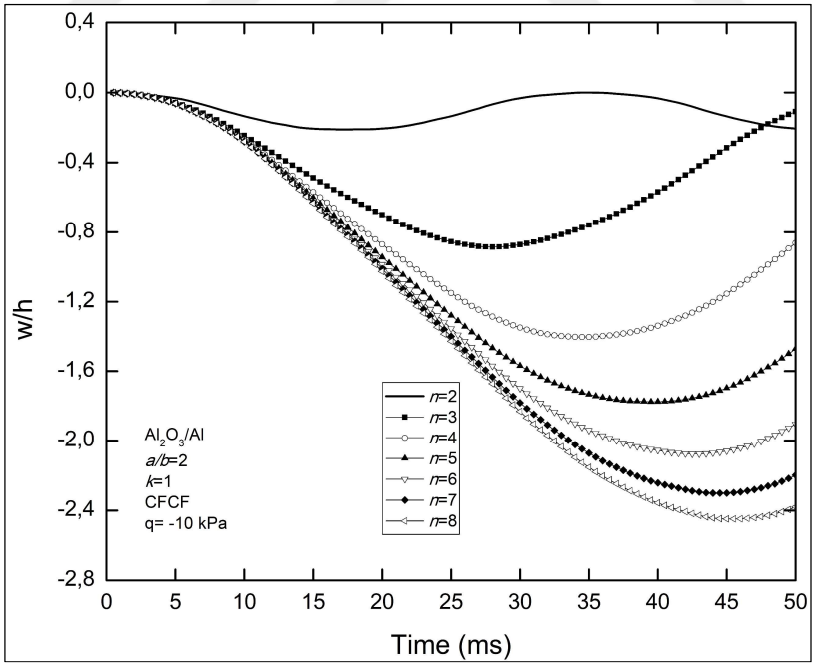

Figure 4.64**:** The effect of ovality value (*n*) on transverse displacement time history (CFCF, Aluminum/Alumina, *k*=1).

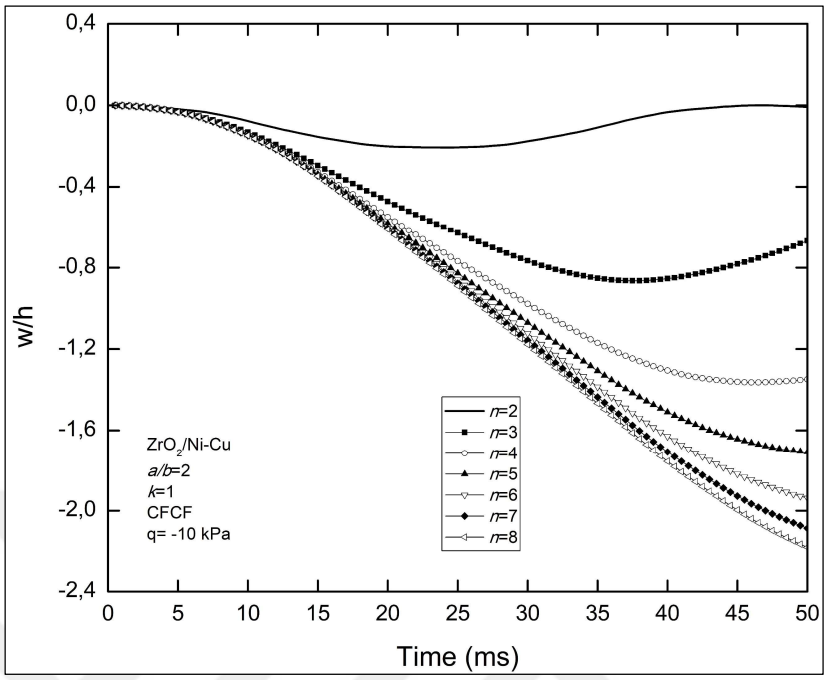

Figure 4.65**:** The effect of ovality value (*n*) on transverse displacement time history (CFCF, Zirconia/Monel, *k*=1).

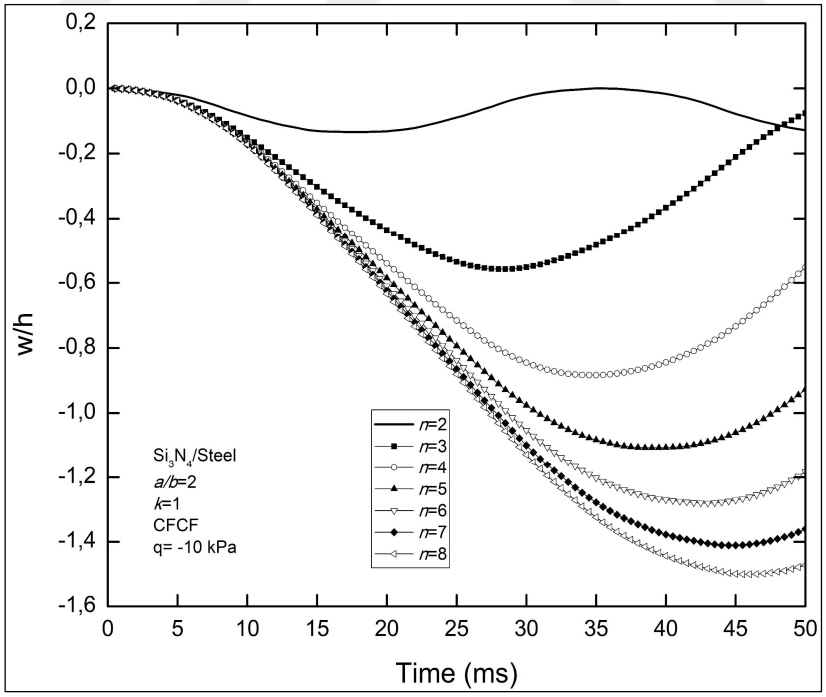

Figure 4.66**:** The effect of ovality value (*n*) on transverse displacement time history (CFCF, Silicon Nitride/Steel, *k*=1).

Lastly, nonlinear dynamic behavior of FGM super-elliptic shells (tubes) with different ovality values under uniformly distributed pressure is investigated. In this example, super-elliptic tube dimensions are taken as the same in the previous example (a=2 m, b=1 m and a/b=2). Regarding CC boundary condition, analyses are performed for Zirconia/Aluminum (ZrO_2/Al) material pair with volume fraction coefficient of k=2. In Figures 4.67 and 4.68 non-dimensional transverse displacement time histories at FGM super-elliptic tube upper and lateral centers are presented, respectively. In the analyses, 1x16 GDQ elements and 11x9 grids in each element were utilized to obtain converged results.

Figures 4.68 and 4.68 illustrate that the increase in the ovality values led to an increase in displacement values for both upper and lateral centers of super-elliptic tube. Lowest displacement values are observed in the elliptical shell case (n=2). From the Figure 4.67, it can be seen that nonlinear transient responses at the upper center of tube get closer to each other with increasing values of n. In addition, displacement values at the upper center of super-elliptic tube are much higher than those at the lateral center.

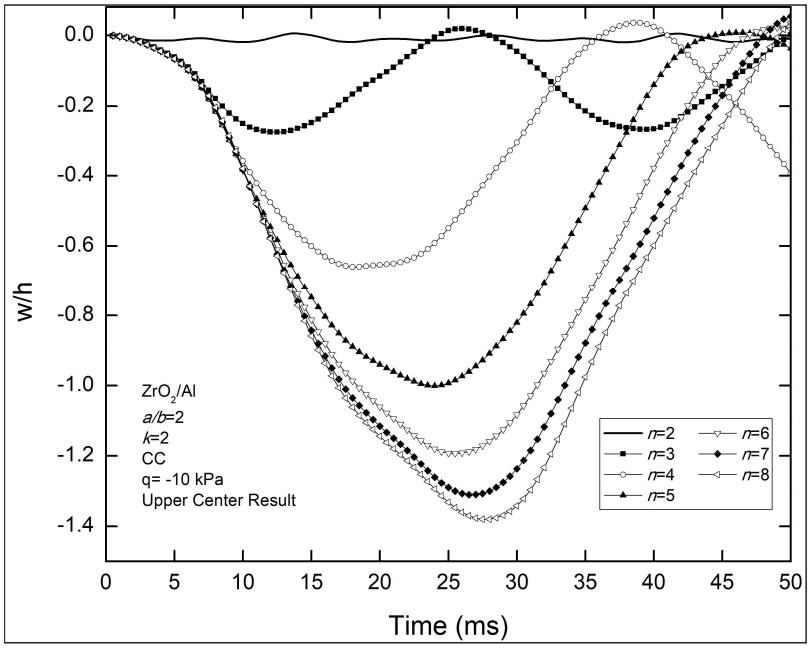

Figure 4.67**:** The effect of ovality value (n) on transverse displacement time history (CC, Zirconia/Aluminum, k=2, at the upper center of tube).

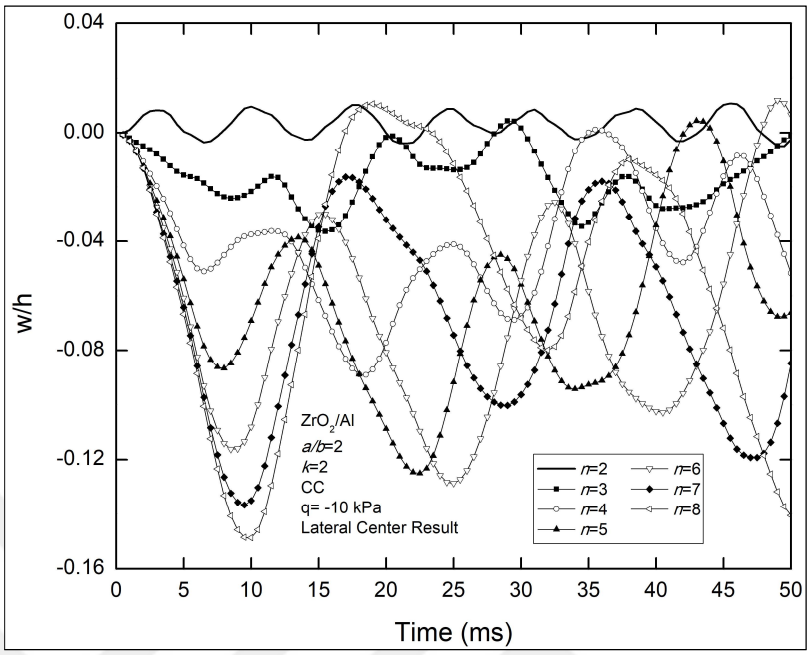

Figure 4.68**:** The effect of ovality value (*n*) on transverse displacement time history (CC, Zirconia/Aluminum, *k*=2, at the lateral center of tube).

4.3.2. Super-Elliptic Shells Made of Different FGMs

Here, the effect of different FGM material pairs on nonlinear transient behavior is examined using five different material combinations namely Alumina/Steel (Al_2O_3/Steel), Zirconia/Aluminum (ZrO_2/Al), Alumina/Aluminum (Al_2O_3/Al), Zirconia/Monel (ZrO_2/Ni-Cu) and Silicon Nitride/Steel (Si_3N_4/Steel). Geometric characteristics of super-elliptic shells are taken as a=2 m, b=1 m (a/b=2). Ovality and volume fraction coefficient values are considered as n=2, 4, 8 and k=1, respectively. Figures 4.69 and 4.70 show non-dimensional transverse displacement time histories at FGM super-elliptic shell (panel) centers made of different FGMs with ovality values 2, 4, 8 considering CCCC and CFCF cases, respectively. 1x8 GDQ elements and in each element 11x9 grids were utilized.

Figure 4.69 (a) shows that Zirconia/Aluminum material pair has the largest displacement values for fully clamped boundary condition and ovality value n=2. As seen in Figures 4.69 (b) and (c), same result is valid for ovality values n=4 and 8. Displacements are nearly identical for Alumina/Steel and Silicon Nitride/Steel material pairs. The vibration amplitude of Alumina/Aluminum and Zirconia/Monel are very close to each other. However, the frequency of transient response of

Zirconia/Monel is lower than that of Alumina/Aluminum. This may be due to mass of Zirconia/Monel is higher than that of Alumina/Aluminum. From Figure 4.70, one can see that Zirconia/Aluminum material pair has the largest displacement values considering CFCF case and ovality values n=2, 4 and 8. Alumina/Steel and Silicon Nitride/Steel have almost the same transient responses.

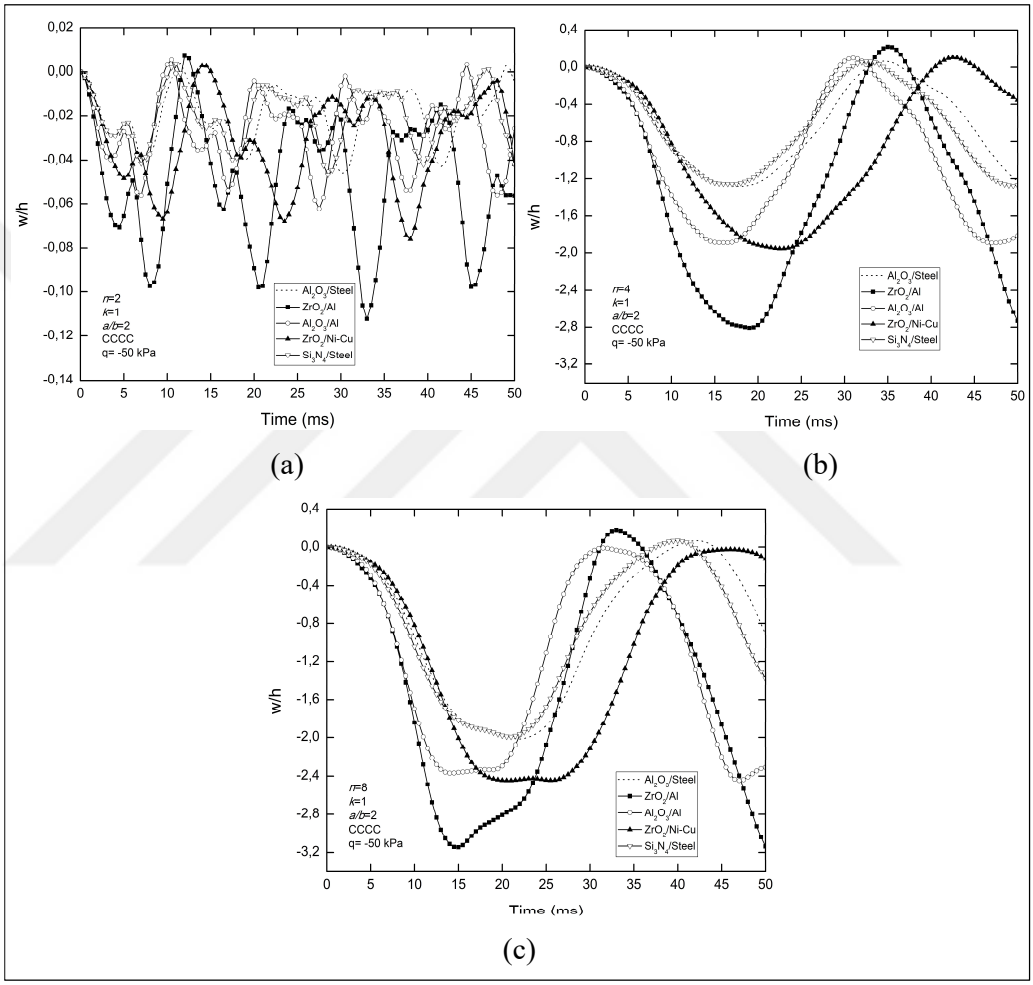

Figure 4.69**:** Non-dimensional transverse displacement time history of FGM super-elliptic shells made of different FGMs (CCCC, k=1): (a) ovality value n=2; (b) ovality value n=4; (c) ovality value n=8.

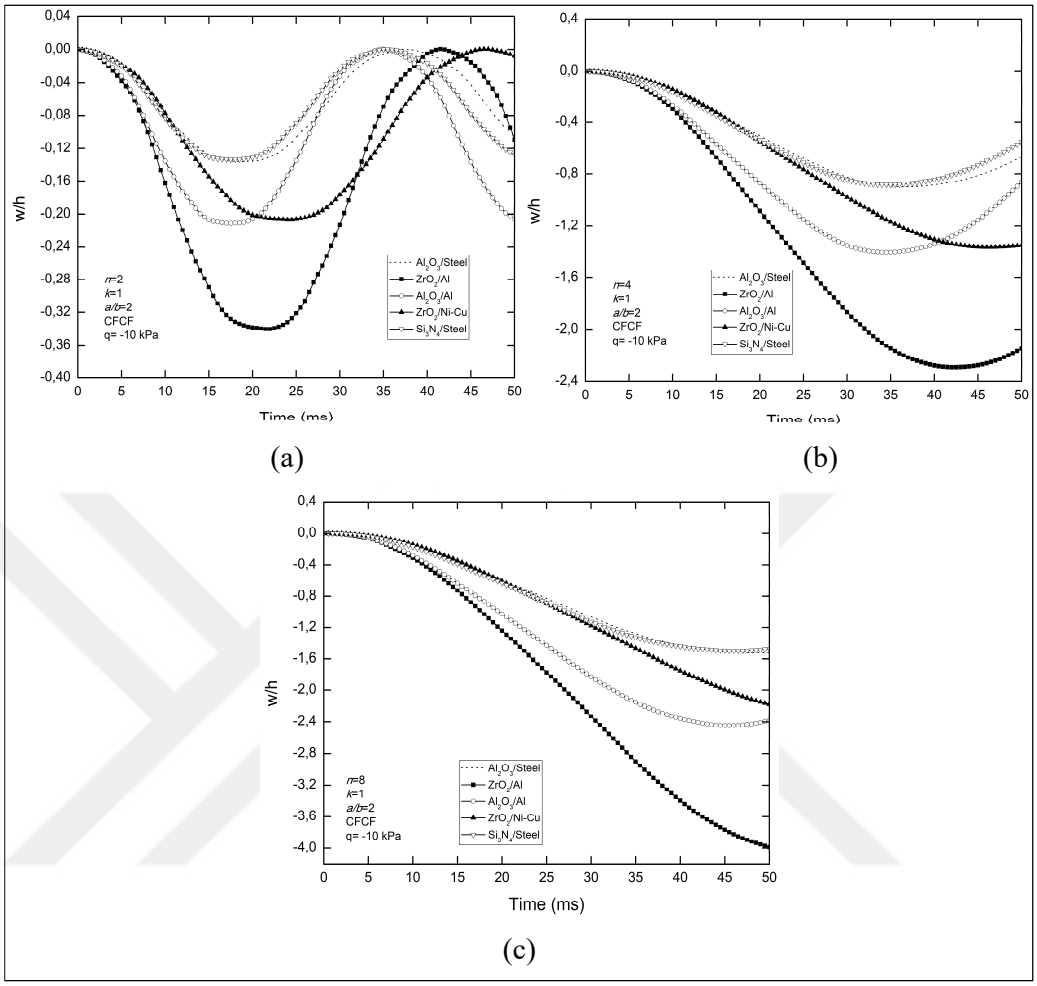

Figure 4.70**:** Non-dimensional transverse displacement time history of FGM super-elliptic shells made of different FGMs (CFCF, k=1): (a) ovality value n=2; (b) ovality value n=4; (c) ovality value n=8.

In addition, regarding CC boundary condition, effect of different material pairs on nonlinear dynamic behavior of super-elliptic tubes is investigated. Geometric characteristics are considered the same as the previous example (a=2 m, b=1 m and a/b=2). Figures 4.71 and 4.72 show non-dimensional transverse displacement time histories at FGM super-elliptic tube upper and lateral centers considering ovality value n=4 and volume fraction coefficient k=2, respectively. 1x16 GDQ elements and in each element 11x9 grids were utilized.

As it is seen in Figures 4.71 and 4.72, super-elliptic tube made of Zirconia/Aluminum material pair has the largest displacement values. Displacements are almost identical for Alumina/Steel and Silicon Nitride/Steel material pairs as in the panel versions. In the previous example, the vibration amplitude of

Alumina/Aluminum and Zirconia/Monel are very close to each other (see Figures 4.69 (b) and 4.70 (b)). However, in this example, the vibration amplitude of Zirconia/Monel is lower than that of Alumina/Aluminum because volume fraction number is considered as k=2.

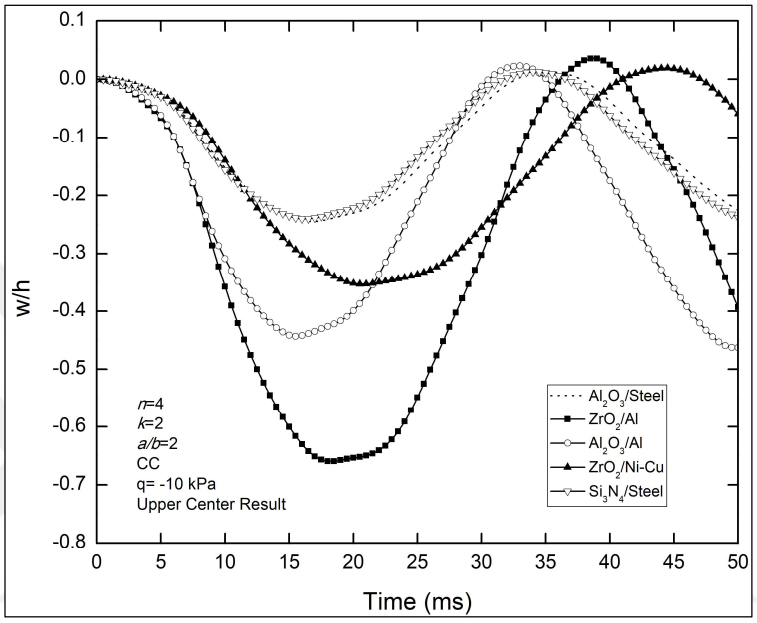

Figure 4.71**:** Non-dimensional transverse displacement time history of FGM super-elliptic shells made of different FGMs (CC, n=4, k=2, at the upper center of tube).

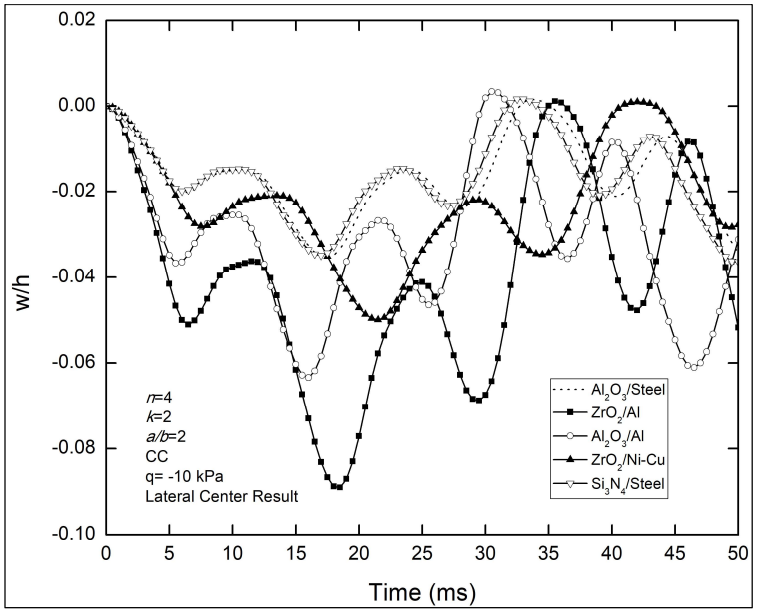

Figure 4.72**:** Non-dimensional transverse displacement time history of FGM super-elliptic shells made of different FGMs (CC, n=4, k=2, at the lateral center of tube).

4.3.3. Effect of Volume Fraction Coefficient (k) on Nonlinear Dynamic Behavior

In this section, effect of volume fraction coefficient (k) on nonlinear dynamic behavior of FGM super-elliptic shells (panels) is investigated. In this context, five different volume fraction coefficients k=0, 1, 5, 20 and 50 are considered. Geometric characteristics are taken as: a=2 m, b=1 m (a/b=2). In this example, analyses are performed for aforementioned material combinations and ovality value is taken as n=4. Non-dimensional transverse displacement time histories at FGM super-elliptic shell centers considering CCCC case are plotted in Figure 4.73 for each FGM. Similarly, in Figure 4.74, non-dimensional transverse displacement histories are presented for each FGM considering CFCF case. In the analyses, 1x8 GDQ elements and 11x9 grids in each element was used to obtain converged results.

Figure 4.73 shows that as the volume fraction coefficient (k) value increases, transverse displacement values show an increasing trend considering all FGMs excluding Zirconia/Monel for CCCC case. Likewise, one can conclude that same result is valid for CFCF boundary condition (Figure 4.74). Alumina/Aluminum has the highest change in displacement with increasing volume fraction coefficient and Zirconia/Monel has the lowest change in displacement with increasing volume fraction coefficient for both boundary conditions. Figures 4.73 and 4.74 show that transient responses are very similar for volume fraction coefficient values higher than 20. Nevertheless, the difference between the transient responses of Alumina/Aluminum with k=20 and k=50 is higher than that of other FGMs.

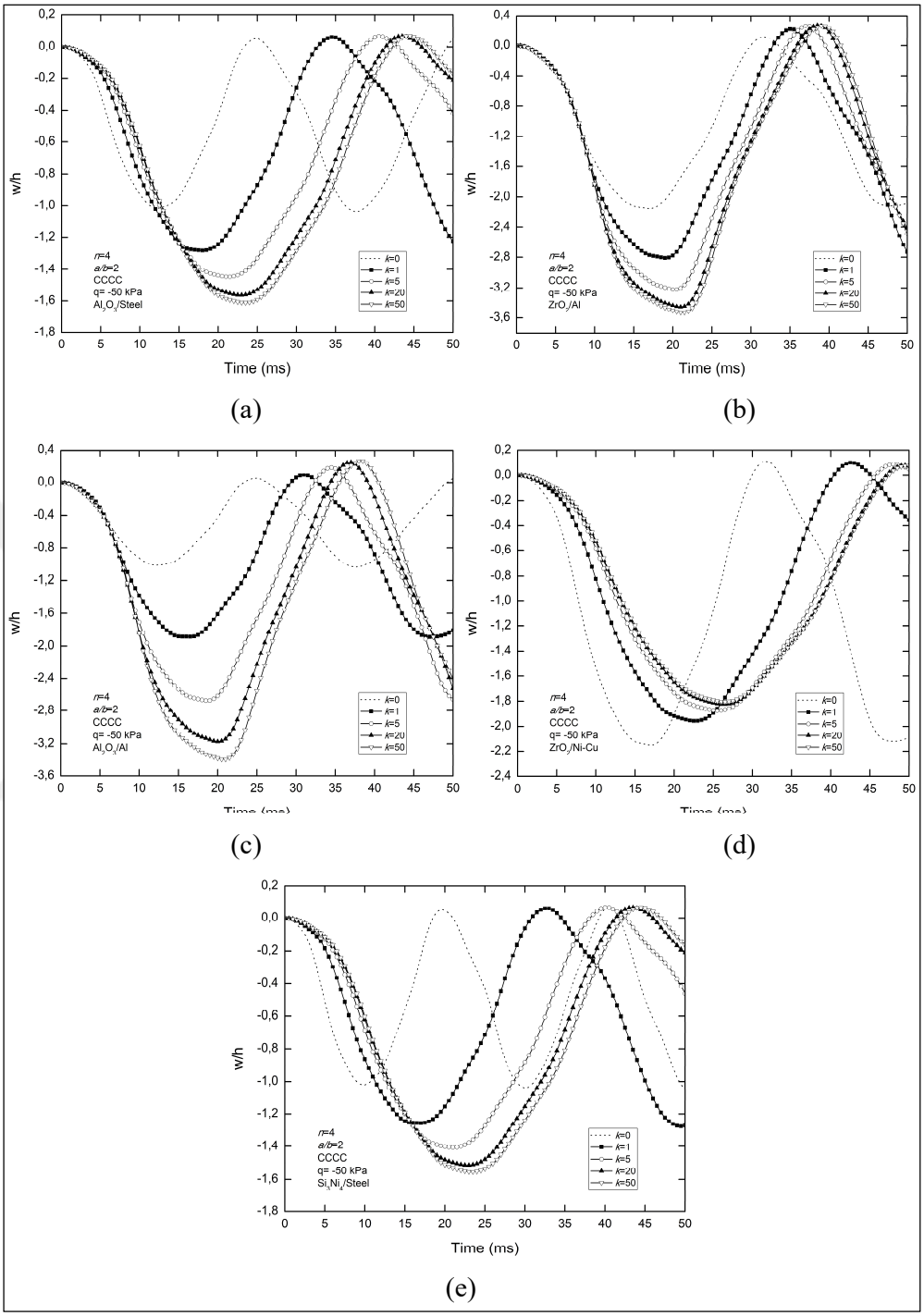

Figure 4.73**:** The effect of volume fraction coefficient on transverse displacement time history for CCCC boundary condition (*n*=4): (a) Alumina/Steel; (b) Zirconia/Aluminum; (c) Alumina/Aluminum; (d) Zirconia/Monel; (e) Silicon Nitride/Steel.

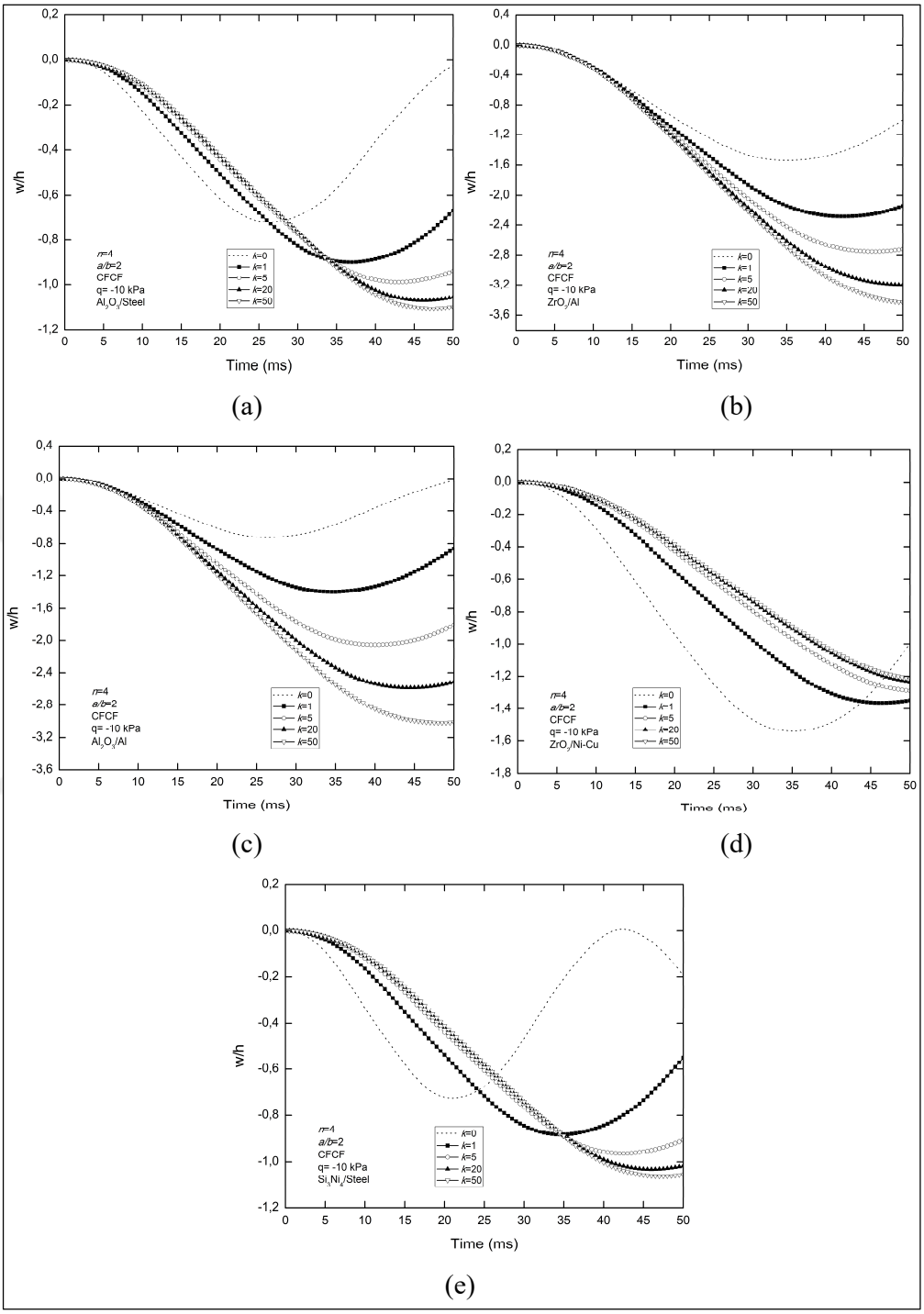

Figure 4.74**:** The effect of volume fraction coefficient on transverse displacement time history for CFCF boundary condition (n=4): (a) Alumina/Steel; (b) Zirconia/Aluminum; (c) Alumina/Aluminum; (d) Zirconia/Monel; (e) Silicon Nitride/Steel.

4.3.4. Effect of Ellipticity (*a/b*) on Nonlinear Dynamic Behavior

Here, effect of ellipticity (*a*/*b*) on nonlinear dynamic behavior of FGM super-elliptic shells (panels) is examined. Considered ellipticity values are: *a*/*b*=1, 3/2 and 2 where major radius is considered as *a*=2 m. Considered ovality values are: *n*=2, 4 and 8. Material of the shell is Silicon Nitride/Steel with volume fraction coefficient *k*=1. Figures 4.75 and 4.76 show the non-dimensional transverse displacement time histories at FGM super-elliptic shell centers considering fully clamped and CFCF cases, respectively. For the converged results, different mesh numbers were utilized by trial such that 1x4 GDQ elements and 11x17 grids for ellipticity value *a*/*b*=1, 1x6 GDQ elements and 11x15 grids for *a*/*b*=3/2 and 1x8 GDQ elements and 11x9 grids for *a*/*b*=2.

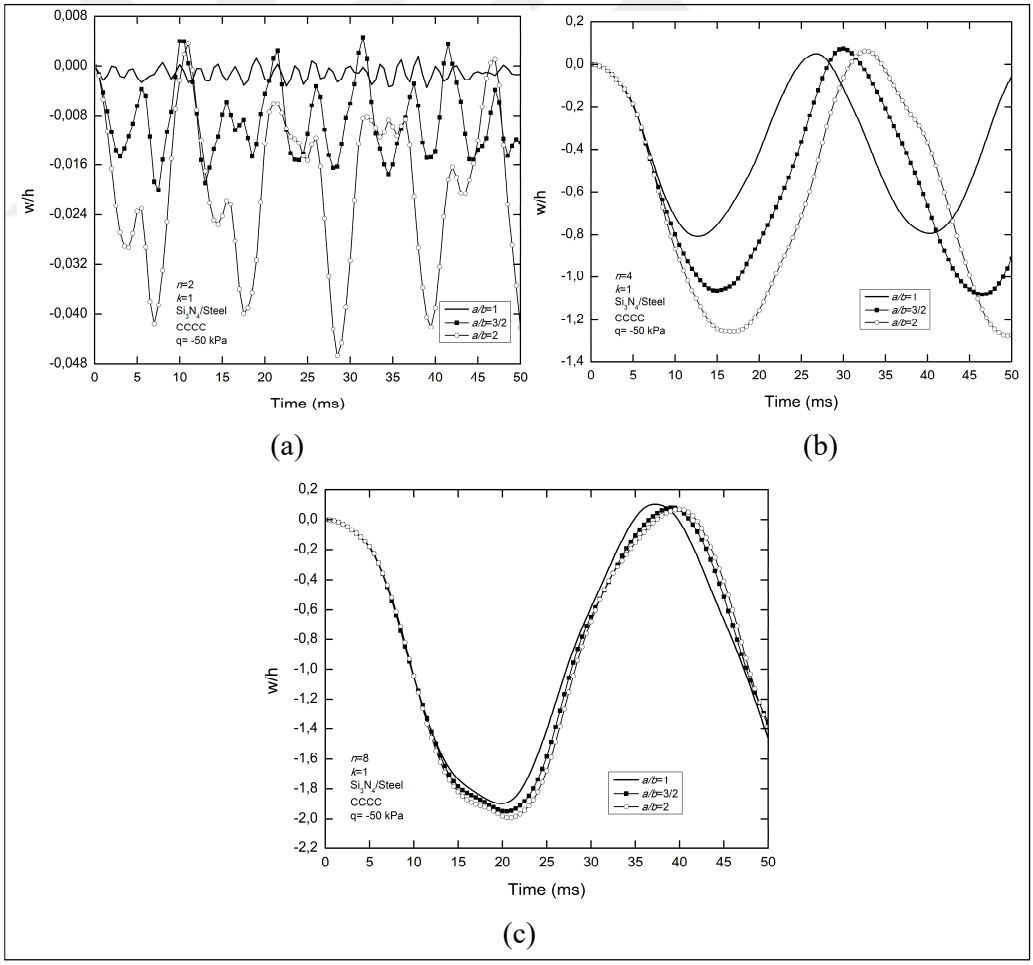

Figure 4.75**:** The effect of ellipticity on transverse displacement time history for CCCC boundary condition (Silicon Nitride/Steel, *k*=1): (a) for ovality value *n*=2; (b) for ovality value *n*=4; (c) for ovality value *n*=8.

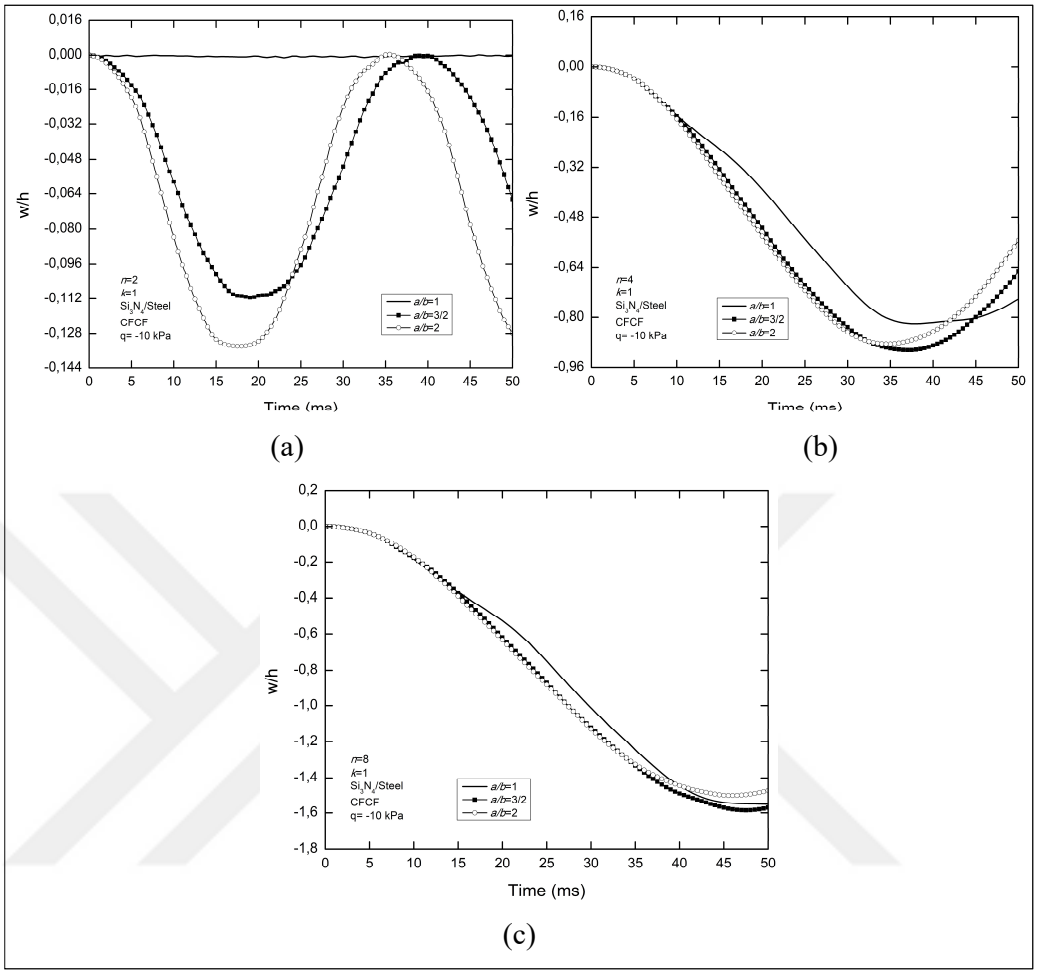

Figure 4.76**:** The effect of ellipticity on transverse displacement time history for CFCF boundary condition (Silicon Nitride/Steel, *k*=1): (a) for ovality value *n*=2; (b) for ovality value *n*=4; (c) for ovality value *n*=8.

Figures 4.75 (a) and (b) show that displacement values increase as the ellipticity of the shell increases for ovality values *n*=2 and 4 considering CCCC boundary condition. However, displacements are very close to each other for ovality value *n*=8 (Figure 4.75 (c)). For CFCF boundary condition, a remarkable increase in displacements is observed with the increasing values of ellipticity considering ovality value *n*=2 (Figure 4.76 (a)). In Figures 4.76 (b) and (c), it is seen that transient responses are very similar for ovality values *n*=4 and 8. Lowest displacements are observed in the cylindrical shell case (*a*/*b*=1 and *n*=2) for both boundary conditions as seen in Figures 4.75 and 4.76.

5. CONCLUSIONS

In this thesis, geometrically nonlinear dynamic behavior of super-elliptic shells (both panel and tube type) made of laminated composite materials and FGMs is investigated using GDQ method. A super-elliptic shell can represent cylindrical, elliptical or quasi-rectangular shell by adjusting parameters in super-ellipse formulation (also known as Lamé curve formulation). In this study, Green–Lagrange nonlinear strain–displacement relations for super-elliptic shells are derived retaining full non-linear terms in all degree of freedom parameters to take geometric nonlinearity into account. Transverse shear effect is considered through the FSDT. Virtual work principle is utilized to obtain equations of motion. Spatial derivatives in equation of motion is expressed with GDQ method and Newmark average acceleration method is utilized in time integration. Several super-elliptic shell problems under uniform distributed load are solved to investigate the effects of laminated composite and functionally graded material properties (layer orientations, volume fraction coefficient of FGM, different ceramic/metal pairs like Alumina/Steel (Al_2O_3/Steel), Zirconia/Aluminum (ZrO_2/Al), Alumina/Aluminum (Al_2O_3/Al), Zirconia/Monel (ZrO_2/Ni-Cu) and Silicon Nitride/Steel (Si_3N_4/Steel)) on dynamic behavior. In addition, effects of super-elliptic shell geometric characteristics (ellipticity and ovality) and boundary conditions on dynamic behavior are examined. Transient dynamic responses are compared with finite element solutions.

Considering laminated composite super-elliptic shells, outlines of this study can be summarized as follows:

- Transverse displacement values increase in magnitude for increasing ovality values for CCCC and CFCF boundary conditions for laminated composite super-elliptic shells with stacking schemes considered in this study.
- Elliptical shell ($n=2$) has lower displacement values in magnitude than other super-elliptic shells for CCCC and CFCF boundary conditions for all stacking schemes considered.
- For CCCC and CFCF boundary conditions, ε_x and ε_y values of elliptical shell (n=2) are much lower than those for n>2.

- In-plane shear stresses become significant in angle-ply stacking schemes and magnitude of τ_{xy} values of elliptical shell (n=2) are lower than those for n>2.
- Regarding CC boundary condition, an increase in transverse displacement values is observed with increasing values of the ovality at the upper and lateral center of laminated composite super-elliptic tubes with stacking scheme [0°/90°/0°/90°/0°].
- Lowest displacement values are obtained for elliptical tube (n=2) considering CC boundary condition and [0°/90°/0°/90°/0°] stacking scheme.
- [60°/-60°/60°/-60°/60°] stacking scheme gives the lowest displacement values in magnitude for CFCF boundary condition for n=2,4 and 8.
- Regarding CC boundary condition and n=4, for both upper and lateral centers of laminated composite super-elliptic tube, [0°/90°/0°/90°/0°] stacking scheme leads highest displacement values.
- Ellipticity has a slight effect on the dynamic behavior of the super-elliptic shell with the ovality n=8 for CCCC boundary condition for [60°/-60°/60°/-60°/60°] stacking scheme.
- For [60°/-60°/60°/-60°/60°] stacking scheme, ellipticity has a slight effect on the dynamic behavior of the super-elliptic shell for the ovality n=4 and 8 for CFCF boundary condition.
- Cylindrical shell (a/b=1 and n=2) leads to lowest displacement values for CCCC and CFCF boundary conditions among the ellipticity values considered (for n=2,4 and 8).

Considering super-elliptic shells made of FGMs, outlines of this study can be summarized as follows:

- As the ovality value of FGM super-elliptic shell increases, larger transverse displacement values were observed for all FGMs considered in this study considering CCCC and CFCF cases.
- For elliptic shell cases (n=2 and $a/b\neq1$), displacement values are quite lower than for other cases for all FGMs considered in this study regarding CCCC and CFCF cases. However, lowest displacement values were observed for cylindrical shell case (a/b=1 and n=2).

- Regarding CC boundary condition, increase in the ovality values led to an increase in displacement values for both upper and lateral centers of FGM super-elliptic tube made of Zirconia/Aluminum material pair (k=2).
- Largest displacements are observed for Zirconia/Aluminum material pair and displacements are nearly identical for Alumina/Steel and Silicon Nitride/Steel material pairs.
- Volume fraction coefficient has an increasing effect on transverse displacements for all FGMs considered in the present work except for Zirconia/Monel.
- Alumina/Aluminum has the highest change in displacement with increasing volume fraction coefficient and Zirconia/Monel has the lowest change in displacement with increasing volume fraction coefficient.
- Considering CCCC boundary condition, the effect of ellipticity on transient response of FGM super-elliptic shells made of Silicon Nitride/Steel is very low for the ovality value n=8. Similarly, same inference is valid for ovalities n=4 and 8 considering CFCF case.
- This study also shows that GDQ method is an efficient and effective method in the non-linear transient analysis of super-elliptic shell structures made of laminated composite materials and FGMs.

Lastly, this study can be extended to investigation of non-linear free vibration and stability analyses of super-elliptic shell structures as a future work. Also, it will be crucial to investigate the dynamic behavior of such structures experimentally.

REFERENCES

Alijani F., Amabili M., (2014), "Non-linear vibrations of shells: A literature review from 2003 to 2013", International Journal of Non-Linear Mechanics, 58 233–57.

Alijani F., Amabili M., Karagiozis K., Bakhtiari-Nejad F., (2011), "Nonlinear vibrations of functionally graded doubly curved shallow shells", Journal of Sound and Vibration, 330 (7), 1432–54.

Amabili M., (2015), "A new third-order shear deformation theory with non-linearities in shear for static and dynamic analysis of laminated doubly curved shells", Composite Structures, 128 260–73.

Amabili M., (2008), "Nonlinear Vibrations and Stability of Shells and Plates", 1st Edition, Cambridge University Press.

Amabili M., Païdoussis M. P., (2003), "Review of studies on geometrically nonlinear vibrations and dynamics of circular cylindrical shells and panels, with and without fluid-structure interaction", Applied Mechanics Reviews, 56 (4), 349.

Bacciocchi M., Eisenberger M., Fantuzzi N., Tornabene F., Viola E., (2016), "Vibration analysis of variable thickness plates and shells by the generalized differential quadrature method", Composite Structures, 156 218–37.

Bellman R., Casti J., (1971), "Differential quadrature and long-term integration", Journal of Mathematical Analysis and Applications, 34 (2), 235–38.

Bellman R., Kashef B. G., Casti J., (1972), "Differential quadrature: A technique for the rapid solution of nonlinear partial differential equations", Journal of Computational Physics, 10 (1), 40–52.

Bert C. W., Malik M., (1996), "Differential quadrature method in computational mechanics: A review", Appl Mech Rev, 49 (1), 1–28.

Chan S. H., (2001), "Performance and emissions characteristics of a partially insulated gasoline engine", International Journal of Thermal Sciences, 40 (3), 255–61.

Chen C. N., (2006), "Discrete element analysis methods of generic differential quadratures", Springer.

Choi S. T., Chou Y. T., (2003), "Vibration analysis of non-circular curved panels by the differential quadrature method", Journal of Sound and Vibration, 259 (3), 525–39.

Dey T., Ramachandra L. S., (2017), "Non-linear vibration analysis of laminated composite circular cylindrical shells", Composite Structures, 163 89–100.

Duc N. D., Tuan N. D., Tran P., Dao N. T., Dat N. T., (2015), "Nonlinear dynamic analysis of Sigmoid functionally graded circular cylindrical shells on elastic foundations using the third order shear deformation theory in thermal environments", International Journal of Mechanical Sciences, 101–102 338–48.

Elishakoff I., Pentaras D., Gentilini C., (2016), "Mechanics of Functionally Graded Material Structures", World Scientific.

Fluegge W., (1973), "Stresses in Shells", 2nd Edition, Springer.

Ganapathi M., Patel B. P., Gupta S. S., Khatri K. N., Sambandam C. T., Giri S. N., (2004), "Free-vibration characteristics of laminated angle-ply non-circular cylindrical shells", Defence Science Journal, 54 (4), 429–42.

Ganapathi M., Patel B. P., Patel H. G., Pawargi D. S., (2003), "Vibration analysis of laminated cross-ply oval cylindrical shells", Journal of Sound and Vibration, 262 (1), 65–86.

Ganapathi M., Patel B. P., Pawargi D. S., (2002), "Dynamic analysis of laminated cross-ply composite non-circular thick cylindrical shells using higher-order theory", International Journal of Solids and Structures, 39 (24), 5945–62.

Hirai T., Chen L., (1999), "Recent and prospective development of functionally graded materials in Japan", Materials Science Forum, 308–311, 509–14.

Isoldi L. A., Awruch A. M., Teixeira P. R., Morsch I. B., (2008), "Geometrically nonlinear static and dynamic analysis of composite laminates shells with a triangular finite element", Journal of the Brazilian Society of Mechanical Sciences and Engineering, 30 (1), 84–93.

Khalifa M., (2015), "Effects of non-uniform Winkler foundation and non-homogeneity on the free vibration of an orthotropic elliptical cylindrical shell", European Journal of Mechanics, A/Solids, 49, 570–81.

Koizumi M., (1997), "FGM activities in Japan", Composites Part B: Engineering, 28 (1–2), 1–4.

Kurtaran H., (2015a), "Geometrically nonlinear transient analysis of moderately thick laminated composite shallow shells with generalized differential quadrature method", Composite Structures, 125, 605–14.

Kurtaran H., (2015b), "Geometrically nonlinear transient analysis of thick deep composite curved beams with generalized differential quadrature method", Composite Structures, 128, 241–50.

Kurtaran H., (2015c), "Large displacement static and transient analysis of functionally graded deep curved beams with generalized differential quadrature method", Composite Structures, 131, 821–31.

Liu B., Ferreira A. J. M., Xing Y. F., Neves A. M. A., (2016), "Analysis of functionally graded sandwich and laminated shells using a layerwise theory and a differential quadrature finite element method", Composite Structures, 136, 546–53.

Ma Y. Q., Wang C. M., Ang K. K., (2008), "Buckling of super ellipsoidal shells under uniform pressure", Thin-Walled Structures, 46 (6), 584–91.

Patel B. P., Gupta S. S., Loknath M. S., Kadu C. P., (2005), "Free vibration analysis of functionally graded elliptical cylindrical shells using higher-order theory", Composite Structures, 69 (3), 259–70.

Patel B. P., Nath Y., Shukla K. K., (2007), "Thermo-elastic buckling characteristics of angle-ply laminated elliptical cylindrical shells", Composite Structures, 77 (1), 120–24.

Patel B. P., Shukla K. K., Nath Y., (2004), "Thermal buckling of laminated cross-ply oval cylindrical shells", Composite Structures, 65 (2), 217–29.

Pradyumna S., Nanda N., (2013), "Geometrically nonlinear transient response of functionally graded shell panels with initial geometric imperfection", Mechanics of Advanced Materials and Structures, 20 (3), 217–26.

Qatu M. S., (2004), "Vibration of laminated shells and plates", Elsevier.

Reddy J. N., (2004a), "An Introduction to Nonlinear Finite Element Analysis", 1st Edition, Oxford University Press.

Reddy J. N., (2003), "Mechanics of Laminated Composite Plate and Shells: Theory and Analysis", 2nd Edition, CRC Press.

Saada A. S., (1974), "Elasticity Theory and Applications", Pergamon press Inc.

Shen H.-S., (2009), "Functionally graded materials Nonlinear Analysis of Plates and Shells", CRC Press.

Shu C., (2000), "Differential quadrature and its applications in engineering", Springer-Verlag.

Soedel W., (2004), "Vibrations of shells and plates", CRC Press.

Sofiyev A. H., Karaca Z., Zerin Z., (2017), "Non-linear vibration of composite orthotropic cylindrical shells on the non-linear elastic foundations within the shear deformation theory", Composite Structures, 159, 53–62.

Srinivasan R. S., Bobby W., (1976), "Free vibration of non-circular cylindrical shell panels", Journal of Sound and Vibration, 46 (1), 43–49.

Struik D. J., (1988), "Lectures on classical differential geometry", Dover Publications Inc.

Thamburaj P., Sun J. Q., (2001), "Modal analysis of a non-circular cylindrical laminated shell using conformal mapping", Journal of Sandwich Structures and Materials, 3 (1), 50–74.

To C. W. S., Wang B., (1998), "Transient responses of geometrically nonlinear laminated composite shell structures", Finite Elements in Analysis and Design, 31 (2), 117–34.

Tornabene F., Bacciocchi M., (2018), "Anisotropic Doubly-Curved Shells: Higher-Order Strong and Weak Formulations for Arbitrarily Shaped Shell Structures", First Edition, Società Editrice Esculapio.

Tornabene F., Fantuzzi N., Bacciocchi M., Dimitri R., (2015a), "Dynamic analysis of thick and thin elliptic shell structures made of laminated composite materials", Composite Structures, 133, 278–99.

Tornabene F., Fantuzzi N., Bacciocchi M., Dimitri R., (2015b), "Free vibrations of composite oval and elliptic cylinders by the generalized differential quadrature method", Thin-Walled Structures, 97, 114–29.

Tornabene F., Fantuzzi N., Bacciocchi M., Viola E., Reddy, J. N., (2017), "A numerical investigation on the natural frequencies of FGM sandwich shells with variable thickness by the local generalized differential quadrature method", Applied Sciences, 7 (2), 131.

Tornabene F., Fantuzzi N., Ubertini F., Viola E., (2015), "Strong formulation finite element method based on differential quadrature: A survey", Applied Mechanics Reviews, 67 (2), 020801.

Uemura S., (2003), "The Activities of FGM on New Application", Materials Science Forum, 423–425, 1–10.

Uysal M. U., (2013), "Investigation of thermal and mechanical loading on functional graded material plates", International Journal of Mechanical, Aerospace, Industrial, Mechatronic and Manufacturing Engineering, 7 (11), 2283–89.

Vorovich I. I., (1999), "Nonlinear theory of shallow shells", Springer Science & Business Media.

Web 1, (2019), https://www.rockwestcomposites.com/shaped-tubing/oval-tubing/26000, (Date Accessed: 02/11/2019).

Web 2, (2019), http://www.escoeng.com/business/tunnel.php, (Date Accessed: 02/11/2019).

Web 3, (2019), https://elpais.com/elpais/2018/07/18/inenglish/1531905099_853875.html, (Date Accessed: 02/11/2019).

Web 4, (2019), https://www.airbus.com/search.image.html?tags=products-and-solutions%3Acommercial-aircraft%2Fa380-family&tagLogicChoice=OR#searchresult-image-all-13, (Date Accessed: 02/11/2019).

Wu Y. C., Yang T. Y., Saigal S., (1987), "Free and forced nonlinear dynamics of composite shell structures", Journal of Composite Materials, 21, 898–909.

Xing Y., Liu B., Liu G., (2010), "A differential quadrature finite element method", International Journal of Applied Mechanics, 02 (01), 207–27.

Yang J., Shen H. S., (2002), "Vibration characteristics and transient response of shear-deformable functionally graded plates in thermal environments", Journal of Sound and Vibration, 255 (3), 579–602.

Zhang J. H., Li G. Z., and Li S. R., (2015), "Analysis of transient displacements for a ceramic-metal functionally graded cylindrical shell under dynamic thermal loading", Ceramics International, 41 (9), 12378–85.

Zong Z., Zhang Y., (2009), "Advanced differential quadrature methods", CRC Press.

BIOGRAPHY

Gökçe AKGÜN was born in 1986 in Samsun/Turkey. In 2009, he received the B.Sc. degree in Mechanical Engineering from Ege University, Department of Mechanical Engineering (İzmir/Turkey). He received the M.Sc. degree in the graduate program of mechanical design from İstanbul Technical University, Graduate School of Science, Engineering and Technology (İstanbul/Turkey) in 2013. He worked as a lecturer in İstanbul Aydın University between 2012 – 2013. He started his doctoral studies at Gebze Technical University, Graduate School of Natural and Applied Sciences, Department of Mechanical Engineering in 2013. He has been working as a research assistant in Gebze Technical University, Department of Mechanical Engineering since 2013.

APPENDICES

Appendix A: Articles Published During the Thesis Study

Akgün G., Kurtaran H., (2019), "Large displacement transient analysis of FGM super-elliptic shells using GDQ method", Thin-Walled Structures, 141, 133-152.

Akgün G., Kurtaran H., (2018), "Geometrically nonlinear transient analysis of laminated composite super-elliptic shell structures with generalized differential quadrature method", International Journal of Non-Linear Mechanics, 105, 221-241.

Appendix B: Details of Laminate Stiffness Coefficients

The laminate stiffness coefficients A_{ij}, B_{ij}, C_{ij}, D_{ij}, E_{ij}, F_{ij}, G_{ij}, H_{ij} and I_{ij} for the laminated composite super-elliptic shells (see equations (2.139) and (2.140)) can be expressed as follows

$$\begin{aligned}&\left\{A_{ij},B_{ij},C_{ij},D_{ij},E_{ij},F_{ij},G_{ij},H_{ij},I_{ij}\right\}\\&=\sum_{k=1}^{n}\int_{z_{k-1}}^{z_k}\left\{1,z,z^2,z^3,z^4,z^5,z^6,z^7,z^8\right\}\bar{Q}_{ij}^{(k)}A_2(1+z/R_2)dz\quad(i,j=1,2,6)\end{aligned}\tag{B.1}$$

$$\begin{aligned}&\left\{A_{ij},B_{ij},C_{ij},D_{ij},E_{ij},F_{ij},G_{ij}\right\}\\&=\sum_{k=1}^{n}k_ik_j\int_{z_{k-1}}^{z_k}\left\{1,z,z^2,z^3,z^4,z^5,z^6\right\}\bar{Q}_{ij}^{(k)}A_2(1+z/R_2)dz\quad(i,j=4,5)\end{aligned}\tag{B.2}$$

where $\bar{Q}_{ij}^{(k)}$ are transformed stiffness coefficients of k-th layer and can be expressed as follows

$$\bar{Q}_{11}^{(k)}=Q_{11}^{(k)}\cos^4(\alpha)+2\left[Q_{12}^{(k)}+2Q_{66}^{(k)}\right]\sin^2(\alpha)\cos^2(\alpha)+Q_{22}^{(k)}\sin^4(\alpha)\tag{B.3}$$

$$\bar{Q}_{12}^{(k)}=\left[Q_{11}^{(k)}+Q_{22}^{(k)}-4Q_{66}^{(k)}\right]\sin^2(\alpha)\cos^2(\alpha)+Q_{12}^{(k)}\left[\sin^4(\alpha)+\cos^4(\alpha)\right]\tag{B.4}$$

$$\bar{Q}_{22}^{(k)} = Q_{11}^{(k)} \sin^4(\alpha) + 2\left[Q_{12}^{(k)} + 2Q_{66}^{(k)}\right]\sin^2(\alpha)\cos^2(\alpha) + Q_{22}^{(k)} \cos^4(\alpha) \tag{B.5}$$

$$\begin{aligned}\bar{Q}_{16}^{(k)} = &\left[Q_{11}^{(k)} - Q_{12}^{(k)} - 2Q_{66}^{(k)}\right]\sin(\alpha)\cos^3(\alpha) \\ &+\left[Q_{12}^{(k)} - Q_{22}^{(k)} + 2Q_{66}^{(k)}\right]\sin^3(\alpha)\cos(\alpha)\end{aligned} \tag{B.6}$$

$$\begin{aligned}\bar{Q}_{26}^{(k)} = &\left[Q_{11}^{(k)} - Q_{12}^{(k)} - 2Q_{66}^{(k)}\right]\sin^3(\alpha)\cos(\alpha) \\ &+\left[Q_{12}^{(k)} - Q_{22}^{(k)} + 2Q_{66}^{(k)}\right]\sin(\alpha)\cos^3(\alpha)\end{aligned} \tag{B.7}$$

$$\begin{aligned}\bar{Q}_{66}^{(k)} = &\left[Q_{11}^{(k)} + Q_{22}^{(k)} - 2Q_{12}^{(k)} - 2Q_{66}^{(k)}\right]\sin^2(\alpha)\cos^2(\alpha) \\ &+Q_{66}^{(k)}\left[\sin^4(\alpha) + \cos^4(\alpha)\right]\end{aligned} \tag{B.8}$$

$$\bar{Q}_{44}^{(k)} = Q_{44}^{(k)} \cos^2(\alpha) + Q_{55}^{(k)} \sin^2(\alpha) \tag{B.9}$$

$$\bar{Q}_{45}^{(k)} = \left[Q_{55}^{(k)} - Q_{44}^{(k)}\right]\sin(\alpha)\cos(\alpha) \tag{B.10}$$

$$\bar{Q}_{55}^{(k)} = Q_{55}^{(k)} \cos^2(\alpha) + Q_{44}^{(k)} \sin^2(\alpha) \tag{B.11}$$

In equations (B.3-11), α indicates the fiber orientation angle for each layer according to the x axis (see Figure 4.5 in chapter 4). Since the composite material properties (elastic modulus, shear modulus and Poisson's ratios) remains the same for each layer, the components of transformed stiffness coefficients $\bar{Q}_{ij}^{(k)}$ can be stated as:

$$Q_{11}^{(k)} = \frac{E_1}{1 - v_{12}v_{21}} \tag{B.12}$$

$$Q_{12}^{(k)} = Q_{21}^{(k)} = \frac{v_{12}E_2}{1 - v_{12}v_{21}} = \frac{v_{21}E_1}{1 - v_{12}v_{21}} \tag{B.13}$$

$$Q_{22}^{(k)} = \frac{E_2}{1 - v_{12} v_{21}} \tag{B.14}$$

$$Q_{66}^{(k)} = G_{12} \tag{B.15}$$

$$Q_{44}^{(k)} = G_{23} \tag{B.16}$$

$$Q_{55}^{(k)} = G_{13} \tag{B.17}$$

where E_1 and E_2 are the elastic modulus and v_{12} and v_{21} are the Poisson's ratios of composite layer in orthogonal directions and $v_{21} = v_{12}(E_2 / E_1)$ is considered. G_{12}, G_{23} and G_{13} are shear moduli and $G_{23} = G_{13} = G_{12}$ is considered.